

NASA/TM—2005-213137



# A Spreadsheet for the Mixing of a Row of Jets With a Confined Crossflow

J.D. Holdeman and T.D. Smith  
Glenn Research Center, Cleveland, Ohio

J.R. Clisset and W.E. Lear  
University of Florida, Gainesville, Florida

## The NASA STI Program Office . . . in Profile

Since its founding, NASA has been dedicated to the advancement of aeronautics and space science. The NASA Scientific and Technical Information (STI) Program Office plays a key part in helping NASA maintain this important role.

The NASA STI Program Office is operated by Langley Research Center, the Lead Center for NASA's scientific and technical information. The NASA STI Program Office provides access to the NASA STI Database, the largest collection of aeronautical and space science STI in the world. The Program Office is also NASA's institutional mechanism for disseminating the results of its research and development activities. These results are published by NASA in the NASA STI Report Series, which includes the following report types:

- **TECHNICAL PUBLICATION.** Reports of completed research or a major significant phase of research that present the results of NASA programs and include extensive data or theoretical analysis. Includes compilations of significant scientific and technical data and information deemed to be of continuing reference value. NASA's counterpart of peer-reviewed formal professional papers but has less stringent limitations on manuscript length and extent of graphic presentations.
- **TECHNICAL MEMORANDUM.** Scientific and technical findings that are preliminary or of specialized interest, e.g., quick release reports, working papers, and bibliographies that contain minimal annotation. Does not contain extensive analysis.
- **CONTRACTOR REPORT.** Scientific and technical findings by NASA-sponsored contractors and grantees.

- **CONFERENCE PUBLICATION.** Collected papers from scientific and technical conferences, symposia, seminars, or other meetings sponsored or cosponsored by NASA.
- **SPECIAL PUBLICATION.** Scientific, technical, or historical information from NASA programs, projects, and missions, often concerned with subjects having substantial public interest.
- **TECHNICAL TRANSLATION.** English-language translations of foreign scientific and technical material pertinent to NASA's mission.

Specialized services that complement the STI Program Office's diverse offerings include creating custom thesauri, building customized databases, organizing and publishing research results . . . even providing videos.

For more information about the NASA STI Program Office, see the following:

- Access the NASA STI Program Home Page at <http://www.sti.nasa.gov>
- E-mail your question via the Internet to [help@sti.nasa.gov](mailto:help@sti.nasa.gov)
- Fax your question to the NASA Access Help Desk at 301-621-0134
- Telephone the NASA Access Help Desk at 301-621-0390
- Write to:  
NASA Access Help Desk  
NASA Center for AeroSpace Information  
7121 Standard Drive  
Hanover, MD 21076

NASA/TM—2005-213137



# A Spreadsheet for the Mixing of a Row of Jets With a Confined Crossflow

J.D. Holdeman and T.D. Smith  
Glenn Research Center, Cleveland, Ohio

J.R. Clisset and W.E. Lear  
University of Florida, Gainesville, Florida

National Aeronautics and  
Space Administration

Glenn Research Center

---

February 2005

## Acknowledgments

The authors appreciate the contributions to this project made by G.H. Canton, University of Florida, J.S. Scheuer, Case Western Reserve University, and Dr. C.J. Marek, NASA Glenn Research Center. Dr. Marek has long been a supporter of the usefulness of the JIC confined-flow empirical model. He contributed many helpful ideas to the current project, and did the original FORTRAN programming several years ago. Mr. Canton did much of the original Microsoft Excel (Microsoft Corporation, Redmond, WA) programming, and Mr. Scheuer did much of the programming for user inputs and contributed many helpful ideas in that endeavor. The authors would also like to thank Professor G.S. Samuelsen, University of California at Irvine, Dr. R. Srinivasan, then of Honeywell Engines, Mr. D.S. Liscinsky, United Technologies Research Center, Mr. C.E. Smith, CFD Research Corporation, and Mr. R.E. Walker (ret.), Aerojet Liquid Rocket Company, for testing an earlier version of this spreadsheet. The authors would like to thank the late Arthur Lefebvre, Professor Emeritus at Cranfield and Purdue, who encouraged the NASA JIC work over the last several decades.

Trade names or manufacturers' names are used in this report for identification only. This usage does not constitute an official endorsement, either expressed or implied, by the National Aeronautics and Space Administration.

Available from

NASA Center for Aerospace Information  
7121 Standard Drive  
Hanover, MD 21076

National Technical Information Service  
5285 Port Royal Road  
Springfield, VA 22100

Available electronically at <http://gltrs.grc.nasa.gov>

# A Spreadsheet for the Mixing of a Row of Jets With a Confined Crossflow

J.D. Holdeman and T.D. Smith  
National Aeronautics and Space Administration  
Glenn Research Center  
Cleveland, Ohio 44135

J.R. Clisset and W.E. Lear  
University of Florida  
Gainesville, Florida 32611

## Abstract

An interactive computer code, written with a readily available software program, MS Excel (Microsoft Corporation, Redmond, WA), is presented which displays three-dimensional oblique plots of a conserved scalar distribution downstream of jets mixing with a confined crossflow for a single row, axial-staged double rows, or opposed rows of jets with or without flow area convergence and/or a nonuniform crossflow scalar distribution.

The program uses multiple spreadsheets in a single Excel notebook to carry out the modeling using a previously-published empirical model. Comparisons are also made between results from the version of the empirical model implemented in the spreadsheet and versions originally written in Applesoft BASIC on an Apple //e computer (Apple Computer, Cupertino, CA) in the 1980's.

## Nomenclature

$A_J/A_M$	jet-to-mainstream area ratio for each row, $(\pi/4)/((S/H)(H/d)^2) = (\pi/4)/((S/d)(H/d))$
$C$	$(S/H)(\text{sqrt}(J))$ ; same as eq. (2)
$C_d$	orifice discharge coefficient
$d$	diameter of a round-hole orifice, or the diameter of an equivalent-area round hole if a noncircular orifice is specified.
$d_J$	$(d)(\text{sqrt}(C_d))$
$DR$	jet-to-mainstream density ratio. For an incompressible flow, and for gases of the same chemical composition, this ratio is approximately equal to the mainstream-to-jet temperature ratio, $T_M/T_J$
$dH/dx$	duct convergence rate; see eq. (4)
$H$	duct height at first row of holes (called $H_0$ in several previous publications)
$H_{eq}$	effective duct height (= $H$ except for opposed rows of inline jets); see eq. (8)
$H(x)$	local duct height for converging ducts (= $H$ for $x \leq 0$ ); see eq. (4)
$J$	jet-to-mainstream momentum-flux ratio, $(DR)(V_J/U_M)^2 = (MR)^2/DR/(C_d)^2/(A_J/A_M)^2$ (incorrectly called the momentum ratio in early publications)
$L/W$	(long dimension)/(short dimension) for noncircular orifices; see eqs. (5) and (6)

(Note that this definition is different than in several previous publications. wherein the orifice length-to-width ratio was often called the aspect ratio. Later  $L/W$  was called the Aspect Ratio, but used the definition of (long dimension)/(short dimension))

$m_J$	jet mass flow
$m_M$	mainstream mass flow
$m_T$	total mass flow, $m_J + m_M$
$m_J/m_T$	jet-to-total mass-flow ratio = $MR/(1 + MR)$
$MR$	jet-to-mainstream mass-flow ratio, $m_J/m_M = (DR)(V_J/U_M)(C_d)(A_J/A_M)$
$M$	jet-to-mainstream mass-flux ratio = $(DR)(V_J/U_M) = \text{sqrt}(J^*DR)$ ; see ref. 2
$PF$	pattern factor, $(MR)(1 - \theta_{\min}/\theta_{EB})$
$R$	jet-to-mainstream velocity ratio = $(V_J/U_M) = \text{sqrt}(J/DR)$ ; see ref. 2
$R_{eff}$	jet-to-mainstream “effective” velocity ratio = $\text{sqrt}(J)$
$S$	lateral spacing between equal locations for adjacent orifices, e.g., between orifice centers
$S/d$	ratio of orifice spacing to orifice diameter
$S/L$	ratio of orifice spacing to actual orifice lateral dimension for bluff slots; see eq. (6), replaces $S/d$ in correlation equations in appendix C
$S/W$	ratio of orifice spacing to actual orifice lateral dimension for streamlined slots; see eq. (5), replaces $S/d$ in correlation equations in appendix C
$S_X$	axial spacing between orifice centers for double rows
$T$	local scalar variable
$T_J$	jet exit scalar variable
$T_M$	mainstream scalar variable
$U$	axial velocity
$U_M$	mainstream velocity
$V_J$	jet exit velocity
$W_{1/2}^-$	jet half-value width ( $W_{1/2}^-/H$ ) on injection side of profile; i.e., for $y/H < y_c/H$ , see figure 2 (note that $y = 0$ is at the top wall in fig. 2)
$W_{1/2}^+$	jet half-value width ( $W_{1/2}^+/H$ ) on opposite side of profile; i.e., for $y/H > y_c/H$ see figure 2 (note that $y = 0$ is at the top wall)
$x$	downstream coordinate; $x = 0$ at center of the first row of orifices unless noted otherwise
$y$	cross-stream coordinate; $y = 0$ at wall
$y_c$	scalar trajectory
$z$	lateral coordinate; $z = 0$ at centerplane
$\Delta(z/S)$	lateral translation of profiles for slanted slots = $(\sin[(\pi/2)(a)])$ ; same as eq. (7)
$\theta$	$(T_M - T)/(T_M - T_J)$
$\theta_c$	maximum scalar difference ratio defines location of scalar trajectory, $y/H = y_c/H$
$\theta_I$	$\theta_1$ and $\theta_2$ are the components of $\theta$ in the superposition formula; see eq. (3)
$\theta_{EB}$	equilibrium $\theta \sim m_J/m_T$ (called TB in ref. 12)
$\theta_{\min}^-$	minimum scalar difference ratio on injection side of profile; (i.e., for $y/H < y_c/H$ ), see figure 2
$\theta_{\min}^+$	minimum scalar difference ratio on opposite side of profile (i.e., for $y/H > y_c/H$ ), see figure 2

## Introduction

The problem of jets in crossflow (JIC or JICF) has been rather extensively treated in the literature, to the point that it can almost be considered to be a ‘classical’ three-dimensional flow problem. Numerous previous JIC studies have yielded insight into such flow field characteristics as the jet structure, jet penetration, the development of vortices, the jet entrainment of crossflow fluid, and the flow field distributions resulting from jet mixing. Extensive listings of JIC publications from studies performed in the past several decades can be found in Margason (ref. 1), Holdeman (ref. 2), Holdeman et al. (ref. 3), and Holdeman et al. (ref. 4). PDF’s of the NASA JIC reports from GRC; Technical Notes (TN), Technical Papers (TP), Technical Memorandums (TM), and Contractor Reports (CR) later than 1970 are posted on [gltrs.grc.nasa.gov](http://gltrs.grc.nasa.gov).

Although all previous studies have contributed additional understanding of the general problem, the information obtained in any given study is determined by its motivation, and it may not satisfy the specific needs of diverse applications. The motivating application may determine such important flowfield parameters as the region of interest, the degree of confinement, and orifice configuration. For example, many of the studies summarized in reference 1 were motivated by V/STOL aircraft (such as the Harrier) in ground proximity; the studies summarized in reference 2 were motivated by mixing of dilution jets in conventional combustion chambers for gas turbine engines; and the studies summarized in references 3 and 4 focused on optimizing the mixing section in the RQL scheme proposed for low emissions combustors.

Note that many of the studies cited in references 1 to 4 are of a single jet in an unbounded crossflow. Although the single jet is a key component in combustor flow fields, flows in combustors and other engineering devices are usually confined and interaction between jets is critical to their performance. Combustor flows are also usually turbulent and reacting, the region of interest may not be very far downstream, and high inlet pressures and temperatures are typical. Thus, single jet studies may be inadequate for direct application to combustor mixing problems.

Many of the techniques suggested for a steady confined JIC, do an excellent job of decreasing jet penetration, but designers are usually looking for something that will increase penetration. So far nothing has been identified for a steady JIC that penetrates significantly farther than a single, round, unbounded JIC, so the unbounded JIC from a round hole should be considered as the upper limit for jet penetration.

The need to design or tailor the temperature pattern at the combustor exit in gas turbine engines was the motivation for the original development of an empirical JIC model for confined flows. In the combustor dilution zone, for which the results in references 5 to 16 were a generic model, rapid mixing of the diluent air with the primary airstream is desired to provide a suitable profile at the turbine inlet, quench any continuing chemical reactions, and reduce combustor length. From the data in references 5, 11, and 14 to 16, an empirical model was developed for predicting the scalar field downstream of a row of jets mixing with a confined crossflow.

Further development of the correlations and publication of those results in reference 17 extended the “basic” model to include variations typically found in combustors for gas turbine engines (ref. 18), e.g., double rows, and opposed rows of jets with or without flow area convergence and/or a nonuniform crossflow scalar distribution. Listings of the Applesoft BASIC programs used in reference 17 are included here as appendixes A and B.

Note, however, that the confined JIC empirical model cannot be used for unconfined jet flows because the relations used therein for orifice size and spacing do not extrapolate properly for the single unconfined JIC. Also, as with any empirical model, one would be more confident in results obtained for interpolation within the range of the generating experiments, rather than for results from extrapolations.

Programs modeling jets in crossflow have been developed using languages such as BASIC and FORTRAN, but a JIC model using a spreadsheet has not been heretofore published in the open literature. MS Excel is an excellent tool to use in order to create a JIC spreadsheet because the model requires both calculation and plotting. The three-dimensional (rotated) carpet plots generated by this program are really just a series of offset two-dimensional plots wherein part of the current profile may not be visible because it is behind previously-plotted profiles.

The Excel program makes it straight-forward to accomplish tasks such as adapting the program input for specific needs or applications, adjusting the viewing angle, and animating the results. A final advantage is that Excel is widely available.

The purpose of this program is to provide an engineering tool to reduce development time and cost by allowing the designer to investigate the effects of varying flow and/or geometric parameters on jet penetration and mixing. This report presents a spreadsheet that is functionally equivalent to the capability of the BASIC programs used in references 12 and 17. To facilitate comparison, the data figures calculated with the spreadsheet presented in this report are cases from references 12 and 17; however, the trajectory correlation used in these earlier reports is slightly different for some of the cases that are common to both, and the differences are also discussed herein. Note too that the nomenclature has evolved during the last three decades; most parameters are defined the same, but some have changed and the reader should be aware of this.

## Flow Field Model

Figure 1 is a schematic of the flow field. The jets are shown here entering the mainstream flow through orifices in the top duct wall (although bottom injection is an option). The primary independent geometric variables are the lateral spacing between the centerlines of adjacent orifices, and the orifice size. These are often expressed in dimensionless form as the ratio of the orifice spacing to orifice diameter,  $S/d$ , and the ratio of the duct height to orifice diameter,  $H/d$ .

Because the ratio of these,  $S/H$ , was found to be very important for confined JIC flows, and the orifice size (inversely proportional to  $H/d$ ) is a generally specified variable,  $S/H$  and  $H/d$  are used herein as independent variables, and  $S/d = (S/H)*(H/d)$  is calculated. (Any two of the parameters  $S/d$ ,  $S/H$ , and  $H/d$  may be considered as independent variables—just not all three.) Input for the  $S/H$  parameter is only allowed in the spreadsheet for the top front row; the user must be aware that although  $S/H$  for other rows is dependent on the value specified, it may not be the same.

Downstream distances are specified in terms of  $x/H$ , and  $x/d (= (H/d)*(x/H))$  which is commonly used in single JIC studies, is readily calculated. Note that  $x/d$  is proportional to  $H/d$  for a given  $x/H$ . The use of  $x/H$  to specify downstream distance is appropriate because the designers' objective is usually to identify orifice configurations to optimize the mixing within a given length, or to adjust an unacceptable exit distribution, and the downstream stations of interest are usually independent of the orifice diameter.

A major assumption in the empirical model for the scalar field downstream of jets mixing with a confined crossflow is based on the observation that nondimensionalized vertical scalar profiles everywhere in the flow field can usually be expressed in the following form:

$$\frac{\theta - \theta_{\min}^{+/-}}{\theta_c - \theta_{\min}^{+/-}} = \exp \frac{(-\ln 2)(y/H - y_c/H)^2}{(W_{1/2}^{+/-}/H)^2} \quad (1)$$

where  $\theta$  ( $= (T_M - T)/(T_M - T_J)$ ) is the dimensionless local scalar difference ratio, and  $T$ ,  $T_M$ , and  $T_J$  are, respectively, the local, mainstream and jet values.  $y/H$  is the local dimensionless distance from the injection wall,  $y_c/H$  is the scalar trajectory, and  $W_{1/2}^{+/-}/H$  is the profile half-value width on the injection or opposite side of the trajectory as appropriate. Note that  $\theta = (\theta_c + \theta_{\min}^{+/-})/2$  if  $|y/H - y_c/H| = W_{1/2}^{+/-}/H$ . It appears that eq. (1) was first applied to confined JIC data in references 9 and 10. A similar equation was applied to centerplane data for a single, unconfined JIC ( $\theta_{\min}^{+/-} = 0$ ) in references 19 to 21.

Note that the trajectory defined by the maximum scalar in the centerplane,  $y_c$ , is not the same as the trajectory defined by the maximum velocity (the point of maximum velocity is usually farther from the injection wall). Note also that  $\theta$  should physically be between 0 and 1, with zero usually representing unmixed mainstream fluid, and one representing unmixed jet fluid (but  $\theta = 1$  often represents mainstream fluid so the reader must be observant here too).

$\theta$  should be neither  $<0$  nor  $>1$  if the parameter represented is a conserved scalar (no sources or sinks). Although  $\theta$  was originally formulated from temperature data, it is dimensionless, and applies to any conserved scalar (see e.g., refs. 3 and 4). Note that although temperature is a conserved scalar in a nonreacting and incompressible flow, it is not a conserved scalar in a compressible and/or reacting flow.

As shown in figure 2,  $\theta_c$ ,  $\theta_{\min}^+$ ,  $\theta_{\min}^-$ ,  $W_{1/2}^+/H$ ,  $W_{1/2}^-/H$ , and  $y_c/H$  are scaling parameters. (Note that  $y = 0$  is at the top wall in fig. 2). For all calculations, the dimensionless flow and geometric variables that must be specified are the jet-to-mainstream density ratio ( $DR$ ), jet-to-mainstream momentum-flux ratio ( $J$ ), jet discharge coefficient ( $Cd$ ), orifice spacing-to-duct-height ratio ( $S/H$ ), duct height-to-orifice diameter ratio ( $H/d$ ), and the downstream distance ( $x/H$ ).

The user must also specify the mainstream scalar distribution for flows with a nonuniform mainstream scalar, the duct convergence rate,  $dH/dx$ , for converging ducts, and the ratio of the long to short dimensions of the orifice,  $L/W$ , for noncircular orifices (all orifices are considered to have semi-circular ends, so they reduce to round holes for  $L/W = 1$ ). Note also, that  $L/W > 1$  by definition, and the definition used here is different from that in reference 2, but is the same as that used in references 3 and 4.

Correlations were developed for each of the scaling parameters. The independent and dependent variables are identified in table 1. The correlations used in this Excel workbook are the same as those included in reference 2 (any differences are due to clarification, changes in nomenclature, or correction of errors) and are also the same as those used and published in reference 17 (and appendixes A and B herein), and NASA TM-104412 (AIAA Paper 91-2458) which was the precursor to reference 2. The complete set of correlation equations used herein is given in appendix C.

A schematic of the several orifice row configurations for which calculations were performed are shown in figure 3. The orifice configurations are in order of their round hole size ( $H/d$  first, then  $S/H$  if  $H/d$  is the same). Only one identifying letter is used for configurations that differ only

by a lateral shift. The orifice configuration for each figure is listed in table 2. The corresponding figures in references 12 and 17 are also listed to facilitate comparison. Whenever possible the closest experimental data in references 5, 11, 14, and 15 are identified in table 2.

The present version of this spreadsheet provides a three-dimensional pictorial representation of the field of a conserved scalar. The ordinate and oblique coordinates are the  $y$  and  $z$  directions, which are respectively, normal to and along the orifice row in an axial (constant- $x$ ) plane. The  $z$ -distance shown in the oblique plots is twice (or 4 times) the orifice spacing for each configuration. There are 21 profiles in this span. Thus for two jets,  $\Delta z/S = 0.1$ ; for four jets,  $\Delta z/S = 0.2$ . Of the 21 profiles only 6 jet profiles are calculated. The others are generated by assuming symmetry about both the centerplane and midplane.

Typical profiles are shown in figure 4 (configuration F in fig. 3,  $S/H = 0.5$ ,  $H/d = 5.66$ ,  $J = 26.4$ ). Profile distributions may be calculated at any user-specified downstream location ( $x$ ), for a single-row, double rows, or opposed rows of jets in a rectangular duct with or without flow area convergence and/or a nonuniform crossflow scalar distribution. The mainstream duct is noncurving. (It is not annular, nor is it a reverse-flow combustor geometry; correlations for curvature effects are given in refs. 22 and 23.)

Independent variables are given in the figure titles and legends. (Key and/or common dependent variables are also shown in parentheses for completeness, although they can be calculated from the independent variables.) Variables that are common to all parts of the figure usually appear in the title; those that are not are given in the legends.

Although calculations can be performed for most flow and geometric conditions of interest, they will be most reliable for conditions within the range of the experiments on which the empirical model is based. Note that not all combinations of the independent variables listed in table 1 were tested. The spreadsheet checks to determine if the inputs specified are within the range of the experiments and warns the user if extrapolation is being specified. The specifics and operation of this program are described in the following section of this report.

## Program Specifics

### Spreadsheet Operation

Included on the CD is a supplemental Microsoft® Excel spreadsheet containing three sheets as described in the following text ([TM—2005-213137/ SUPPL1](#)).

**Input Sheet.**—The first sheet in the Microsoft® Excel workbook is the Input sheet where input values are entered by the user through either the blue-bordered cells (sections A, C, D, and E), the option boxes (sec. B and C), or the check boxes (sec. D). Section A queries the user to enter dimensionless inputs for up to four rows of orifices; section B is a button-input section that defines which of the four available rows are being utilized (inactive rows have a gray background); section C is also button-input used to define the shape of the orifices; section D can be used to initiate several special case scenarios; and section E asks for a user-defined scalar field if a nonuniform mainstream  $\theta$  is specified.

*Section A:* queries the user to enter up to 19 dimensionless inputs to define the physical situation for up to four rows of round holes or slots. The blue-bordered cells are for input of the

independent variables. The input cells are separated into four columns, one for each of the four possible locations of orifices (two rows, top or bottom) the red bordered cells are dependent variables for reference only and cannot be input directly; for example,  $C = S/H \cdot \sqrt{J}$  has been found to be useful in categorizing JIC configurations, and is calculated but its value cannot be input. Similarly,  $M = \sqrt{DR \cdot J}$ ,  $R = \sqrt{J/DR}$ ,  $R_{eff} = \sqrt{J}$ ,  $S/d = (S/H)(H/d)$ , and  $x/d = (x/H)(H/d)$  are considered to be dependent variables and cannot be input.

The user is required to input several dimensionless parameters which will define the flow and geometry conditions and location of the plot. These are:  $x/H$ ,  $DR$ ,  $J$ ,  $H/d$ ,  $S/H$ ,  $C_d$ , and  $S_x/H$ . The input cells show two things simultaneously. The first is the active rows, which can be discerned by whether the boxes in the columns are grayed or not (if the desired row is grayed, it should be activated in section B). The second thing is an obvious distinction between the independent and dependent variables (blue versus red outlines on the cells). This is a little tricky for a variable like  $S/H$ , which can only be defined once—variables such as this are set in the top/front row. Therefore, if this row is inactive, the user will have to adjust a grayed out cell in jet row 1 top, and then verify that the desired value appear in active rows.

For  $x/H$  inputs the user must also be particularly careful. Input is allowed only in the top/front row. All other rows are calculated from the input value of  $x/H$  for the top/front and  $S_x/H$ . Note that  $S_x/H$  is only input once, so rows on the top and bottom will be at the same axial location. Again, and particularly if the top/front row is not active, the user must ascertain that the expected values appear for other rows.

Note that  $x/H$  values will always be from the center of the orifices in the first row. Thus if a downstream distance is desired from another location, e.g., from midway between the rows where the  $x/H$  input from the top front row must be  $(S_x/H)/2$  larger than the value that would be obtained if  $x = 0$  was midway between rows.

*Section B:* is a simple row of buttons for specifying the orifice location and apparent spacing for each of the four possible active rows: first row, top; second row, top; first row, bottom; second row, bottom. In each row is a choice of five scenarios: the row is inactive (contains no orifices); a row of two orifices shows the centerplane at the edge; a row of two orifices shows the midplane at the edge; a row of four orifices shows the centerplane at the edge; a row of four orifices shows the midplane at the edge. The spacing shown for rows of four orifices is double that of 2-hole distributions. This is usually just scaling though, as the same profiles can usually be displayed in either the 2-hole or 4-hole format, as will be shown subsequently.

*Section C:* is a row of buttons and an input box for specifying the shape of the orifices. Again, there is a possibility of four active rows: each row has four options to choose from: round holes, streamlined slots, bluff slots, and 45° slanted slots. If a noncircular orifice is selected, the user must also enter the length to width ratio of the slot in the input box. In the length to width ratio,  $L/W$ ,  $L$  is the long dimension and  $W$  is the short dimension of the orifice. Hence  $L/W$  is independent of orifice orientation, and is always greater than, or equal to, one. Slots are assumed to have semicircular ends so if  $L/W = 1$ , the slot will reduce to a round hole, and of course, is independent of bluff, streamlined, or slanted orientation. (Note that this definition is the same as used in refs. 3 and 4, but is different from that in ref. 2.)

*Section D:* is a random array of check and input boxes to further modify the flow configuration.

Hot/Cold: This check box inverts the scalar profile of the plot (no physical changes). The standard definition of  $\theta$  (see the discussion following eq. (1)), where the numerator is the local difference from the mainstream fluid, is used unless otherwise noted. In the alternate definition (i.e.,  $1 - \theta$ ), the numerator is the local difference from the jets. This option is discussed further in the View Options section below.

Duct Convergence: This allows the height of the duct to change with downstream distance; convergence begins at  $x/H = 0$  and is assumed to be symmetric. The rate of convergence is adjusted by changing the parameter ( $dH/dx$ ) in the formula  $H(x)/H = 1 - (dH/dx)(x/H)$ . The box must be checked to invoke convergence, and if it is checked  $dH/dx$  must be specified. Note that although the local duct height is becoming smaller, profiles are scaled to the duct height at  $x/H = 0$ , so the duct height always appears the same.

Mainstream Scalar: A nonuniform mainstream scalar may be invoked by checking the appropriate box. If the user chooses to specify a nonuniform mainstream scalar, the desired distribution is input in section E; all values should be between 0 and 1.

Perspective: The user may adjust the appearance of the output plot by changing the perspective (no physical changes). To change the perspective, specify a multiple of 0.01; an  $x$ -perspective = 0.04 and a  $y$ -perspective = 0.02 work well. Note that the “back” of the profiles is not shown, although it could be visible in some cases (see, for example, the profiles in refs. 5 to 7).

*Section E:* allows the user to specify the mainstream scalar distribution. The identification of a nonuniform mainstream scalar in section D requires input of a 21x21 cell array (101 [ $y$ ] × 21 [ $z$ ]) that allows for any mainstream profile that the user desires to specify. These values must be entered in section E. This capability expands the earlier programs which were limited to preset mainstream distributions which varied only in the  $y$ -direction.

The rows represent the scalar profile from the top of the duct to the bottom of the duct; the columns represent the mainstream profile from the left side of the duct (closest profile) to the right (farthest profile). Note that columns 1 and 21 should be the same; if they are not, a discontinuity will exist outside of the field of view that is displayed. The specified distribution does not decay as  $x/H$  increases, so the distribution that is input can be viewed by specifying that all rows of jets are inactive in section B.

**Error messages.**—Warnings occur if the input falls outside of the range of the experimental data from which the empirical relations were formulated. This program is intended to be user friendly; however, the user must be aware of the limitations of the empirical relations and the limitations of this program. Several common input errors are outlined below.

First there is a narrative error box stretching from columns C to M in row 30. This error box does not indicate an error in the traditional sense; rather, it alerts the user if an input parameter is outside the range of the generating experiments. The existence of an error will be shown in rows 6 to 29 in column O which will show either OK or ERROR. If an ERROR occurs, this indicates that a value for an active row is outside the range of the data that were used in formulating the empirical model (see table 1). The number of warnings for each row in the spreadsheet is given in rows 6 to 26, and is totaled in row 30 of column P. ERROR does not stop the calculation.

**As an example.** To get opposed rows, pick jet rows 1 top and bottom, or 2 top and bottom in section A, then select in-line or staggered in section B, the orifice shape in section C, the flow

convergence in section D, and give specifications for a nonuniform scalar in sections D and E. If both rows are the same in section B, either spreadsheet rows 33 or 34 for two orifices (or 35 or 36 for 4 orifices), then the orifices are in-line, for staggered make them different, depending on whether a centerplane or midplane is desired at the edge on top.

For double (axial staged) rows, pick jet rows 1 and 2 top or 1 and 2 bottom and specify the axial separation between centerlines,  $S_x/H$ . Identify either centerplane or midplane at the edge in section B. If these are the same the holes are aligned, if they're different the holes are staggered.

Note that  $S/H$  must be specified in row 1, even if that row is inactive, and that inactive rows are grayed. The default in section B is no orifices, so  $\theta$  will be = 0 unless a row is active or a nonuniform scalar distribution is specified. Effects can be ganged, like double axial rows of opposed jets from noncircular orifices in a converging duct with a nonuniform mainstream scalar (but there is no experimental data for this case).

The user should be aware that the geometry of the setup should be checked for physical consistency; the program will not warn of this. For example, slots or holes may overlap, the mainstream passage can be set to converge to a zero or negative height, or the empirical model may return a value of  $\theta$  greater than 1.

Also, although  $x/H$  is allowed to vary according to the inputs, near the orifice the potential core may not have closed yet and  $\theta$  could approach infinity.  $x/H_{\min}$  in spreadsheet row 22 gives the lowest value for  $x/H$  that will yield a  $\theta_{\max}$  of one. In other words, a value of  $x/H$  less than  $x/H_{\min}$  will yield  $\theta$  values over one, which are not physically realistic. Note that the downstream distance should be downstream of the trailing edge of the last row of orifices ( $x/H > S_x/H + 0.5/(H/d)$ ). The user should ensure this in their input specification.

A protected section of this sheet also carries out most of the computation and is discussed in the Spreadsheet Structure section below. Calculations are performed based on the inputs to derive the nondimensional parameters for use in the program. The Excel workbook is protected except where user input is necessary. The spreadsheet may be customized by unprotecting it; however, the user would be well advised to customize a copy. The password for unprotecting the spreadsheet is "symmetry."

**Plot Sheet.**—The second sheet in the Excel workbook is labeled "Plots." This sheet provides the output as determined from the user-defined input variables and the code subroutines.

The first plot (Theta Profile) displays the three-dimensional scalar profile for the input conditions. The profiles that are output have the dependent variable ( $\theta$  on the horizontal axis and the independent coordinate ( $y$ ) on the vertical axis). (Note that this is opposite to convention, where the dependent variable is customarily on the vertical axis). Even though Excel does not usually allow for three-dimensional plotting, this program is able to plot a virtual three-dimensional profile in which the transverse axis is created by shifting a series of two-dimensional profiles by a predetermined amount.

The axis scales may show values greater than one. This may be simply a function of the plotting method, although the empirical model can return  $\theta$  values greater than one. These are nonphysical results though; all physical  $\theta$  results should be between 0 and 1. (Also note that  $\theta$  will be equal to 0 unless at least one row of jets in section B is active or a nonuniform scalar distribution is specified in sections D and E.)

The second plot (Maximum and Minimum Scalar Profiles in Vertical Planes) generates two curves displaying the vertical scalar profiles in planes that have the maximum and minimum average  $\theta$  values. The spreadsheet selects, of all the profiles in  $y$ -theta planes, those with the

highest and lowest average  $\theta$ . These two profiles are plotted as “maximum” and “minimum.” The  $z$  location of the profiles does not matter; however, these profiles are usually for the planes through the orifice center (centerplane) and midway between orifices (midplane). (But note that if 4 orifices are displayed, so the actual  $\Delta z/S = 0.2$ , then the midplane will not be displayed if the centerplane is at the edge, and the centerplane will not be displayed if the midplane is at the edge.)

An animation macro, accessed by a button on the Plots sheet, allows the user to watch the development of the profiles with increasing downstream distance. To activate it simply press the Time Flow button (macros must be enabled). The user can set the initial and final  $x/H$  positions and the  $x/H$  increments. The macro may not be stoppable once the program is running so one must choose the boundaries and increment levels carefully.

**3-D Sheet.**—The reader will note that the profile plots generated by this spreadsheet can also be rendered as more conventional contour plots. Importing the data allows the user to generate both profile and contour plots using the same data. The final sheet labeled “3-D” is simply an array of the plotted data with three rows of data that provides the user a means to generate his/her own 3-D plots using a three-dimensional plotting program, such as Plot 3-D or Tecplot (Tecplot, Inc., Bellevue, WA).

Column A is the  $\theta$  distribution. Column B shows  $z/S$ , column C shows  $y/H$ .  $y/H$  increases by 0.01 from 0 to 1 over every 101 rows. After 101 rows,  $z/S$  increases by 0.1, from 0 to 2.0 (21 times). Note that 21 profiles are necessary because a nonuniform scalar distribution may be specified which does not assume symmetry in the span displayed. If the mainstream flow is uniform, or only varies as a function of  $y/H$ , then only the first 6  $\theta$  profiles will be different; e.g., if a display is chosen for 2 orifices with the centerplane at the edge (spreadsheet row 33), then profiles for  $z/S = 0 = 1 = 2$ ,  $0.1 = 0.9 = 1.1 = 1.9$ ,  $0.2 = 0.8 = 1.2 = 1.8$ ,  $0.3 = 0.7 = 1.3 = 0.7 = 1.3 = 1.7$ ,  $0.4 = 0.6 = 1.4 = 1.6$ , and  $0.5 = 1.5$ . Note also that  $\theta$  will be = 0 in column A unless at least one row of jets in section B is active or a nonuniform scalar distribution is specified in sections D and E.

### Spreadsheet Structure

The main empirical relations as published in reference 2 are calculated in columns A to F of rows 164 to 240 (columns H to M of rows 164 to 185 are conditions called from the option or check boxes). Most of the relations are straightforward; the  $\theta_c$ 's and  $y_c$ 's have 5 conditional statements: one for each of the five options in the boxes of section B.

Columns A to S of rows 241 to 2363 make the calculations needed to initiate the plots. Columns A to C hold the data one would use for a conventional three-dimensional plot, and these columns are reproduced in the three-dimensional sheet.

Columns D, E, G, and H calculate  $\theta$  for each possible active row: row 1, top; row 2, top; row 1, bottom; and row 2, bottom; respectively (column F reverses  $y/H$  to calculate the bottom hole configurations). If jets are opposed in-line, D and E (and/or G and H) calculate the resultant symmetrical distribution.

Column I plots the mainstream scalar configuration from the user input in section E. Unless user checks the nonuniform checkbox, this column returns all zeros.

Columns J, K, M, and N function to turn off the  $\theta$ 's of columns C, D, F, and G if “none” is selected in the option box of section B. Also, M and N turn off if part of the opposed in-line jets case.

Column L determines the values for the max/min plot by averaging values from the first ten rows in the  $z$ -direction and plotting the maximum average and the minimum average.

Column O calculates the final  $\theta$  values by combining jet rows 1 + 2, top + bottom, plus the mainstream  $\theta$  (columns H, J, K, M, and N). These are combined by an extension of the superposition formula, except for the case of in-line opposed jets, where the symmetry is called for that case Superposition is extended to any other jets and a nonuniform mainstream scalar.

Column P inverts the  $\theta$ 's for the Hot/Cold button. It also increases the  $\theta$  slightly for each increase in  $z$  by the  $x$ -perspective value in section D.

Column Q hides values of ‘covered’ lines to create the three-dimensional effect. It shows the value of the row with the highest value that was calculated most recently.

Column R shows the value which should be plotted from analyzing column Q. This is the value that is plotted on the  $x$ -axis.

Column S recreates the  $y/H$  values, by increasing the  $y$ -perspective value for each new line on the plot. This is the value plotted on the  $y$ -axis.

## View Options

**Plane of Symmetry.**—Different features may be apparent depending on whether the centerplane or midplane is at the edge in the oblique plot. As an example, compare the distribution in figure 5, with the midplane at the edge for  $J = 26.4$  and F:  $S/H = 0.5$ ,  $H/d = 5.66$ , with the distributions in figure 4, where the centerplane is at the edge.

**$\theta$  Definition.**—The flow also can appear quite different depending on the definition used for  $\theta$ . Profiles may be shown as either “cold” ( $\theta = (T_M - T)/(T_M - T_J)$ ), as in figure 5 where pure jet fluid would be  $\theta = 1$ , or as “hot” ( $\theta = (T - T_J)/(T_M - T_J)$ ), as in figure 6 where pure jet fluid would be  $\theta = 0$ , again with F:  $S/H = 0.5$ ,  $H/d = 5.66$ , and  $J = 26.4$ . In the “cold” distribution, the numerator is the difference between the local and the undisturbed mainstream, and the jet flow appears as peaks in the distribution. However, for the “hot”  $\theta$  distribution (i.e.,  $1 - \theta_{\text{cold}}$ ), the numerator is the local difference from the jets, wherein the fluid originating from the jets causes depressions in the  $\theta$  distribution. “Cold” distributions will be shown in this report unless noted otherwise.

**Injection location.**—As shown in figure 7, profiles for bottom wall injection of the jets can be created. This figure provides an additional view of “cold”  $\theta$  profiles for F:  $S/H = 0.5$ ,  $H/d = 5.66$ , and  $J = 26.4$ . As in figure 5, the profiles shown in figure 7 have the midplane at the edge. Note that even if the top-front row is inactive, the jet spacing must be entered there and then the user must check the bottom rows to be sure the values there are the desired ones.

## The Effects of Flow Conditions and Geometry

Figures 8 to 23 show example variations in  $\theta$  profiles as a function of the several independent flow and geometric variables. (Important or common dependent variables are often shown in

parentheses.) The profile plots were created with the spreadsheet, and are formatted as in references 12 and 17 to facilitate comparisons. The corresponding figure numbers from these references are given in table 2. The spreadsheet is functionally equivalent to the Apple// program used in NASA TM–87294 reference 17. The trajectory equation used in NASA TM–83457 reference 12 gives slightly different results for some cases. The spreadsheet was modified to duplicate the results in reference 12. These results are shown in figures 24 to 26. In figures 8 to 14 and 24 to 26 the centerplane (i.e., the plane through the center of an orifice) is at the edge in the profile plots, and in figures 15 to 23 the midplane (i.e., the vertical plane midway between adjacent orifices) is at the edge.

### “Basic” Effects of a Confined JIC

**Downstream Distance ( $x/H$ ).**—Figure 8 shows the variation in scalar distributions with downstream distance; the locations shown are  $x/H = 0.25, 0.5, 1.0,$  and  $2.0$ , with the centerplane at the edge in the profile plots (as in fig. 4). In figure 8(a) the orifice configuration is C in figure 3 ( $S/H = 0.25, H/d = 8$ ), with  $J = 26.4$ ; and in figure 8(b) it’s I ( $S/H = 1, H/d = 4$ ), also with  $J = 26.4$ . In figure 8, the momentum-flux ratio ( $J$ ) and the ratio of cross sectional area to orifice area ( $= (4/\pi)(S/H)(H/d)^2$ ), and hence the jet to mainstream mass-flow ratio ( $MR$ ), are constant. Thus, the range of distributions from under-penetration in part (a) to over-penetration in part (b) results entirely from variation in orifice size end spacing at a fixed operating condition and total orifice area. Profiles for the optimum configuration for this condition are show in figure 4.

**Momentum-flux Ratio ( $J$ ).**—Figure 9 shows the increase in jet penetration that occurs with increasing  $J$  for orifice configuration F:  $S/H = 0.5$  and  $H/d = 5.66$  (see fig. 3). These profiles are at a downstream distance equal to one-half of the duct height ( $x/H = 0.5$ ), although the downstream distance that is shown is arbitrary and the same trends would be apparent for different  $x/H$  values. As expected, the jet penetration increases with increasing  $J$ . Since the orifice geometry is constant in this figure, the jet-to-mainstream mass-flow ratio increases with momentum-flux ratio from left to right across the row. Note that the jets are underpenetrating on the left, and overpenetrating on the right.

**Density Ratio ( $DR$ ).**—The effect of increasing  $DR$  at constant  $J$  can be seen in figure 10 where there is minimal change due to variations in the density ratio. In the figure, the density ratio varies from 0.5 to 2 at a momentum-flux ratio ( $J$ ) of 26.4 at a downstream distance of  $x/H = 0.5$  for the same orifice geometry (F:  $S/H = 0.5$  and  $H/d = 5.66$ ) shown in figure 4. Note that the magnitude of  $\theta$  increases slightly as the jet-to-mainstream mass-flow ratio increases. Other than this, there is little difference between hot-jets-in-a-cold-mainstream and cold-jets-in-a-hot-mainstream at a constant momentum-flux ratio.

Analyses of the experimental data in reference 5 suggested that the effect of varying the density ratio ( $DR$ ) had a minor effect for flows with a constant momentum-flux ratio ( $J$ ). This is shown in reference 2 too. The similarity in the distributions at constant  $J$  is in contrast to the experimental observations of (1) increased penetration with increasing  $DR$  at constant  $R (= \text{sqrt}(J/DR))$ , and (2) decreased penetration with increasing  $DR$  at constant  $M (= \text{sqrt}(J*DR))$  that are shown in figures 17 and 18 in reference 2.

**Orifice Spacing ( $S/H$ ).**—Figure 11 shows the effect on the profiles of decreasing the lateral spacing between orifices for configurations E ( $S/H = 1$ ), D ( $S/H = 0.5$ ), and C ( $S/H = 0.25$ ) at a downstream distance equal to one-half of the duct height. ( $x/H = 0.5$ ). Note that the lateral uniformity of the profiles increases as the orifice spacing decreases, but the penetration decreases as a result of the confinement. Note also that the jet-to-mainstream mass-flow ratio increases as the spacing decreases, since the orifice size is constant ( $H/d = 8$  in all cases). Thus, figure 11 shows that jet penetration increases as orifice spacing ( $S/H$ ) increases (actually penetration decreases as spacing decreases), because the maximum penetration for a given  $J$  will occur for an unconfined JIC).

**Orifice Size at Constant  $S/d$ .**—Figure 12 shows the increased jet penetration, and increased lateral nonuniformity that result from increasing the orifice size with the orifice spacing-to-diameter ratio ( $S/d$ ) held constant. Note that as orifice size increases ( $H/d$  decreases), the orifice spacing ( $S/H$ ) must increase to maintain a constant  $S/d$  since  $S/d = (S/H)*(H/d)$ . In the left column  $S/H = 0.125$  and  $H/d = 16$  (configuration A); in the middle column  $S/H = 0.25$  and  $H/d = 8$  (C); and in the right column  $S/H = 0.5$  and  $H/d = 4$  (F). Note that since these profiles are at a constant downstream distance ( $x/H = 0.5$ ), the dimensionless downstream distance expressed in terms of the orifice size ( $x/d$ ) varies in proportion to  $H/d$  ( $x/d = (x/H)*(H/d)$ ), so  $x/d = 8$  in the leftmost figure,  $x/d = 4$  in the center, and  $x/d = 2$  in the right figure. Jet penetration increases as orifice size increases at constant  $S/d$ . The reader should also note that the lateral nonuniformity increases as  $H/d$  decreases, and  $x/d$  decreases.

**Orifice Size at Constant  $S/H$ .**—In contrast to the profile variations seen in figure 12 for  $S/d = 2$ , the profiles in figure 13 for  $S/H = 0.5$  ( $S/d = (S/H)(H/d)$  varies) remain similar when the orifice diameter increases ( $H/d$  decreases) at a constant  $S/H$ . The profiles in parts (a) and (b) are at downstream distances equal to one-half and two duct heights respectively. The orifice diameter doubles as  $H/d$  is varied from 8 to 4, resulting in a four-fold increase in the ratio of the jet-to-mainstream mass flow. The result is that the distributions are shifted to higher  $\theta$  values, consistent with the larger jet flow, but the shape of the distributions remains similar. Since  $x/d = (x/H)(H/d)$ ,  $x/d$  decreases from 4 to 2 as  $H/d$  decreases from 8 to 4

**Coupled Orifice Spacing ( $S/H$ ) and Momentum-flux Ratio ( $J$ ).**—Analysis of the experimental data in references 5 and 11 suggested a coupling between the momentum-flux ratio ( $J$ ) and the orifice spacing ( $S/H$ ), and led to the conclusion that for a given momentum-flux ratio there exists an orifice spacing for which the most efficient mixing occurs, independent of orifice size. (Conversely, for a given orifice spacing ( $S/H$ ) there is a  $J$  for which the most efficient mixing occurs.) This relationship can be stated as

$$C = (S/H)(\text{sqrt}(J)) \quad (2)$$

$C$  can be useful in characterizing the jet penetration. For one sided injection, optimum mixing was found to occur when  $C$  is  $\sim 2.5$ . Under-penetration is expected if  $C$  is approximately half of the optimum value, and over-penetration is expected when  $C$  is  $\sim$  double the optimum value.

The profiles shown in figure 14 represent optimum mixing conditions ( $C = 2.57$ ), and show the profiles which result at different momentum-flux ratios ( $J$  increases from left to right), when the orifice spacing is adjusted according to the relation in equation (2). (For  $J = 6.6$ ,  $S/H = 1$

{e.g., configuration I}; for  $J = 26.4$ ,  $S/H = 0.5$  {e.g., F}; and for  $J = 105.6$ ,  $S/H = 0.25$  {e.g., B}.) The profiles in parts (a) and (b) are at downstream distances equal to one-half and two duct heights respectively. Clearly, similar distributions are obtained over a range of momentum-flux ratios if  $J$  and  $S/H$  are correctly coupled. Here, the mass-flow ratio is constant, since the orifice size decreases as  $J$  increases.

Note that the lateral uniformity increases as  $J$  increases. It is evident that flows with smaller momentum-flux ratios (larger spacing) need greater downstream distances to achieve equivalent mixing. Also, the reader should note that the optimum mixer at a given  $J$  may appear to give worse mixing than a nonoptimum mixer at a higher momentum-flux ratio. ( $J$  will increase as the orifice  $\Delta P$  is increased for a constant mainstream condition. Increasing  $J$  will usually promote better mixing, but often at the “cost” of a higher  $\Delta P$ .) Thus one should always examine the anticipated distributions and not base a configuration selection solely on a “mixing parameter.”

As can be seen from equation (2), and inferred from perusing figures 9 and 11, there is usually a trade-off between momentum-flux ratio ( $J$ ) and orifice spacing ( $S/H$ ), but note that, for example, the top left figure in figure 9 and the bottom one in figure 11 have significant differences in lateral uniformity but they have similar  $C$  values ( $C = 1.28$ ), and very similar penetration.

### Effects Typical of JICs in Gas Turbine Combustors

**Nonuniform Mainstream Scalar Distribution.**—The influence of a nonuniform mainstream flow on the profiles is expected to be significant. The effect of nonuniform velocity is unknown; however, the effect of a nonuniform mainstream scalar distribution is included in the empirical model through superposition; the results can be seen by examining figure 15.

In part (a), underpenetrating jets were chosen to fill in a deficit in the mainstream scalar distribution near the injection wall ( $J = 6.6$  and configuration F:  $S/H = 0.5$ ,  $H/d = 5.66$ ;  $J = 26.4$  and configuration C:  $S/H = 25$ ,  $H/d = 8$ —both cases with  $C = 1.28$ ); in part (b), the jets were positioned to fill a center deficit in the mainstream scalar distribution ( $J = 6.6$  and configuration I:  $S/H = 1$ ,  $H/d = 4$ ;  $J = 26.4$  and configuration F:  $S/H = 0.5$ ,  $H/d = 5.66$ ;  $J = 105.6$  and configuration C:  $S/H = 25$ ,  $H/d = 8$ —all cases with  $C = 2.57$ ); and in part (c), over penetrating jets were chosen for a mainstream which had a scalar deficit adjacent to the opposite wall ( $J = 26.4$  and configuration I:  $S/H = 1$ ,  $H/d = 4$ ;  $J = 105.6$  and configuration F:  $S/H = 0.5$ ,  $H/d = 5.66$ —both cases with  $C = 5.14$ ). (Orifice configurations are shown in fig. 3.)

The mainstream  $\theta$  profiles look piecewise linear in reference 2, but are sinusoidal in reference 17. The  $\theta$  profiles that are both easy to specify and give results that are reasonably similar to those in figure 11 in reference 17 result from specifying a parabolic  $\theta$  between the walls in (a) and (c) with  $\theta$  from 0 to 0.5; for (b)  $\theta$  varies from 0.25 to 0.5 on both sides of  $y = 0.5$ .

The composite empirical profiles were obtained by superimposing the upstream profile and the corresponding profile for jets in a uniform mainstream according to the following equation:

$$\theta = [\theta_1 + \theta_2 - (2)(\theta_1\theta_2)]/[1 - \theta_1\theta_2] \quad (3)$$

Note that here  $\theta_1$  is the mainstream distribution and  $\theta_2$  is the distribution for jets in a uniform mainstream. Note that for a uniform mainstream,  $\theta_1 = 0$  and  $\theta = \theta_2$ . Superposition gives a good approximation to the experimental data, but it must be realized that this is only an approximation, since there can be cross-stream transport due to the flow of mainstream fluid

over and around the jets (and to different y locations), and this is not accounted for in superimposing the distributions.

Equation 3 is extended as necessary if more than two  $\theta$ 's are needed by beginning with equation 3 for two  $\theta$ 's, and inserting equation (3) again for  $\theta_2$  and so on. E.g., there would be five  $\theta$ 's for double rows of opposed, staggered jets with a nonuniform mainstream scalar distribution. (Superposition is not used herein for opposed rows of in-line jets.)

**Flow Area Convergence.**—Converging ducts are assumed to converge symmetrically with convergence commencing at the center of the upstream orifices ( $x/H = 0$ ), according to the following.

$$H(x)/H = 1 - (dH/dx)(x/H) \quad (4)$$

Figure 16 shows the effect of flow area convergence on the scalar profiles for  $J = 26.4$  and orifice geometry  $H$  in figure 3 ( $S/H = 0.5$ ,  $H/d = 4$ ). In parts (a) and (b) the duct converges to  $1/2$  of the injection plane height in a downstream distance equal to twice and 1 times the injection plane height respectively (i.e.,  $dH/dx = 0.25$  and  $0.5$ ). These profiles show increasing jet penetration and slightly increased lateral nonuniformity with increasing convergence, and hence these profiles do not support the observation in Holdeman et al. reference 13 that convergence improves the mixing. Note that although the local duct height is becoming smaller, these profiles are scaled to the duct height at  $x/H = 0$  so the amount of convergence is not visually evident.

### **Noncircular Orifices.**

**Bluff and Streamlined Slots:** It was observed in Srinivasan et al. reference 15 that bluff slots resulted in slightly less jet penetration and more two-dimensional profiles than circular holes, and that streamlined slots resulted in slightly greater jet penetration and more three-dimensional profiles. This effect is modeled by using the actual ratio of the orifice spacing to the orifice lateral dimension,  $S/W$  or  $S/L$ , as appropriate, in lieu of  $S/d$  in the correlation equations in appendix C.  $H/d$  is not changed.

For slots that are rectangular orifices with semi-circular ends.

$$S/W = (S/d)[1 + (4/\pi)((L/W - 1))]^{0.5} \quad (5)$$

and

$$S/L = (S/W)/(L/W) = (S/d)[1 + (4/\pi)((L/W - 1))]^{0.5}/(L/W) \quad (6)$$

where  $L/W$  is the ratio of the long to short dimensions of the slot, and “d” is the diameter of a round orifice of equal area.

For a streamlined slot the long dimension of the slot ( $L$ ) is parallel to the mainstream flow and the short dimension ( $W$ ) is the actual lateral dimension. For bluff slots the long dimension of the slot is perpendicular to the mainstream flow and  $L$  is the actual lateral dimension of the slot. Note that  $L/W \geq 1$ , so  $S/W > S/d$  ( $W < d$ ) for a streamlined slot, and  $S/L < S/d$  ( $L > d$ ) for a bluff slot. If  $L/W = 1$  then the “slot” is a round hole, and  $S/L = S/W = S/d$ .

Dimensionless distributions are shown in figure 17 for jets issuing from orifice row configurations with bluff and streamlined slots of  $L/W$  equal to 2.8 at  $x/H = 0.25$ ,  $0.5$ , and  $1$ .

These configurations are shown in rows K and L in figure 3, and have the same orifice spacing,  $S/H$ , and open area as the circular holes in configuration H in figure 3:  $S/H = 0.5$ ,  $H/d = 4$ . The momentum-flux ratio,  $J$ , is 26.4. The jets from the bluff slots in figure 17(a) penetrate less and are more two-dimensional across the orifice centerplane compared to the circular holes, whereas the jets from streamlined slots, figure 17(b), are highly three-dimensional and have deeper penetration. At downstream locations both the slot configurations and circular holes produce very similar completely mixed distributions.

*Slanted Slots:* Two effects were noted in the experimental results for slanted slots, namely that the centerplanes shifted laterally with increasing downstream distance and the axes of the kidney-shaped scalar contours were inclined with respect to the injection direction. The distributions are assumed to be the same as those for a round hole of equal area, but are shifted according to the following.

$$\Delta(z/S) = (\sin[(\pi/2)(a)]) \quad (7)$$

where  $a = \min[1, (x/H_{eq})(J/26.4)^{0.25}]$  and the argument of the sine function is here expressed in radians.

Figure 18 shows profiles for the same slot as in figure 17, but oriented at  $45^\circ$  to the mainstream flow direction. The orifice configuration in figure 3 ( $M$ :  $S/H = 0.5$ ,  $H/d = 4$ ) has the same orifice spacing and area as the round holes in  $H$ , and the momentum-flux ratio,  $J$ , is 26.4. Although the first downstream station at  $x/H = 0.25$  seems to suggest that this is a centerplane plot [ ]--0--( ], figure 18 here is indeed a midplane plot [ -0--0- ] to be consistent with figure 17 and most of the other figures in the range 15 to 23 and indicates that a lateral shift equal to almost half the orifice spacing has occurred by  $x/H = 0.25$ . The profile plot at  $x/H = 1$  clearly shows the midplane at the edge, so it appears that the profiles have shifted a full orifice spacing by this location.

The empirical model profiles in figure 18 illustrate the observed shift, but the asymmetry and rotation of the distributions observed in the experimental data is not modeled (see e.g., fig. 13 in fig. 2). Note that figure 18 herein does not agree with figure 14 in reference 17; figure 18 in this report shows the expected profile shift, figure 14 in reference 17 does not.

### ***Opposed Rows of Jets.***

*Centerlines In-line:* The empirical model was used to calculate profiles for opposed rows of jets with their centerlines in-line, by assuming that the confining effect of an opposite wall is similar to that of a plane of symmetry between opposed jets.

The concept of an “equivalent” duct height was utilized by Cox reference 24 and later Wittig et al. reference 25 to allow empirical correlations from single side injection data to be applied to opposed jet injection. This is confirmed by the experimental results in Srinivasan et al. reference 14 also.

In general, flows of opposed rows of jets with centerlines in-line can be modeled by calculating an effective duct height as proposed in reference 25, namely;

$$[H_{eq}]_{top} = (H) \left( \frac{[(A_j/A_M)(J^{0.5})]_{top}}{[(A_j/A_M)(J^{0.5})]_{top} + [(A_j/A_M)(J^{0.5})]_{bottom}} \right) \quad (8)$$

and

$$[H_{eq}]_{bottom} = H - [H_{eq}]_{top}$$

Note that for the symmetric case (as shown here),  $J_{\text{top}} = J_{\text{bottom}}$  so  $H_{\text{eq}} = (H)/2$ . Note also that equation (8) does not contain the hole diameter,  $d$ , (other than its inclusion in  $A_J/A_M$ ). Alternative definitions were investigated in reference 26, but the one in equation (8) was verified by the experimental data. Results for single side and opposed jet injection at  $x/H = 0.5$  for  $H/d = 8$  is shown for both experimental data and the empirical model in reference 27.

Profiles for opposed jets with a momentum-flux ratio,  $J$ , of 6.6, for configuration D:  $S/H = 0.5$  and  $H/d = 8$ , are shown in figure 19(a) and profiles with a momentum-flux ratio,  $J$ , of 26.4 for configuration C:  $S/H = 0.25$  and  $H/d = 8$ , are shown in figure 19(b), both for downstream distances from  $x/H = 0.25$  to 1.5. The single side optimum with the same orifice area for  $J = 6.6$  is I:  $S/H = 1$ ,  $H/d = 4$  and for  $J = 26.4$  is H:  $S/H = .5$ ,  $H/d = 4$ . Note that the appropriate orifice spacing for opposed jets with centerlines in-line is half that for a single side injection case (see fig. 5).

The interested reader will note that there is no figure here comparable to figure 16 in reference 17 for opposed rows of jets with centerlines in-line but with different momentum-flux ratios on opposite walls. The figures from the spreadsheet look OK, but there would be a nonphysical discontinuity in  $\theta$  if  $\theta_{\text{min}}^+$  values from the top and bottom were not equal. The apparent “fix” would be to average the two  $\theta_{\text{min}}^+$ ’s, but it was not within the scope of the current effort to modify the correlations.

*Centerlines Staggered:* For opposed rows of jets of the same orifice spacing and diameter, but with their orifice centerlines staggered, the optimum ratio of orifice spacing to duct height is double the optimum value for single-side injection at the same momentum-flux ratio reference 17 thus every other orifice from the one-side optimum is moved to the opposite wall.

The result of implementing this relationship for  $J = 26.4$  with orifice configuration E:  $S/H = 1$ ,  $H/d = 8$ , and for  $J = 105.6$  with configuration D:  $S/H = 0.5$ ,  $H/d = 8$ , is shown in figure 20, parts (a) and (b) respectively. Note that because the orifice size is constant, there are twice as many orifices in the case shown in figure 20(b), and  $J$  is increased, the jet-to-mainstream mass-flow ratio for the case shown in figure 20(b) is 4 times that for the case shown figure 20(a).

The profiles in figure 20(a) may be compared to the corresponding profiles for one-side injection in figure 20(c) ( $J = 26.4$  and D:  $S/H = 0.5$ ,  $H/d = 8$ ). The z-span of the figure includes four orifices rather than two, and note that figure 20(c) shows a centerplane at the edge. Note also that  $C$  is  $\sim 2$  1/2 for the one-side injection shown in part (c), whereas for opposed/staggered jets  $C$  is  $\sim 5$  for both parts (a) and (b) in figure 20.

The specification for figure 17 in reference 17 appears to be incomplete.  $H/d = 4$  in 17(a) and 17(c) in reference 17, whereas  $H/d = 8$  in figures 20(a) and 20(c). Complete specifications for the cases in figure 20 are given therein and in table 2. Because the orifice size is different, figure 20 here is not identical to figure 17 in reference 17, but the conclusions are the same.

The superposition equation (3) is used for this case where  $\theta_1$  is the distribution from the top row of jets, and  $\theta_2$  is the distribution from the bottom row of jets. It was shown in reference 17 that the empirical model does not compare favorably with the data in this complex case as the individual jets are usually overpenetrating and these distributions are often not consistent with the Gaussian profile assumption in equation (1) and the superposition modeling (eq. (3)) that is appropriate for many of the single-side and opposed-jet cases of interest. In fact, over-penetration is usually desired for opposed rows of staggered jets as jets originating from one wall must pass those from the opposite wall.

**Double Rows of Jets.**—For double axial rows of holes, as shown in figures 21 to 23, the empirical calculations were obtained by superimposing separate calculations for the two rows. Again the superposition formula in equation (3) was used; this time  $\theta_1$  is the front row and  $\theta_2$  is the trailing row.

In this report  $x/H$  is always specified from the center of the front row; thus the reader must do some arithmetic to make comparisons with the double-row figures in reference 17, but the corresponding profiles are there. The calculated  $x/H$  planes should be no farther upstream than the trailing edge of the orifices in the farthest downstream row, i.e.,  $x/H$  must be larger than  $(S_x/H) + (1/(2(H/d)))|_{\text{row2}}$ .

**Centerlines In-line:** It was observed from the experimental profiles in references 2 and 18 that the single-and double-row configurations for in-line rows of round jets have very similar distributions, as can be seen by comparing the profiles in figure 21 with the results from the single row of equally spaced and equal area round holes.

Figure 21 shows dimensionless scalar distributions for an orifice configuration with two in-line rows of round jets for three different values of the axial spacing between the rows. Profiles are shown at downstream distances equal to 0, 25, 0.5, 1, and 1.5 duct height from the location midway between the rows for  $S_x/H = 0, 0.5, \text{ and } 1$ . (Note that  $S_x/H = 0$  is a nonphysical case; the two rows of in-line orifices are co-located.) Both rows shown in figure 21 are identical (F:  $S/H = 0.5, H/d = 5.66$ ). These profiles may be compared with a single row of jets from equally spaced and equally sized holes in figure 5 and profiles for an equally spaced and equal-area round holes (H:  $S/H = 0.5, H/d = 4$ ; shown in the lower right profile distributions in fig. 13).

The  $x/H$  for each active row is from the center of the top, front row, and  $S_x/H$  is the axial distance between the centers of the front and back rows. Thus to get an  $x/H$  from midway between the rows, as in figure 18 in reference 17, the  $x/H$  for row 1 needs to be specified as the desired overall  $x/H + (S_x/H)/2$  and the  $x/H$  for row 2 needs to be specified as the desired  $x/H - (S_x/H)/2$ .

**Staggered Orifices:** Figure 22 shows dimensionless scalar profiles for a double-row configuration where the trailing row is staggered with respect to the lead row (both rows are configuration I:  $S/H = 1, H/d = 4$ ). In each row in the figure, profiles are given at distances equal to 0, 25, 0.5, 1, and 1.5 duct height downstream from the center of the trailing row of holes for  $S_x/H = 0, 0.5, \text{ and } 1$ . For the cases in figure 19 in reference 17, one needs to specify  $x/H$  for row 1 as the desired  $x/H$  from the center of the trailing row  $+ S_x/H$ .

Overpenetration is evident for both rows at all  $S_x/H$  values in parts (a) and (c) in figure 22, as would be expected as  $C = 5.14$  for both rows, and there is no influence between the rows in the superposition formula used in the model. Note that for  $S_x/H = 0$  this distribution should be the same as the bottom row in H:  $S/H = 0.5, H/d = 4$  (shown in the lower right profile distributions in fig. 13), but it is not.

The distribution shown in figure 20(c) is similar but the orifice diameter is smaller than that in figure 22(a). Note also that the centerplane is at the edge in figures 13, 20(c), and 22(a), but figures 22(a) and 20(c) are 4-hole distributions whereas figure 13 shows 2-holes.

Note that the empirical model does not extrapolate properly as the offset goes to zero. The increased penetration in figure 22(a) is not surprising since the interaction of adjacent jets is very

important and the independent calculation of each row in figure 22(a) does not consider the confining effect of the closest jets.

*Different Number of Orifices:* Scalar profiles are shown in figure 23 for a double-row configuration where the trailing row has twice as many orifices as the leading row, but with equal orifice areas in each row (Row 1 = F:  $S/H = 0.5$ ,  $H/d = 5.66$ ; row 2 = C:  $S/H = 0.25$ ,  $H/d = 8$ ). ( $X/d$  is intentionally not given in fig. 23 as  $d$  is different in rows 1 and 2 and thus an “overall”  $x/d$  would be ambiguous.)

In part (a), the momentum-flux ratio is the same,  $J = 26.4$ , for both rows, but it is optimum only for the lead row. The under-penetration of the trailing row is evident even at the farthest downstream location. In figure 23(b), the momentum-flux ratio of the lead row is increased to  $J = 105.6$  resulting in over-penetration of these jets, but this is compensated for by the under-penetration of the trailing row jets and a well mixed distribution is approached with increasing distance downstream.

In figure 23(c), the momentum-flux ratios of the leading and trailing rows are switched with the same orifice configuration so that both rows have the optimum combination of spacing ( $S/H$ ) and momentum-flux ratio ( $J$ ). This yields a well-mixed profile, as expected. The profiles in figures 23(b) and (c) are different, but both of them will decay to a well-mixed distribution. The designer’s choice would depend on the application.

The result shown here in figure 23(c) is almost the same as in figure 20(c) in reference 17, but the results are not identical. Just changing  $J$  is much easier than changing spacing, hole size, and switching 2-holers and 4-holers, but the distributions are slightly different because the  $x/H$  for the higher and lower  $J$  rows are slightly different.

### Comparison of Results from Correlations used in Previous Publications

In duplicating and verifying the figures in 12 with the spreadsheet, it was noted that the jet scalar trajectory equation was changed between publication of 12 and 17 to give a better fit to the data in references 11, 14, and 15.

The term that was changed was  $0.539 = >0.3575(a1)$  where  $a1 = \min [(1 + S/H), 2]$ . The trajectories are almost identical for  $S/H \sim 0.5$ . Differences exist both for  $S/H < 0.5$  and  $S/H > 0.5$ , but are most apparent when  $S/H \sim 1$ . ( $S/H > 1$  was never investigated, and it is unlikely that the lateral spread of a confined JIC would be greater than its vertical penetration and spread.)

Note also that, although the term wasn’t changed, if  $C = (S/H)(J)^{0.5} > 3.5$  in “ $\exp(-b)$ ”, where  $b = (0.091)(x/H)^2 [1 - (S/H)(J)^{0.5}/3.5]/(S/H)$ , then “ $-b$ ” becomes positive, and this term results in an increase in the trajectory. This can cause a trajectory “growth” that was not observed experimentally, so when input values are outside the range of the experiments they are flagged in the spreadsheet, and it is suggested that they be examined carefully.

An example of the different results obtained with the trajectory correlation used in reference 12 is given in figure 24(a) and (b) which show profiles respectively with  $C = 1.28$  ( $J = 26.4$  and configuration C:  $S/H = 0.25$ ,  $H/d = 8$ ), and  $C = 5.14$  ( $J = 26.4$  and I:  $S/H = 1$ ,  $H/d = 4$ ) calculated with the equations used in reference 12. These are the same conditions as used previously in figure 8. Other figures for which a change is apparent are figures 11 and 14.

Figure 25 shows calculations for the profile variation with decreased orifice spacing at constant orifice size using the equations used in 12. The conditions here are the same as shown previously in figure 11. Note that the figure in the left column of figure 11 ( $S/H = 1$ ) shows

greater jet penetration than for the equation used in figure 25 and the jet penetration in the right column in figures 11 ( $S/H = 0.25$ ) is slightly less than for the equation used in figure 25.

Figure 26(a) and (b) show calculations at  $x/H = 0.5$  and  $x/H = 2$  for the profile variation with coupled orifice spacing and momentum-flux ratio using the equations used in reference 12. These are the same conditions as shown previously in figure 14(a) and (b). Note that the figures in the left columns of figures 14 and 26 for  $S/H = 1$  show greater jet penetration for the equations used in figure 14, but note also that the lateral variation is much greater for the larger spacing and smaller momentum-flux ratio in both figures. Although it is not so apparent, note also that the figures in the right column of figures 14 and 26 for  $S/H = 0.25$  show less jet penetration for the equation used in figure 14.

## Design Procedures

The calculated results shown here suggest that, for a given momentum-flux ratio, the design procedure should first identify the orifice spacing and total orifice area needed to obtain the desired jet penetration and profile shape. The orifice size should then be chosen to provide the desired jet-to-mainstream mass-flow ratio. Some adjustments might be needed to arrive at a final configuration, because pressure drop and orifice geometry must be monitored to ensure that the suggested configuration is physically realistic. Also, it should be noted that since jet penetration usually varies with axial distance, one must consider both ‘what’ and ‘where’ in the optimization.

Thus, the suggested procedure is.

- Determine given momentum-flux ratio
- Select orifice spacing for desired jet penetration
- Calculate total orifice area needed for desired mass-flow ratio
- Calculate individual orifice size
- Determine blockage, fit, etc. and make sure the specified case is “physical”
- Iterate to solution if necessary

The interested reader will note that this procedure is different from the Cranfield Design Method described in reference 28 which emphasizes the size of individual orifices.

## Conclusions

An interactive computer code, written with an MS Excel spreadsheet is presented which displays three-dimensional oblique plots of the distributions of a conserved scalar downstream of mixing with a confined crossflow, for either single-side or opposed jet injection.

Profiles calculated with the Excel JIC spreadsheet are presented to show the effects of flow and geometric variables on the mixing. These are shown by the profiles in figures 4 to 23, and confirm the conclusions reached previously from examination of the experimental data. Unless multiple downstream distances are shown in the figures,  $x/H$  is assumed constant in the following conclusions.

1. Mixing improves with downstream distance (see figs. 4 to 8).
2. Momentum-flux ratio ( $J$ ) is the most significant flow variable (see fig. 9).
3. The effect of density ratio ( $DR$ ) is small if the momentum-flux ratio ( $J$ ) is constant. (See fig. 10; note that  $J = ((R)^2 * DR) = ((M)^2 / DR)$  so that  $R$  must decrease as  $DR$  increases, and  $M$  must increase as  $DR$  increases, if  $J$  is to be held constant.)
4. Decreasing spacing at constant orifice diameter ( $H/d$ ) reduces penetration and increases lateral uniformity. (See fig. 11; note that  $x/d$  is also constant when  $H/d$  and  $x/H$  are constant.)
5. Increasing orifice diameter at a constant ratio of spacing to orifice diameter ( $S/d$ ) increases penetration but also increases lateral nonuniformity. (See fig. 12; note that  $x/d$  decreases at a fixed  $x/H$  when  $H/d$  decreases.)
6. Increasing orifice diameter at a constant ratio of spacing to duct height ( $S/H$ ) increases the magnitude of the scalar difference, but jet penetration and profile shape remain similar. (See fig. 13; note that  $x/d$  decreases because  $H/d$  decreases.)
7. Similar distributions may be obtained over a range of momentum-flux ratios, independent of orifice diameter, if orifice spacing and momentum-flux ratio are coupled. (See fig. 14; note that  $x/d$  increases at constant  $x/H$  when  $H/d$  increases.)
8. Smaller momentum-flux ratios = > larger orifice spacing and require a greater distance for equivalent mixing (see fig. 14).
9. The mixing of jets with flows that have a nonuniform scalar mainstream distribution can be approximated by superimposing the jets-in-a-uniform-mainstream and upstream profiles (see fig. 15).
10. Flow area convergence results in slightly increased jet penetration and cross-stream mixing, but the lateral profiles are less uniform than for the straight duct case (see fig. 16).
11. For jets from noncircular orifices that are symmetric with respect to the main flow direction, the effects of shape are most significant in the region close to the injection plane, but farther downstream both streamlined and bluff slot geometries yield well mixed distributions similar to those from equally-spaced, equivalent-area circular holes (see fig. 17).
12. Profiles for jets from 45° slanted slots rotate and shift laterally ( $z$ ) as a function of momentum-flux ratio and downstream distance. The lateral shift is included in the empirical model; but the rotation is not (see fig. 18).
13. The empirical model may be used to calculate profiles for opposed rows of jets with their centerlines in-line, by assuming that the confining effect of a plane of symmetry between opposed jets is similar to that of an opposite wall. For this case, the optimum ratio of orifice spacing to duct height is one-half of the optimum value for single-side injection at the same momentum-flux ratio (see fig. 19).
14. For opposed rows of jets, with the orifice centerlines staggered, the optimum ratio of orifice spacing to duct height is double the optimum value for single-side injection at the same momentum-flux ratio (see fig. 20).
15. At the same momentum-flux ratio, and with the same orifice spacing, double rows of in-line jets have profile distributions similar to those from a single row of equally-spaced, equivalent-area circular orifices (see fig. 21).
16. Superimposing independent calculations of the two rows may be used to calculate flow for jets from double (axially-staged) rows with orifices staggered, but caution should be exercised using this model for very small offsets between the rows as there is significant interaction between adjacent jets that is not considered (see fig. 22).

17. Superimposing independent calculations of the two rows is used to approximate jets from double rows of orifices of different size and spacing (see fig. 23).

The spreadsheet used herein is capable of calculating flowfields which are physically unrealistic, and/or represent large extrapolations from the test conditions in the data base on which the model is based. These conditions are flagged in the program with warnings, but, of course, the user must always exercise judgment in using this or any other analytical tool.

## Appendix A

### Listing of Applesoft BASIC program used in Reference 17: Part I

```

5 PRINT CHR$(4)"MAXFILES 1"
10 HI = PEEK (115) + 256 * PEEK (116) - 642: HIMEM: HI
20 IF PEEK (104) < > 64 THEN POKE 104,64: POKE 16384,0:: POKE
115,HI / 256 - INT (HI / 256): POKE 116, INT (HI / 256): PRINT
"RELOAD FILES2.1A": PRINT CHR$(4)"RUN FILES2.1A"
30 PRINT CHR$(4)"BLOAD SHPS,A"HI + 1: POKE 233, INT ((HI + 1) /
256): POKE 232,HI + 1 - INT ((HI + 1) / 256) * 256
31 IF FL = 1 THEN 500
32 DIM T%(100,25),CM%(148),SD(4),H(4),HD(4),CD(4),DR(4),J(4),MR(4),TB(4),
WN(4),WP(4),YC(4),TC(4),TP(4),TN(4):NN = 1
33 DIM TE%(100,25),X(4),XH(4),A1(4),A2(4),A3(4),A4(4),A5(4),C0(4),AX(4),
SH(4)
34 DIM T$(4),P$(4),E$(4),MS%(100): PRINT FRE (0)
500 PI = 3.1415926:CO = - LOG (2):W$ = CHR$(14):D$ = CHR$(4):
ROT= 0: SCALE= 1: PRINT D$"OPEN PARAM1": PRINT D$"READ PARAM1": INPUT
P$,T$,E$,CD$,DR$,J$,SD$,H$,X$: PRINT D$"CLOSE PARAM1"
501 NN = 1:T$(NN) = T$:P$(NN) = P$:E$(NN) = E$:AX(NN) = 1
502 CD(NN) = VAL (CD$):DR(NN) = VAL (DR$):J(NN) = VAL (J$):SD(NN)
= VAL (SD$):H(NN) = VAL (H$):X(NN) = VAL (X$):XH(NN) = X(NN)
503 PRINT D$"OPEN PARAM2": PRINT D$"READ PARAM2": INPUT
P$,T$,E$,CD$,DR$,J$,SD$,H$,X$: PRINT D$"CLOSE PARAM2"
504 NN = 2:T$(NN) = T$:P$(NN) = P$:E$(NN) = E$:AX(NN) = 1
505 CD(NN) = VAL (CD$):DR(NN) = VAL (DR$):J(NN) = VAL (J$):SD(NN)
= VAL (SD$):H(NN) = VAL (H$):X(NN) = VAL (X$):XH(NN) = X(NN)
506 NN = 1
510 TEXT : HOME : PRINT : PRINT TAB( 5)"Dilution Jet Mixing
PROFILES v2.1": PRINT : PRINT TAB( 3)"Type new value & <Return> to
change;": PRINT "<Return> alone to accept default entry;"
520 PRINT TAB( 6)"or <Tab> & <Return> to restart": POKE 34,7
521 HOME : VTAB 9
522 PRINT W$;"View Parameters:": PRINT " _____ "
523 DV$ = "S": PRINT : PRINT "S)ingle or D)ouble rows (axial &
opposed/staggered), or O)pposed/in-line ";: INPUT DU$: IF DU$ < > ""
THEN DV$ = DU$
524 PRINT : PRINT W$;"Jets: <T>op; <B>ottom; or opposed <T&B> ?
";T$(NN);: INPUT "":DU$: IF DU$ < > "" THEN T$(NN) = DU$: IF DU$ =
CHR$( 9) THEN 510
525 IF DV$ = "S" THEN MR(2) = 0
526 PRINT : PRINT "<C>enterplane or <M>idplane at edge? "P$(NN);:
INPUT "":DU$: IF DU$ < > "" THEN P$(NN) = DU$: IF DU$ = CHR$( 9)
THEN 510
527 SP$(NN) = "2": PRINT : PRINT W$;"Profile span (# of orifices)
";SP$(NN);: INPUT DU$: IF DU$ < > "" THEN SP$(NN) = DU$: IF DU$ =
CHR$( 9) THEN 510
528 PRINT : PRINT W$;"<H>ot or <C>old Theta? ";E$(NN);: INPUT
"":DU$: IF DU$ < > "" THEN E$(NN) = DU$: IF DU$ = CHR$( 9) THEN 510
530 HOME : VTAB 9
540 PRINT W$;"Flow & Orifice Parameters:": PRINT
" _____ ": PRINT : PRINT W$; TAB( 10)"CD=";CD(NN)
550 PRINT W$; TAB( 10)"DR=";: PRINT DR(NN)
560 PRINT W$; TAB( 10)"J=";: PRINT J(NN)
570 PRINT : PRINT TAB( 10);"H0/D=";: PRINT H(NN)
580 PRINT TAB( 10);"S/H0=";: PRINT SD(NN)

```

```

590 PRINT TAB( 10)"X/H0=";: PRINT X(NN)
600 PRINT : INPUT " ok? ";FP$:FP$ = LEFT$(FP$,1): IF FP$
= "N" THEN 610
601 IF FP$ = CHR$( 9) THEN 510
602 IF NN = 1 AND (DV$ = "D" OR T$(1) = "T&B" AND T$(2) = T$(1))
THEN NN = 2: GOTO 510
603 IF DV$ = "S" THEN SP$(2) = SP$(1):T$(2) = T$(1):P$(2) =
P$(1):E$(2) = E$(1):DR(2) = DR(1):CD(2) = CD(1):J(2) = J(1):SD(2) =
SD(1):H(2) = H(1):X(2) = X(1)
604 SD(1) = SD(1) * H(1):SD(2) = SD(2) * H(2):HD(1) = H(1):HD(2) =
H(2):HT = HD(1):XH(1) = X(1):XH(2) = X(2)
605 AR(1) = CD(1) * PI / 4 / SD(1) / HD(1):AR(2) = CD(2) * PI / 4 /
SD(2) / HD(2)
606 MR(1) = SQR (DR(1) * J(1)) * AR(1):MR(2) = SQR (DR(2) * J(2))
* AR(2):HS = 1: IF T$(1) = "T&B" THEN HS = AR(1) * SQR (J(1)) /
(AR(1) * SQR (J(1)) + AR(2) * SQR (J(2)))
607 IF T$(1) = "T&B" THEN HD(1) = HD(1) * HS:XH(1) = XH(1) / HS
608 IF T$(2) = "T&B" THEN HD(2) = HD(2) * (1 - HS):XH(2) = XH(2) / (1 - HS)
609 NN = 1: GOTO 661
610 VTAB 12: HTAB 20: INPUT CD$: IF CD$ < > "" THEN CD(NN) = VAL
(CD$): IF CD$ = CHR$( 9) THEN 530
620 VTAB 13: HTAB 20: INPUT DR$: IF DR$ < > "" THEN DR(NN) = VAL
(DR$): IF DR$ = CHR$( 9) THEN 530
630 VTAB 14: HTAB 20: INPUT J$: IF J$ < > "" THEN J(NN) = VAL
(J$): IF J$ = CHR$( 9) THEN 530
635 VTAB 16: HTAB 20: INPUT H$: IF H$ < > "" THEN H(NN) = VAL
(H$): IF H$ = CHR$( 0) THEN 530
640 VTAB 17: HTAB 20: INPUT SD$: IF SD$ < > "" THEN SD(NN) = VAL
(SD$): IF SD$ = CHR$( 9) THEN 530
650 VTAB 18: HTAB 20: INPUT XX$: IF XX$ < > "" THEN X(NN) = VAL
(XX$): IF XX$ = CHR$( 9) THEN 530
660 GOTO 600
661 HOME : INPUT "Axial offset = ";SX$:FC(NN) = 0:TA(NN) = 0:BA(NN)
= 0:XH(NN) = XH(NN) + VAL (SX$): IF SX$ = CHR$( 9) THEN 510
662 PRINT : PRINT "Flow area convergence ? (Y/N): ";: INPUT "":DU$:
IF DU$ = CHR$( 9) THEN 510
663 IF DU$ < > "Y" THEN 669
664 PRINT : PRINT " Convergence rate = ";: INPUT "":DU$:FC(NN) =
VAL (DU$): PRINT : PRINT " T)op, B)ottom, or S>ymmetric ? ";: INPUT
"":DU$: IF DU$ = "T" AND (T$(NN) = "T" OR T$(NN) = "T&B") THEN TA(NN)
= ATN (FC(NN)):BA(NN) = 0
665 IF DU$ = "B" AND (T$(NN) = "B" OR T$(NN) = "T&B") THEN BA(NN) =
ATN (FC(NN)):TA(NN) = 0
666 IF DU$ < > "T" AND DU$ < > "B" THEN TA(NN) = ATN (FC(NN) /
2):BA(NN) = TA(NN)
667 AX(NN) = 1 - FC(NN) * XH(NN): IF AX(NN) < = 0 THEN PRINT :
PRINT "EXIT <= 0": GOTO 662
668 J(NN) = J(NN) * (AX(NN) * COS (TA(NN))) ^ 2
669 IF NN = 2 THEN 680
670 PRINT : PRINT "Mainstream temperature:": PRINT : PRINT "
U)niform, C)ool top, or H)ot top ";MT$;:MT$ = "U": INPUT "":DU$: IF
DU$ < > "" THEN MT$ = DU$: IF DU$ = CHR$( 9) THEN 669
671 IF DU$ = "" THEN 680
672 IF MT$ < > "U" THEN PRINT " Maximum mainstream Theta = ";:
INPUT DU$:MT = VAL (DU$): IF DU$ = CHR$( 9) THEN 669
673 FOR L = 0 TO 100:YH = L / 100
674 MS%(L) = 0

```

```

675 IF MT$ = "C" THEN MS%(L) = (MT / 2 + MT / 2 * COS (YH * PI)) * 1000 +
    .5
676 IF MT$ = "H" THEN MS%(L) = (MT / 2 + MT / 2 * COS ((YH - 1) *
    PI)) * 10000 + .5
677 IF MT$ = "S" THEN MS%(L) = (MT - MT * SIN (YH * PI)) * 10000 + .5
678 NEXT
680 SL = 0:AR = 1:NC$(NN) = "N": PRINT : PRINT "Non-circular
    orifices? (Y/N) ";NC$;: INPUT ";DU$: IF DU$ < > "" THEN NC$ = DU$:
    IF NC$ = CHR$(9) THEN 510
681 IF NC$ < > "Y" THEN 700
683 PRINT : PRINT " Aspect ratio = ";: INPUT ";DU$: IF DU$ =
    CHR$(9) THEN 510
684 IF DU$ < > "" THEN AR = VAL (DU$): IF ABS (AR) < > 1 THEN 700
686 BE = SGN (AR) * XH(NN) / 2 * (J(NN) / 26.4) ^ .25: IF ABS
    (BE) > .5 THEN BE = SGN (BE) * .5
688 SL = - SIN (PI * BE) / 2
700 AR = ABS (AR): IF P$(NN) = "M" THEN SL = SL + .5
701 IF SL < 0 THEN SL = 1 + SL
710 IF NN = 1 AND T$(1) = "T&B" AND T$(2) = T$(1) THEN MR(1) =
    MR(1) + MR(2):MR(2) = MR(1)
718 T$ = T$(NN):P$ = P$(NN):E$ = E$(NN)
721 AG = 1 + 4 / PI * (AR - 1): IF AR < 1 THEN AG = 1 + 4 / PI *
    (1 / AR - 1)
722 SH(1) = SD(1) / HD(1):SH(2) = SD(2) / HD(2)
723 SD(NN) = SD(NN) * SQR (AG): IF AR > 1 THEN SD(NN) = SD(NN) / AR
724 AR = 1:TB(1) = MR(1) / (MR(1) + 1)
725 TB(2) = MR(2) / (MR(2) + 1)
732 WN(1) = .2 / AX(1) * J(1) ^ .15 * SD(1) ^ .27 * XH(1) ^ .12 /
    HD(1) ^ .38 * SQR (HT / HD(1)) * CD(1) ^ .055:WP(1) = .1623 / AX(1)
    * J(1) ^ .18 / SD(1) ^ .25 * SQR (XH(1)) * SQR (HT / HD(1)) * CD(1)
    ^ .125
733 WN(2) = .2 / AX(2) * J(2) ^ .15 * SD(2) ^ .27 * XH(2) ^ .12 /
    HD(2) ^ .38 * SQR (HT / HD(2)) * CD(2) ^ .055:WP(2) = .1623 / AX(2)
    * J(2) ^ .18 / SD(2) ^ .25 * SQR (XH(2)) * SQR (HT / HD(2)) * CD(2)
    ^ .125
737 A2(1) = 1 + SH(1):A2(2) = 1 + SH(2): IF DV$ = "D" AND (T$(1) =
    "T" AND T$(2) = "B" OR T$(1) = "B" AND T$(2) = "T") THEN A2(1) =
    1.506:A2(2) = 1.506
738 A1(2) = .3575 * A2(2): IF A2(2) > 2 THEN A1(2) = .715
739 A1(1) = .3575 * A2(1): IF A2(1) > 2 THEN A1(1) = .715
741 YC(2) = A1(2) / AX(2) * J(2) ^ .25 * SD(2) ^ .14 * HD(2) ^ -
    .45 * XH(2) ^ .17 * CD(2) ^ .155 * EXP ( - .091 * XH(2) * XH(2) * (1
    / SH(2) - SQR (J(2)) / 3.5))
742 YC(1) = A1(1) / AX(1) * J(1) ^ .25 * SD(1) ^ .14 * HD(1) ^ -
    .45 * XH(1) ^ .17 * CD(1) ^ .155 * EXP ( - .091 * XH(1) * XH(1) * (1
    / SH(1) - SQR (J(1)) / 3.5))
744 TC(1) = TB(1) + (1 - TB(1)) * (A2(1) / J(1) ^ .35 / XH(1) /
    HD(1) * CD(1) ^ .5) ^ (1.15 * SQR (SH(1) / (1 + SH(1))))
745 TC(2) = TB(2) + (1 - TB(2)) * (A2(2) / J(2) ^ .35 / XH(2) /
    HD(2) * CD(2) ^ .5) ^ (1.15 * SQR (SH(2) / (1 + SH(2))))
746 IF YC(1) < = 1 THEN 750
747 YC(1) = 1: PRINT : INVERSE : PRINT "NOTE:";: NORMAL
748 IF T$ = "T" OR T$ = "B" THEN PRINT "Trajectory at opposite
    wall": GOTO 750
749 PRINT " Trajectory at centerline"
750 IF YC(2) < = 1 THEN 785
760 YC(2) = 1: PRINT : INVERSE : PRINT "NOTE:";: NORMAL

```

```

770 IF T$ = "T" OR T$ = "B" OR T$ = "F" OR T$ = "R" THEN PRINT
    "Trajectory at opposite wall": GOTO 785
780 PRINT " Trajectory at centerline"
785 A3(1) = .038: IF YC(1) + WP(1) > = 1 THEN A3(1) = A3(1) * (HT /
    HD(1)) ^ 3.67: IF T$(1) = "T&B" THEN WP(1) = 1 - YC(1): IF WP(1) < =
    0 THEN WP(1) = .001
786 TP(1) = 1 - EXP ( - A3(1) * J(1) ^ 1.62 * SD(1) ^ 1.5 / HD(1) ^
    2.57 * XH(1) ^ 1.1 * CD(1) ^ .535)
787 A3(2) = .038: IF YC(2) + WP(2) > = 1 THEN A3(2) = A3(2) * (HT /
    HD(2)) ^ 3.67: IF T$(2) = "T&B" THEN WP(2) = 1 - YC(2): IF WP(2) < =
    0 THEN WP(2) = .001
788 TP(2) = 1 - EXP ( - A3(2) * J(2) ^ 1.62 * SD(2) ^ 1.5 / HD(2) ^
    2.57 * XH(2) ^ 1.1 * CD(2) ^ .535)
791 C0(2) = 1: IF YC(2) + WP(2) > 1 THEN C0(2) = C0(2) * EXP (.22 *
    XH(2) * XH(2) * ( SQR (J(2)) / 5 - SH(2)))
792 TN(2) = 1 - EXP ( - C0(2) / J(2) ^ .3 / SD(2) ^ 1.4 * XH(2) ^
    .9 * HD(2) ^ .9 * CD(2) ^ .25)
793 C0(1) = 1: IF YC(1) + WP(1) > 1 THEN C0(1) = C0(1) * EXP (.22 *
    XH(1) * XH(1) * ( SQR (J(1)) / 5 - SH(1)))
794 TN(1) = 1 - EXP ( - C0(1) / J(1) ^ .3 / SD(1) ^ 1.4 * XH(1) ^
    .9 * HD(1) ^ .9 * CD(1) ^ .25)
796 PF = 0:TM = TP(1): IF TN(1) < TM THEN TM = TN(1)
797 IF TP(2) < TM THEN TM = TP(2)
798 IF TN(2) < TM THEN TM = TN(2)
800 A4(1) = .227:A4(2) = .227: IF (T$(1) = "T" AND T$(2) = "B" OR
    T$(2) = "B" AND T$(1) = "T") AND DV$ = "D" THEN A4(1) = A4(1) *
    2:A4(2) = A4(2) * 2
801 A5(1) = .452:A5(2) = .452
802 G(1) = EXP ( - A4(1) * J(1) ^ .67 / SD(1) * XH(1) ^ .54 * HD(1)
    ^ .54 * CD(1) ^ .23):G(2) = EXP ( - A4(2) * J(2) ^ .67 / SD(2) *
    XH(2) ^ .54 * HD(2) ^ .54 * CD(2) ^ .23)
803 LI = 100:KI = 5:DK = .1
805 D(1) = EXP ( - A5(1) * J(1) ^ .53 / SD(1) ^ 1.53 * XH(1) ^ .83
    * HD(1) ^ .83 * CD(1) ^ .35)
806 D(2) = EXP ( - A5(2) * J(2) ^ .53 / SD(2) ^ 1.53 * XH(2) ^ .83
    * HD(2) ^ .83 * CD(2) ^ .35)
810 FOR K = 0 TO 2 * KI:ZS = K / KI / 2 * VAL (SP$(NN)) / 2
817 ZS = ZS + SL: IF ZS > = .5 AND ZS < 1 THEN ZS = 1 - ZS
818 IF ZS > = 1 AND ZS < 1.5 THEN ZS = ZS - 1
819 IF ZS > = 1.5 THEN ZS = 2 - ZS: IF ZS > 2 THEN PRINT ZS: END
820 ZF = 4 * ZS * ZS:YK = YC(NN) * (1 - ZF * G(NN)):TK = TC(NN) * (1
    - ZF * D(NN)):TF = (TB(NN) - TM * TK) / (1 - TB(NN)): IF TF > PF THEN
    PF = TF
822 WP = WP(NN)
823 TS = TP(NN)
824 IF T$ < > "T&B" THEN 830
826 IF NN = 1 THEN TS = (TP(1) + TP(2) * TC(2) * (1 - ZF * D(2)) /
    TC(1) / (1 - ZF * D(1))) / 2: GOTO 830
828 TS = (TP(2) + TP(1) * TC(1) * (1 - ZF * D(1)) / TC(2) / (1 - ZF
    * D(2))) / 2
830 REM
831 IF TS > 1 THEN TS = 1
832 FOR L = 0 TO LI:YH = CO * (L / LI - YK) * (L / LI - YK): IF L /
    LI < YK THEN T%(L,K) = (TK * (TN(NN) + (1 - TN(NN)) * EXP (YH /
    WN(NN) / WN(NN)))) * 10000 + .5: GOTO 850
840 T%(L,K) = (TK * (TS + (1 - TS) * EXP (YH / WP / WP))) * 10000 + .5
850 NEXT : PRINT ".":; NEXT : FOR K = 0 TO 2 * KI: FOR L = 0 TO

```

```

      LI:CM%(L) = T%(L,K): IF T$ = "B" THEN CM%(L) = T%(LI - L,K)
860 IF T$ < > "T&B" THEN 890
862 CM%(L) = 0
870 IF NN = 1 AND L < = LI * HS THEN CM%(L) = T%(1 / HS * L,K): GOTO 890
872 IF NN = 2 AND L > LI * HS THEN CM%(L) = T%(1 / (1 - HS) * (LI - L),K)
890 IF E$ = "H" THEN CM%(L) = 100 - CM%(L)
893 NEXT : PRINT ".": FOR L = 0 TO LI
894 T%(L,K) = CM%(L):CM%(L) = 0: IF NN = 1 THEN TE%(L,K) = T%(L,K):
      GOTO 897
895 IF NN = 2 AND DV$ = "D" THEN T%(L,K) = (T%(L,K) + TE%(L,K) - 2
      * T%(L,K) * TE%(L,K) / 10000) / (1 - T%(L,K) * TE%(L,K) / 100000000):
      GOTO 897
896 T%(L,K) = TE%(L,K) + T%(L,K)
897 IF NN = 2 OR DV$ = "S" THEN T%(L,K) = (T%(L,K) + MS%(L) - 2 *
      T%(L,K) * MS%(L) / 10000) / (1 - T%(L,K) * MS%(L) / 100000000)
898 NEXT : PRINT ".": NEXT : IF NN = 1 AND (DV$ = "D" OR T$ =
      "T&B") THEN NN = 2: GOTO 661
900 PRINT : PRINT CHR$(4)"BLOADCHAIN,A520"
910 CALL 520"FILES2.1B"

```



## Appendix B

### Listing of Applesoft BASIC program used in Reference 17: Part II

```

10 SCALE= 1: ROT= 0: DEF FN RO(X) = INT (X * 100 + .5) / 100
20 GOTO 899
40 H PLOT XC, YC: FOR A = AB TO AD STEP 6
50 YP = RH * (1 - YS) * SIN (A / 180 * PI): XP = RH * COS (A / 180
  * PI) + YS / .6 * 2 * YP
60 IF XC + XP > = 0 THEN H PLOT XC + XP, YC - YP
62 NEXT : RETURN
70 FOR CN = 1 TO LEN (N$): Q$ = MID$ (N$, CN): IF ZN = 0 THEN DRAW
  ASC (Q$) - 31 AT XN + 6 * (CN - 1), YN: GOTO 90
80 DRAW ASC (Q$) - 31 AT XN, YN + 6 * (CN - 1)
90 NEXT : ZN = 0: RETURN
100 XN = CC: YN = RC + 124: N$ = "-": GOSUB 70
110 N$ = "O=(TM-T)/(TM-TJ)": IF E$ = "H" THEN N$ = "O=(T-TJ)/TM-TJ"
120 XN = CC: YN = RC + 124: GOSUB 70
130 N$ = "0": XN = CC: YN = RC + 114: GOSUB 70
140 N$ = ".5": XN = CC + 50: YN = RC + 114: GOSUB 70
150 N$ = "1": XN = CC + 100: YN = RC + 114: GOSUB 70
170 N$ = ".5": XN = CC - 22: YN = RC + 50: GOSUB 70
180 N$ = "0": IF T$ = "B" THEN N$ = "1"
190 XN = CC - 18: YN = RC: GOSUB 70
200 N$ = "0": IF T$ = "T" THEN N$ = "1"
210 XN = CC - 18: YN = RC + 100: GOSUB 70
220 N$ = "Y-H": ZN = 1: XN = CC - 36: YN = RC + 44: GOSUB 70
285 NN = 1: YN = 179
290 XN = 2: N$ = "S/H0=" + STR$ ( FN RO (SD (NN) / H (NN))): GOSUB 70
300 XN = 65: N$ = "H0/D=" + STR$ ( FN RO (H (NN))): GOSUB 70
310 XN = 128: N$ = "J=" + STR$ ( FN RO (J (NN))): GOSUB 70
320 XN = 184: N$ = "DR=" + STR$ ( FN RO (DR (NN))): GOSUB 70
330 XN = 240: N$ = "CD=" + STR$ ( FN RO (CD (NN))): GOSUB 70
335 IF (DV$ = "D" OR T$ (NN) = "T&B") AND NN = 1 THEN NN = 2: YN =
  187: GOTO 290
370 RETURN
899 PRINT : PRINT "<3>D or <2>D profiles? ";: GET O$: PRINT : HOME
  : VTAB 22: POKE - 16304, 0: POKE - 16301, 0
900 IF O$ = "2" THEN HCOLOR= 3: RX = 112: CX = 38: OS = 0: NP = 0: RC =
  RX - 100: CC = CX: GOTO 2000
1000 HGR : HCOLOR= 3: POKE - 16302, 0: CC = 99: RC = 42: RI = 2: CI = 4
1010 H PLOT CC + 180, RC - 40 TO CC + 72, RC - 40: H PLOT CC + 80, RC -
  40 TO CC, RC
1015 H PLOT CC + 32, RC - 20 TO CC + 40, RC - 20: H PLOT CC - 8, RC TO
  CC, RC TO CC, RC + 108: H PLOT CC - 8, RC + 50 TO CC, RC + 50
1020 H PLOT CC - 8, RC + 100 TO CC + 100, RC + 100 TO CC + 100, RC +
  108: H PLOT CC + 50, RC + 100 TO CC + 50, RC + 108: XN = 2: YN = 187: N$ =
  "X/H0=" + STR$ ( FN RO (X (NN))): GOSUB 70
1029 XN = 2: YN = 3: N$ = " 2.1": REM : GOSUB 70
1030 N$ = "Z/S"
1040 XN = CC: YN = RC - 22: GOSUB 70: GOSUB 100: AB = 0: AD = 360: YS =
  0: RH = 25 / SD (NN)
1060 YS = .6: IF P$ < > "M" THEN 1100
1070 SX = 25: IF T$ = "B" THEN 1080
1072 XC = CC - 60: IF DV$ = "D" AND DF = 1 AND T$ (1) = T$ (2) THEN
  XC = XC - SX

```

```

1073 YC = RC - 10: GOSUB 40
1074 XC = CC - 20: IF DV$ = "D" AND DF = 1 AND T$(1) = T$(2) THEN
      XC = XC - SX
1075 YC = RC - 30: GOSUB 40: IF DV$ < > "D" THEN 1080
1076 IF T$(1) < > T$(2) AND DF < 1 THEN DF = 1:AB = 180: GOTO 1112
1078 IF T$(1) = T$(2) AND P$(1) = P$(2) AND DF < 1 THEN XC = XC -
      20:DF = 1: GOTO 1072
1079 IF T$(1) = T$(2) AND P$(1) < > P$(2) AND DF < 1 THEN XC = XC
      - 20:DF = 1:AB = 0: GOTO 1102
1080 IF T$ = "T" THEN 1180
1082 XC = CC - 60: IF DV$ = "D" AND DF = 1 AND T$(1) = T$(2) THEN
      XC = XC - SX
1083 YC = RC + 90: GOSUB 40
1084 XC = CC - 20: IF DV$ = "D" AND DF = 1 AND T$(1) = T$(2) THEN
      XC = XC - 2X
1085 YC = RC + 70: GOSUB 40: IF DV$ < > "D" THEN 1180
1086 IF T$(1) < > T$(2) AND DF < 1 THEN DF = 1:AB = 180: GOTO 1102
1088 IF T$(1) = T$(2) AND P$(1) < > P$(2) AND DF < 1 THEN DF =
      1:XC = XC - 20:AB = 0: GOTO 1082
1090 GOTO 1180
1100 IF T$ = "B" THEN 1111
1102 XC = CC - 72: IF DV$ = "D" AND DF = 1 AND T$(1) = T$(2) THEN
      XC = XC - SX
1103 YC = RC:AB = 0:AD = 180: GOSUB 40
1104 XC = CC - 32: IF DV$ = "D" AND DF = 1 AND T$(1) = T$(2) THEN
      XC = XC - SX
1105 YC = RC - 20:AD = 360: GOSUB 40
1106 XC = CC + 8: IF DV$ = "D" AND DF = 1 AND T$(1) = T$(2) THEN XC = XC -
      20
1107 YC = RC - 40:AB = 180: GOSUB 40: IF DV$ < > "D" THEN 1111
1108 IF T$(1) < > T$(2) AND P$(1) = P$(2) AND DF < 1 THEN DF =
      1:AB = 0:AD = 360: GOTO 1082
1109 IF T$(1) = T$(2) AND P$(1) = P$(2) AND DF < 1 THEN XC = XC -
      20:DF = 1: GOTO 1102
1110 GOTO 1180
1111 IF T$ = "B" THEN 1180
1112 XC = CC - 72: IF DV$ = "D" AND DF = 1 AND T$(1) = T$(2) THEN
      XC = XC - SX
1113 YC = RC + 100:AB = 0:AD = 180: GOSUB 40
1114 XC = CC - 32: IF DV$ = "D" AND DF = 1 AND T$(1) = T$(2) THEN
      XC = XC - SX
1115 YC = RC + 80:AD = 360: GOSUB 40: IF DV$ < > "D" THEN 1180
1116 IF T$(1) < > T$(2) AND P$(1) = P$(2) AND DF < 1 THEN DF =
      1:AB = 0:AD = 360: GOTO 1072
1118 IF T$(1) = T$(2) AND P$(1) = P$(2) AND DF < 1 THEN XC = XC -
      20:DF = 1: GOTO 1112
1120 GOTO 1180
1180 FOR D1 = 0 TO 20:CS = CC + CI * D1:RS = RC - RI * D1:K = ABS
      (D1 - 20 * INT (D1 / 10)): IF D1 > 10 AND NC$ = "Y" AND AR = 1 THEN
      K = D1 - 10 * INT (D1 / 10)
1182 FOR D2 = 0 TO 100:L = D2
1190 C = CS + INT (T%(L,K) + 50) / 100
1200 R = RS + D2: IF C < CM%(R) THEN 1220
1210 H PLOT C,R:CM%(R) = C
1220 NEXT : NEXT : PRINT CHR$(6): POKE - 16301,0: FOR ZZ = 0 TO
      148:CM%(ZZ) = 0: NEXT
1230 PRINT "<S>ave to disk, <2>D profiles,          <R>estart, or

```

```

    <E>xit to main menu? ";: GET O$: PRINT : IF O$ = "E" OR O$ = CHR$
    (27) THEN 2230
1240 IF O$ = "R" OR O$ = CHR$ (13) THEN SD(NN) = INT (1000 *
    SD(NN) / H(NN) + .5) / 1000:NN = 1:FL = 1: PRINT CHR$
    (4)"BLOADCHAIN,A520": CALL 520"FILES2.1A,D1"
1250 IF O$ = "S" THEN GOSUB 3000: GOTO 1230
2000 HGR : HCOLOR= 3: HOME : VTAB 22:RX = 112:CX = 38:OS = 0:NP =
    0:RC = RX - 100:CC = CX: GOSUB 100
2010 HPLOT CX - 8,RX - 100 TO CX,RX - 100 TO CX,RX TO CX + 100,RX
    TO CX + 100,RX + 8: HPLOT CX - 8,RX - 50 TO CX,RX - 50: HPLOT CX -
    8,RX TO CX,RX: HPLOT CX,RX TO CX,RX + 8: HPLOT CX + 50,RX TO CX +
    50,RX + 8
2020 IF NP < 5 THEN XN = 2 + NP * 56:YN = 148:N$ = "X/H=" + STR$ (
    FN RO(X)): GOSUB 70
2030 IF OS > 0 THEN HPLOT CX + 104 - OS * 100,RX TO CX + 100,RX TO
    CX + 100,RX + 8:N$ = "1":XN = CX + 100:YN = RX + 14: GOSUB 70
2090 INPUT "Z/S=";Z: IF Z = 1 THEN FOR L = 0 TO 100:T%(L,6) = 0:
    FOR K = 0 TO 5:T%(L,6) = T%(L,6) + T%(L,K): NEXT :T%(L,6) = T%(L,6) /
    6: NEXT :K = 6: GOTO 2120
2100 IF Z < - .05 OR Z > = .55 THEN 2090
2110 K = INT (10 * Z + .5): IF P$ = "M" THEN K = 5 - K
2120 IF NP < 5 THEN XN = 2 + NP * 56:YN = 156:N$ = "Z/S=" + STR$ (
    FN RO(Z)): GOSUB 70
2130 FOR KK = 0 TO 100
2150 RP = RX - 100 + KK:CP = CX + INT (T%(L,K) + 50) / 100: IF T$ =
    "S" THEN CP = CP + INT (T%(LI - L,KI - K) + 50) / 100: IF CP > CX +
    100 THEN CP = CX + 100
2160 HPLOT CP,RP: NEXT
2170 PRINT CHR$ (6): PRINT "<N>ew axes, <O>verlay, <3>D profiles,
    <S>ave to disk, <R>estart, or <E>xit ";: GET O$: PRINT : IF O$ = "N"
    THEN 2000
2180 IF O$ = "3" THEN 1000
2190 IF O$ = "O" THEN INPUT "OFFSET=";OS:CX = CX + OS * 100: IF CX
    + 100 > 279 THEN CX = CX - OS * 100: GOTO 2170
2200 IF O$ = "R" OR O$ = CHR$ (13) THEN SD(NN) = INT (1000 *
    SD(NN) / H(NN) + .5) / 1000:FL = 1: PRINT CHR$
    (4)"BLOAD"CHAIN,A520":CALL 520"FILES2.1A"
2210 IF O$ = "S" THEN GOSUB 3000
2220 IF O$ < > "E" AND O$ < > CHR$ (27) THEN NP = NP + 1: GOTO 2020
2230 NN = 2
2231 POKE 34,0: PRINT D$"OPEN PARAM"NN: PRINT D$"WRITE PARAM"NN:
    PRINT P$: PRINT T$: PRINT E$: PRINT CD(NN): PRINT DR(NN): PRINT
    J(NN): PRINT INT (1000 * SD(NN) / H(NN) + .5) / 1000: PRINT H(NN):
    PRINT X: PRINT D$"CLOSE"
2240 TEXT : HOME : PRINT : PRINT "Loading main menu": POKE 104,96:
    POKE 24576,0: PRINT D$"RUN PRO"
3000 INPUT "PICTURE NAME? ";PN$: IF PN$ = "" THEN RETURN
3004 SU$ = ",D2"
3005 IF RIGHT$(PN$,3) = ",D2" THEN SU$ = ",D2":PN$ = LEFT$(PN$,
    LEN (PN$) - 3)
3006 IF LEFT$(PN$,7) = "CATALOG" THEN TEXT : PRINT CHR$
    (4)"CATALOG";SU$: GOTO 3000
3010 PRINT D$"BSAVE";PN$;" ,A8192,L8192,D2";SU$: RETURN

```



## Appendix C Correlation Equations

### *Jet Centerline Theta Trajectory*

$$y_c/H_{eq} = (a_1)(0.3575)(J)^{0.25}(S/d)^{0.14}(H_{eq}/d)^{-0.45} (C_d)^{0.155} (x/H_{eq})^{0.17} (\exp(-b)) \quad \text{C3-1}$$

where  $a_1 = \min[(1+S/H_{eq}), 2]$   
and  $b = (0.091)(x/H_{eq})^2 [1 - (S/H_{eq})(J^{0.5})/3.5]/(S/H_{eq})$

### *Maximum Theta for Centerplane Profiles*

$$\theta_c = \theta_{EB} + (1 - \theta_{EB}) [(a_1)(J)^{-0.35} (C_d)^{0.5} (H_{eq}/d)^{-1} (x/H_{eq})^{-1}]^f \quad \text{C3-2}$$

where  $f = 1.15 [(S/H_{eq})/(1+S/H_{eq})]^{0.5}$   
and  $\theta_{EB} = \sim m_J/m_T$

### *Minimum Thetas for Centerplane Profiles*

$$(\theta_{\min}^+)/(\theta_c) = 1 - \exp(-c^+) \quad \text{C3-3}$$

where  $c^+ = (a_3)(0.038)(J)^{1.62}(S/d)^{1.5}(H_{eq}/d)^{-2.57}(C_d)^{0.535}(x/H_{eq})^{1.1}$   
and  $a_3 = 1$  if  $(y_c/H_{eq} + W_{1/2}^+/H_{eq}) \leq 1$   
 $= (H/H_{eq})^{3.67}$  if  $(y_c/H_{eq} + W_{1/2}^+/H_{eq}) > 1$

$$(\theta_{\min}^-)/(\theta_c) = 1 - \exp(-c^-)$$

where  $c^- = (Q)(1.57)(J)^{-0.3}(S/d)^{-1.4}(H_{eq}/d)^{0.9}(C_d)^{0.25}(x/H_{eq})^{0.9}$   
and  $Q = 1$  if  $(y_c/H_{eq} + W_{1/2}^+/H_{eq}) \leq 1$   
 $= \exp[(0.22)(x/H_{eq})^2((J^{0.5})/5 - S/H_{eq})]$  if  $(y_c/H_{eq} + W_{1/2}^+/H_{eq}) > 1$

### *Centerplane Half-Widths*

$$(W_{1/2}^+)/H_{eq} = (0.1623)(J)^{0.18}(S/d)^{-0.25}(H/H_{eq})^{0.25}(C_d)^{0.125}(x/H_{eq})^{0.5} \quad \text{C3-4}$$

$$(W_{1/2}^-)/H_{eq} = (0.2)(J)^{0.15}(S/d)^{0.27}(H_{eq}/d)^{-0.38}(H/H_{eq})^{0.5}(C_d)^{0.055}(x/H_{eq})^{0.12}$$

### *Theta Trajectory for Off-Centerplane Profiles*

$$y_{c,z}/y_c = 1 - (4)(z/S)^2(\exp(-g)) \quad \text{C3-5}$$

where  $g = (0.227)(J)^{0.67}(S/d)^{-1}(H_{eq}/d)^{0.54}(C_d)^{0.23}(x/H_{eq})^{0.54}$

**Maximum Theta for Off-Centerplane Profiles**

C3-6

$$\theta_{c,z}/\theta_c = 1 - (4)(z/S)^2 (\exp(-d))$$

where  $d = (0.452)(J)^{0.53}(S/d)^{-1.53} (H_{eq}/d)^{0.83}(C_d)^{0.35}(x/H_{eq})^{0.83}$

**Minimum Thetas for Off-Centerplane Profiles**

C3-7

$$(\theta_{\min,z}^{+/-})/(\theta_{c,z}) = (\theta_{\min}^{+/-})/(\theta_c)$$

**Half-widths for Off-Centerplane Profiles**

C3-8

$$(W_{1/2,z}^{+/-})/H_{eq} = (W_{1/2}^{+/-})/H_{eq}$$

The six scaling parameters,  $y_c/H_{eq}$ ,  $\theta_c$ ,  $\theta_{\min}^+$ ,  $\theta_{\min}^-$ ,  $W_{1/2}^+/H_{eq}$ , and  $W_{1/2}^-/H_{eq}$ , are used in equation (1) to define the vertical profile at any  $x, z$  location in the flow. For all except the case of opposed rows of jets with centerlines in-line,  $H_{eq}$  in the correlation equations is equal to  $H$ , the height of the duct at the injection location.

**Nonuniform Mainstream Scalar; Opposed Rows of Jets with Centerlines Staggered; Double (axially staged) Rows of Jet**

C3-9

It was shown in Holdeman and Srinivasan reference 17 that these flows can be satisfactorily modeled by superimposing independent calculations of the separate elements. This is accomplished as follows:

$$\theta = [\theta_1 + \theta_2 - (2)(\theta_1)(\theta_2)]/[1 - (\theta_1)(\theta_2)]$$

Note that  $\theta = \theta_1$  at any location where  $\theta_2 = 0$  (and  $\theta = \theta_2$  if  $\theta_1 = 0$ ); and that  $\theta \leq 1$  (provided that  $\theta_1$  and  $\theta_2$  are each  $\leq 1$ ). Also, for the completely mixed case  $\theta_{EB}$  is equal to the ratio of the total jet flow to the mainstream flow as required.

**Flow Area Convergence**

C3-10

This case is modeled by assuming that the accelerating mainstream will act to decrease the effective momentum-flux ratio as the flow proceeds downstream, thus:

$$J(x) = (J)[H(x)/H]^2$$

where  $H(x)/H = 1 - (dH/dx)(x/H)$

Note that the trajectory and the jet half-widths are calculated in terms of the duct height at the injection location, so the ordinate must be scaled by the inverse of the convergence rate,  $H/H(x)$ , to show profiles in terms of  $H$  at the axial location of interest.

It was observed in Srinivasan et al. reference 15 that bluff slots resulted in slightly less jet penetration and more two-dimensional profiles than circular holes, and that streamlined slots resulted in slightly greater jet penetration and more three-dimensional profiles. This effect is modeled by using the actual ratio of the orifice spacing to the orifice lateral dimension in lieu of  $S/d$  in the correlation equations.  $H/d$  is not changed.

For rectangular orifices with circular ends;

$$S/W = (S/d)[1 + (4/\pi)(L/W - 1)]^{0.5}$$

for streamlined slots short dimension of slot is perpendicular to mainstream flow

and

$$S/L = \frac{(S/d)[1 + (4/\pi)(L/W - 1)]^{0.5}}{(L/W)}$$

for streamlined slots long dimension of slot is perpendicular to mainstream flow

for bluff slots long dimension of slot is perpendicular to mainstream flow

where “ $d$ ” is the diameter of a round orifice of equal area, and  $L/W$  is the ratio of the long-to-short dimensions of the slot (Note that in this definition  $L/W \geq 1$ , so  $S/W > S/d$  for a streamlined slot, and  $S/L < S/d$  for a bluff slot. However,  $S/L$  cannot be  $< 1$  for a physically realistic bluff slot, so for this case  $1 < S/L < S/d$  (assuming that  $S/d > 1$ ).

**Slanted Slots**

Two effects were noted in the experimental results for slanted slots namely that the centerplanes shifted laterally with increasing downstream distance and the axes of the kidney-shaped scalar contours were inclined with respect to the injection direction. The distributions are assumed to be the same as those for a round hole of equal area, but are shifted according to the following:

$$\Delta(z/S) = (\sin[(\pi/2)(a)])$$

where  $a = \min[1, (x/H_{eq})(J/26.4)^{0.25}]$

The rotation effect observed in the experimental data (e.g. ref. 2) is not modeled.

The reader may notice that some of these correlations may have changed from those published in references 2 and 17. Aside from corrections of typos and other errors, only the formatting was changed, i.e.  $S/H$  and  $H/d$  are now shown as independent variables, and  $S/d$  is a dependent one ( $S/d = S/H)(H/d)$ ). Note that any two of the set  $S/d$ ,  $H/d$ , and  $S/H$  may be chosen, just not all three!

It was observed in Kamotani and Greber reference 8 that the flowfield downstream of opposed jets was similar to that downstream of a single jet injected toward an opposite wall at half the distance between the jets. This is confirmed by the experimental results in Srinivasan et al. reference 14 also. Thus for the symmetric case,  $H_{eq} = (H_o)/2$ .

In general, these flows can be modeled by calculating an effective duct height as proposed in Wittig et al. reference 22, namely;

$$[H_{eq}]_{top} = (H) \left( \frac{[(A_J/A_M)(J^5)]_{top}}{[(A_J/A_M)(J^5)]_{top} + [(A_J/A_M)(J^5)]_{bottom}} \right)$$

and

$$[H_{eq}]_{bottom} = H - [H_{eq}]_{top}$$

## References

1. Margason, R.J., Fifty Years of Jet in Cross Flow Research, Presented at Computational and Experimental Assessment of Jets in Cross Flow, AGARD Conference Proceedings 534, April 1993.
2. Holdeman, J.D., Mixing of Multiple Jets with a Confined Subsonic Crossflow. *Progress in Energy and Combustion Science*, vol. 19, pp. 31–70, August 1993 (see also AIAA Paper 91–2458 and NASA/TM–104412, June 1991).
3. Holdeman, James D., Liscinsky, David S., Oechsle, Victor L., Samuelson, G. Scott, and Smith, Clifford E., Mixing of Multiple Jets With a Confined Subsonic Crossflow: Part I—Cylindrical Ducts. *Journal of Engineering for Gas Turbines and Power*, vol. 119, October 1997 (also ASME Paper 96–GT–482 and NASA TM–107185, June 1996).
4. Holdeman, J.D., Liscinsky, D.S., and Bain, D.B., Mixing of Multiple Jets With a Confined Crossflow: Part II—Opposed Rows of Orifices in Rectangular Ducts. *Journal of Engineering for Gas Turbines and Power*, vol. 121, July 1999 (also ASME Paper 97–GT–439 and NASA TM–107461, June 1997).
5. Walker, R.E. and Kors, D.L., Multiple Jet Study Final Report. NASA CR–121217, June 1973.
6. Holdeman, James D., Walker, R.E., and Kors, D.L., Mixing of Multiple Dilution Jets With a Hot Primary Airstream for Gas Turbine Combustors. AIAA Paper 73–1249 (also NASA TM–71426, November 1973).
7. Walker, R.E., Kors, D.L., and Holdeman, J.D., Mixing of Multiple Jets of Cooling Air with Simulated Combustion Gases. CPIA Publication 243, Proceedings of the 10th JANNAF Combustion Meeting, vol. 2, pp. 377–396, December 1973.
8. Kamotani, Y. and Greber, I., “Experiments on Confined Turbulent Jets in Cross Flow,” NASA CR–2392, March 1974.
9. Walker, R.E. and Eberhardt, R.G., “Multiple Jet Study Data Correlations,” NASA CR–134795, April 1975.
10. Holdeman, J.D., and Walker, R.E., Mixing of a Row of Jets with a Confined Crossflow. *AIAA Journal*, vol. 15, no. 2, pp. 243–249, February 1977 (see also “An Empirical Model for the Mixing of a Row of Dilution Jets with a Confined Crossflow.” AIAA Paper 76–48 and NASA TM–71821).
11. Srinivasan, R., Berenfeld, A., and Mongia, H.C., Dilution Jet Mixing Program—Phase I Report. NASA CR–168031 (Garrett 21–4302), 1982.
12. Holdeman, J.D., Perspectives on the Mixing of a Row of Jets with a Confined Crossflow. AIAA Paper 83–1200 (also NASA TM–83457, June 1983).
13. Holdeman, J.D., Srinivasan, R., and Berenfeld, A., Experiments in Dilution Jet Mixing. *AIAA Journal*, vol. 22, no. 10, pp. 1436–1443, October 1984 (see also AIAA Paper 83–1201 and NASA TM–83434, June 1983).
14. Srinivasan, R., Coleman, E., and Johnson, K., Dilution Jet Mixing Program Phase II Report. NASA CR–174624 (Garret 21–4804), 1984.
15. Srinivasan, R., Meyers, G., Coleman, E., and White, C., Dilution Jet Mixing Program Phase III Report. NASA CR–174884 (Garrett 21–5418), 1985.
16. Srinivasan, R. and White, C.D., Dilution Jet Mixing Program Supplementary Report. NASA CR–175043 (Garrett 21–5705), 1986.
17. Holdeman, J.D., and Srinivasan, R., Perspectives on Dilution Jet Mixing. AIAA Paper 86–

- 1611 (also NASA TM-87294), June 1986.
18. Holdeman, J.D., Srinivasan, R., Meyers, G.D., and White, C.D., Experiments in Dilution Jet Mixing—Effects of Multiple Rows and Noncircular Orifices. *Journal of Propulsion and Power*, vol. 3, no. 3, May/June 1987 (see also AIAA Paper 85-1104 and NASA TM-86996, July 1985).
  19. Kamotani, Y. and Greber, I., Experiments on a Turbulent Jet in a Cross Flow. NASA CR-72893 (also FTAS/TR-71-83, Case Western Reserve University, June 1971).
  20. Kamotani, Y. and Greber, I., Experiments on a Turbulent Jet in a Cross Flow. AIAA J. vol. 10, no. 11, p. 1425, November 1972 (also AIAA Paper 72-149, January 1972).
  21. Holdeman, J.D., Correlation for Temperature Profiles in the Plane of Symmetry Downstream of a Jet Injected Normal to a Crossflow. NASA TN D-6966, September 1972.
  22. Srinivasan, R. and White, C., Transition Mixing Study: Empirical Model Report. NASA CR-182139 (Garrett 21-6689), February 1988.
  23. Holdeman, J.D., Srinivasan, R., and White, C.D., An Empirical Model of the Effects of Curvature and Convergence on Dilution Jet Mixing. AIAA Paper 88-3180 (also NASA TM-100896, July 1988).
  24. Cox, G.B., Jr., An Analytical Model for Predicting Exit Temperature Profile from Gas Turbine Engine Annular Combustors, AIAA Paper 75-1307. October 1975.
  25. Wittig, S.L.K., Elbahar, O.M.F., and Noll, B.E., “Temperature Profile Development in Turbulent Mixing of Coolant Jets with a Confined Hot Cross-Flow,” *Journal of Engineering for Gas Turbines and Power*, vol. 106, 1984, p. 193 (see also ASME Paper no. 83-GT-39).
  26. Liscinsky, D.S., True, B. and Holdeman, J.D., Effect of Inlet Flow Conditions on Crossflow Jet Mixing. AIAA Paper 96-2881 (also NASA TM-107258, July 1996).
  27. Liscinsky, D.S., True, B. and Holdeman, J.D., Mixing Characteristics of Directly Opposed Rows of Jets Injected Normal to a Crossflow in a Rectangular Duct. AIAA Paper 94-0217 (also NASA TM-106477, January 1994).
  28. Lefebvre, Arthur H., *Gas Turbine Combustion, Second Edition*, Taylor and Francis, 1999.

TABLE I.—RANGE OF FLOW AND GEOMETRIC VARIABLES  
ON WHICH THE EMPIRICAL MODEL IS BASED

Independent Variables	
Density ratio, $DR$	0.5 to 2.2
Momentum-flux ratio, $J$	5 to 105.6
Discharge coefficient, $Cd$	0.6 to 1
Downstream distance, $x/H^*$	0 to 2
Orifice spacing to duct height ratio, $S/H^+$	0 to 1
Orifice size, $H/d$	4 to 16
Axial orifice spacing, $S_x/H$	0.25 to 0.5
Orifice $L/W$ ratio	1 to 2.8
Variable mainstream $\theta$	0 to 1
<b>Flow area convergence, <math>dH/dx</math></b>	<b>0 to 0.5</b>
Dependent Variables	
Downstream distance, $x/d$	2 to 32
Spacing to orifice diameter ratio, $S/d$	2 to 6
<b>Area ratio, <math>A_J/A_M</math></b>	<b>0.025 to 0.1</b>
<b>Jet-to-total mass-flow ratio, <math>m_J/m_T</math></b>	<b>0.075 to 0.36</b>
<b>Jet-to-mainstream mass-flow ratio, <math>MR</math></b>	<b>0.08 to 0.6</b>
<b>Jet-to-mainstream mass-flux ratio, <math>M</math></b>	<b>3 to 14</b>
<b>Jet-to-mainstream velocity ratio, <math>R</math></b>	<b>3 to 14</b>
<b>Equilibrium <math>\theta</math>, <math>\theta_{EB}</math></b>	<b>0 to 1</b>
<b>Pattern factor, <math>PF = (MR)(1-\theta_{min}/\theta_{EB})</math></b>	<b>0 to 0.6</b>
<b><math>C = (S/H)(\text{sqrt}(J))</math></b>	<b>0.5 to 10</b>

\*Note that the downstream distance cannot be within the orifice diameter for any row.

+ Note that  $S/d$  must be greater than 1.

TABLE 2.—CROSS REFERENCE BETWEEN CONDITIONS FOR EMPIRICAL MODEL CALCULATIONS IN CURRENT REPORT AND FIGURES IN PREVIOUS PUBLICATIONS AND EXPERIMENTAL DATA IN REFERENCES 5, 11, 14, AND 15

Figure no. (this report)	Row (in fig. 7)	<i>S/H</i>	<i>H/d</i>	<i>J</i>	<i>C*</i>	<i>TM</i>	Figure no. (in TM)	Test no.	Reference no.	Figure no. (in ref.)
4	F	0.5	5.66	26.4	2.57	—	—	96	5	25(b)-3
								II-50	14	123
5	F	.5	5.66	26.4	2.57	83457	11	96	5	25(b)-3
								II-50	14	123
6	F	.5	5.66	26.4	2.57	83457	12	—		
7	F	.5	5.66	26.4	2.57	83457	13(a)	—		
8(a)	C	.25	8	26.4	1.28	83457	4(a)	59	5	20(b)-3
										28(b)-1
								I-5	11	20
8(b)	I	1	4	26.4	5.14	83457	4(b)	88	5	—
								I-4	11	18
9-1	F	.5	5.66	6.6	1.28	82347	5-1	94	5	25(b)-1
								II-49	14	121
9-2	F	.5	5.66	26.4	2.57	83457	5-2	96	5	25(b)-3
								II-50	14	123
9-3	F	.5	5.66	105.6	5.14	83457	5-3	—		
10-1	F	.5	5.66	26.4	2.57	83457	6-1	—		
10-2	F	.5	5.66	26.4	2.57	83457	6-2	—		
10-3	F	.5	5.66	26.4	2.57	83457	6-3	—		
11-1	E	1	8	26.4	5.14	83457	7-1	—		
11-2	D	.5	8	26.4	2.57	83457	7-2	69	5	28(b)-3
								I-7	11	24
11-3	C	.25	8	26.4	1.28	83457	7-3	59	5	20(b)-3
										28(b)-1
								I-5	11	20
12-1	A	.125	16	26.4	0.64	83457	8-1	3	5	20(b)-1
										31(a)-1
12-2	C	.25	8	26.4	1.28	83457	8-2	59	5	20(b)-3
										28(b)-1
								I-5	11	20
12-3	H	.5	4	26.4	2.57	83457	8-3	104	5	20(b)-4
								III-2	15	50
13(a)-1	D	.5	8	26.5	2.57	83457	9(a)-1	I-7	11	24
13(a)-2	F(~)	.5	6	26.4	2.57	83457	9(a)-2	96	5	25(b)-3

Figure no. (this report)	Row (in fig. 7)	<i>S/H</i>	<i>H/d</i>	<i>J</i>	<i>C*</i>	<i>TM</i>	Figure no. (in TM)	Test no.	Reference no.	Figure no. (in ref.)
								II-50	14	123
13(a)-3	G	.5	5	26.4	2.57	83457	9(a)-3	—		
13(a)-4	H	.5	4	26.4	2.57	83457	9(a)-4	104	5	
								III-22	15	50
13(b)-1	D	.5	8	26.4	2.57	83457	9(b)-1	I-7	11	24
13(b)-2	F(~)	.5	6	26.4	2.57	83457	9(b)-2	96	5	25(b)-3
								II-50	14	123
13(b)-3	G	.5	5	26.4	2.57	83457	9(b)-3	—		
13(b)-4	H	.5	4	26.4	2.57	83457	9(b)-4	104	5	20(b)-4
								III-22	15	50
14(a)-1	J	1	2.83	6.6	2.57	83457	10(a)-1	—		
14(a)-2	F	.5	5.66	26.4	2.57	83457	10(a)-2	96	5	25(b)-3
								II-50	14	123
14(a)-3	B	.25	11.32	105.6	2.57	83457	10(a)-3	—		
14(b)-1	J	1	2.83	6.6	2.57	83457	10(b)-1	—		
14(b)-2	F	.5	5.66	26.4	2.57	83457	10(b)-2	96	5	25(b)-3
								II-50	14	123
14(b)-3	B	.25	11.32	105.6	2.57	83457	10(b)-3	—		
15(a)-1	F	.5	5.66	6.6	1.28	87294	11(a)-1	—		
15(a)-2	C	.25	8	26.6	1.28	87294	11(a)-2	—		
15(b)-1	I	1	4	6.6	2.57	87294	11(b)-1	—		11(b)-1
15(b)-2	F	.5	5.66	26.4	2.57	87294	11(b)-2	I-30		11(b)-2
15(b)-3	C	.25	8	105.6	2.57	87294	11(b)-3	—		11(b)-3
15(c)-1	I	1	4	26.4	5.14	87294	11(c)-2	—		11(c)-2
15(c)-2	F	.5	5.66	105.6	5.14	87294	11(c)-3	—		11(c)-3
16(a)	H	.5	4	26.4	2.57	87294	12(a)	III-3	15	12
16(b)	H	.5	4	26.4	2.57	87294	12(b)	III-2	15	10
17(a)	K <sup>+</sup>	.5	4	26.4	2.57	87294	13(a)	III-19	15	44
17(b)	L <sup>+</sup>	.5	4	26.4	2.57	87294	13(b)	III-19	15	44
18	M <sup>+</sup>	.5	4	26.4	2.57	87294	14	III-19	15	44
19(a)	D <sup>**</sup>	.5	8	6.6	1.28	87294	15(a)	II-7	14	26
	D <sup>**</sup>	.5	8	6.6	1.28					
19(b)	C <sup>**</sup>	.25	8	26.4	1.28	87294	15(b)	II-2	14	13
	C <sup>**</sup>	.25	8	26.4	1.28					
20(a)	E <sup>**</sup>	1	8	26.4	5.14	87294	17(a)			
	E <sup>**</sup>	1	8	26.4	5.14					
20(b)	D <sup>**</sup>	.5	8	105.6	5.14	87294	17(b)	II-12	14	36
	D <sup>**</sup>	.5	8	105.6	5.14					
20(c)	D	.5	8	26.4	2.57	87294	17(c)	69 I-7	5 11	28(b)-3 24
21(a)	H	.5	4	26.4	2.57	87294	18(a)	III-22	15	50
21(b)	F	.5	5.66	26.4	2.57	87294	18(b)	III-6	15	18
	F	.5	5.66	26.4	2.57					
21(c)	F	.5	5.66	26.4	2.57	87294	18(c)	—		
	F	.5	5.66	26.4	2.57					
22(a)	H	.5	4	26.4	2.57	87294	19(a)	III-22	15	60
22(b)	I	1	4	26.4	5.14	87294	19(b)	III-9	15	24
	I	1	4	26.4	5.14					
22(c)	I	1	4	26.4	5.14	87294	19(c)	—		
	I	1	4	26.4	5.14					
23(a)	F	.5	5.66	26.4	2.57	87294	20(a)	III-11	15	28
	C	.25	8	26.4	1.28					

Figure no. (this report)	Row (in fig. 7)	$S/H$	$H/d$	$J$	$C^*$	$TM$	Figure no. (in TM)	Test no.	Reference no.	Figure no. (in ref.)
23(b)	F	.5	5.66	105.6	5.14	87294	20(b)	III-15	15	
	C	.25	8	26.4	1.28					
23(c)	C	.25	8	105.6	2.57	87294	20(c)	III-17	15	40
	F	.5	5.66	26.4	2.57					
24(a)	C	.25	8	26.4	1.28	83457	4(a)	59	5	20(b)-3
										28(b)-1
								I-5	11	20
24(b)	I	1	4	26.4	5.14	83457	4(b)	88	5	—
								I-4	11	18
25-1	E	1	8	26.4	5.14	83457	7-1	—		
25-2	D	.5	8	26.4	2.57	83457	7-2	69	5	28(b)-3
								I-7	11	24
25-3	C	.25	8	26.4	1.28	83457	7-3	59	5	20(b)-3
										28(b)-1
								I-5	11	20
26(a)-1	J	1	2.83	6.6	2.57	83457	10(a)-1	—		
26(a)-2	F	.5	5.66	26.4	2.57	83457	10(a)-2	96	5	25(b)-3
								II-50	14	123
26(a)-3	B	.25	11.32	105.6	2.57	83457	10(a)-3	—		
26(b)-1	J	1	2.83	6.6	2.57	83457	10(b)-1	—		
26(b)-2	F	.5	5.66	26.4	2.57	83457	10(b)-2	96	5	25(b)-3
								II-50	14	123
26(b)-3	B	.25	11.32	105.6	2.57	83457	10(b)-3	—		

\*  $C = (S/H)(\text{sqrt}(J))$ .

+ For noncircular orifices, “ $d$ ” is the diameter of a round hole of the same area.

\*\* Top row/bottom row.

++ Front row/back row.

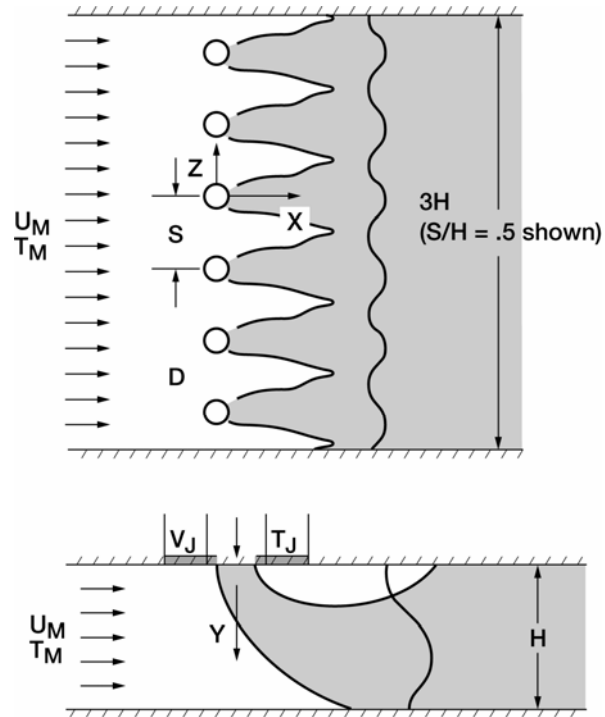


Figure 1.—Schematic of flow field for a confined jet in cross flow (shown for one-side injection of a single row of jets from the top duct wall).

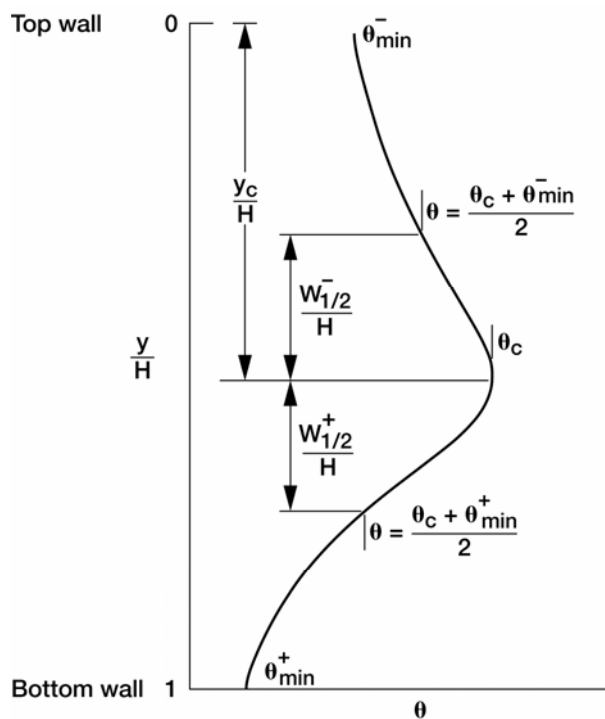


Figure 2.—Schematic of a typical vertical scalar profile showing scaling parameters in empirical model (shown for one-side jet injection from the top duct wall).

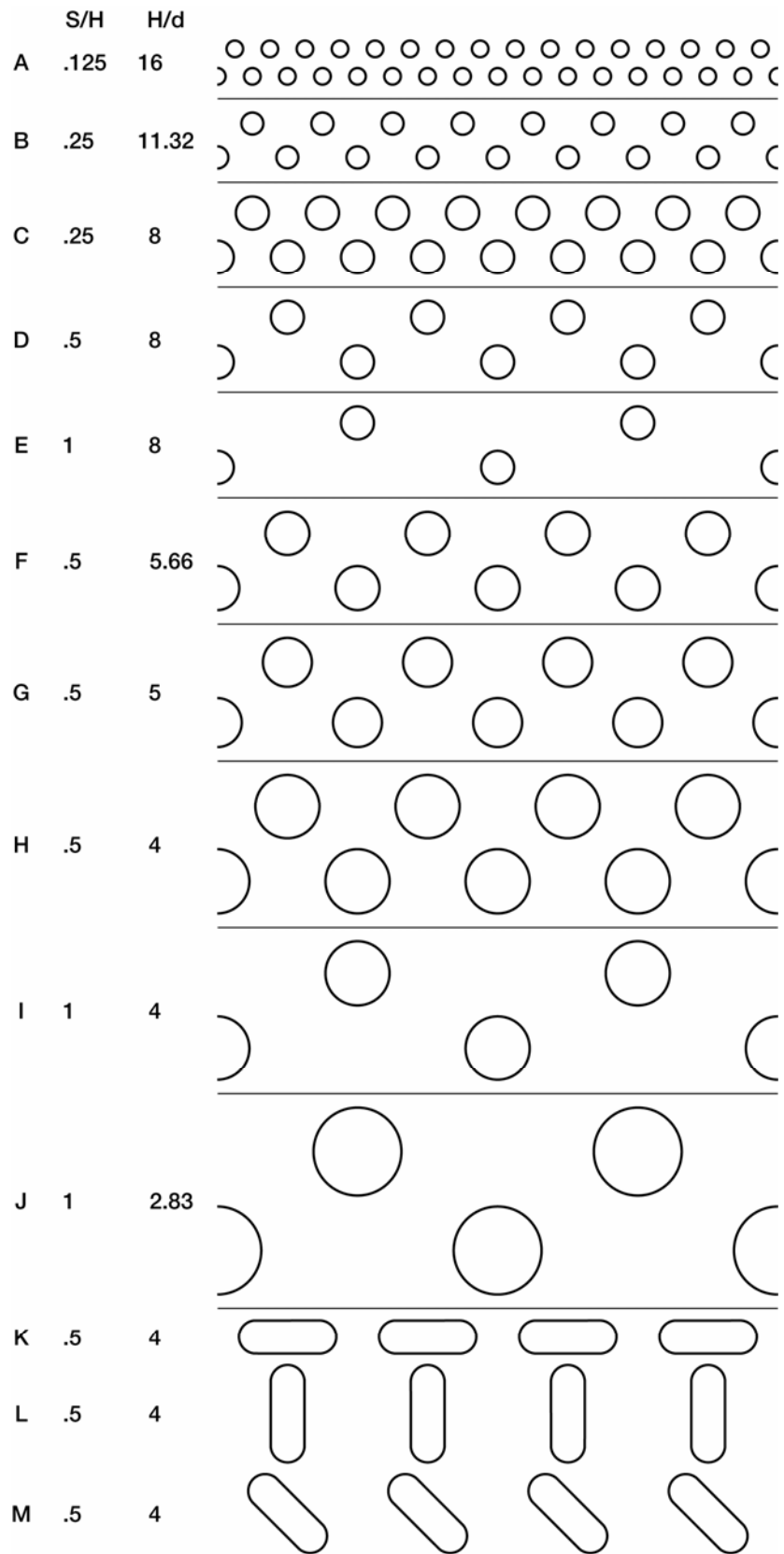


Figure 3.—Orifice configuration.

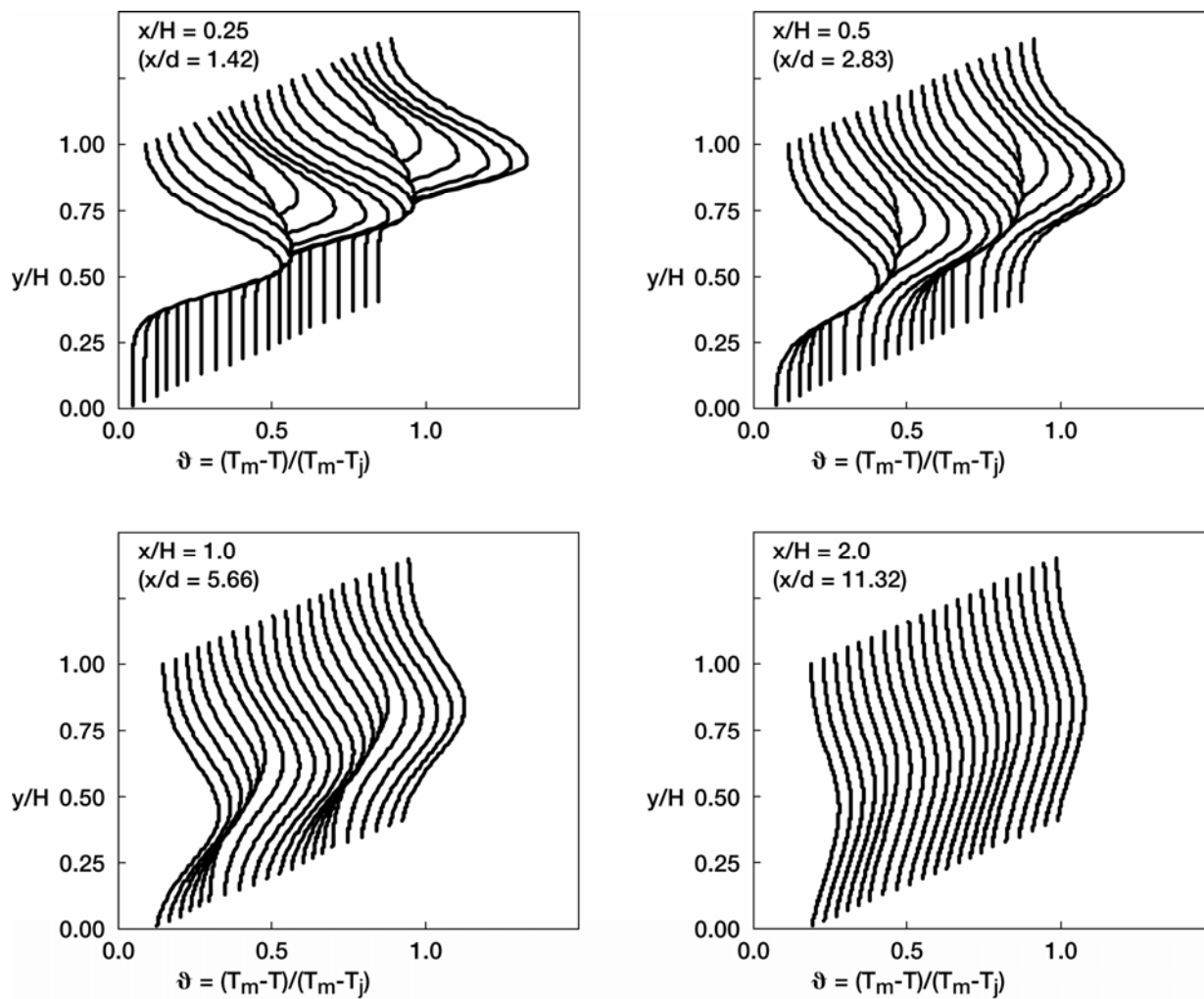


Figure 4.—Variation of scalar profiles with increasing downstream distance: orifice configuration F in figure 3 (centerplane at edge [ ]–0–( in spreadsheet]) for  $S/H = 0.5$ ,  $H/d = 5.66$ , ( $S/d = 2.83$ ),  $DR = 2.2$ ,  $J = 26.4$ , ( $M = 7.62$ ,  $R = 3.46$ ,  $C = 2.57$ ), and  $C_d = 0.64$ .

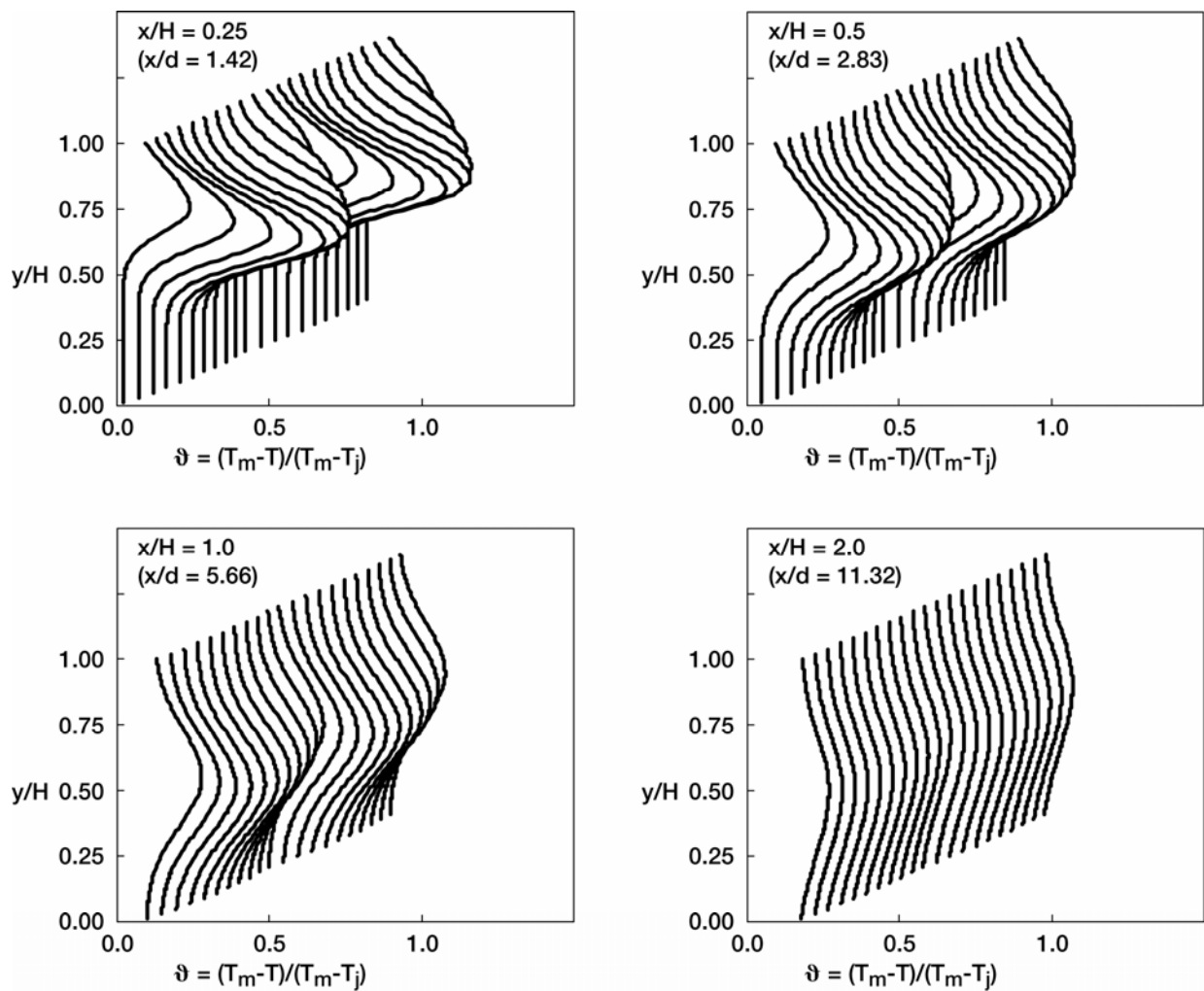


Figure 5.—Variation of scalar profiles with increasing downstream distance: orifice configuration F in figure 3 (midplane at edge [-0-0- in spreadsheet]) for  $S/H = 0.5$ ,  $H/d = 5.66$ , ( $S/d = 2.83$ ),  $DR = 2.2$ ,  $J = 26.4$ , ( $M = 7.62$ ,  $R = 3.46$ ,  $C = 2.57$ ), and  $Cd = 0.64$ .

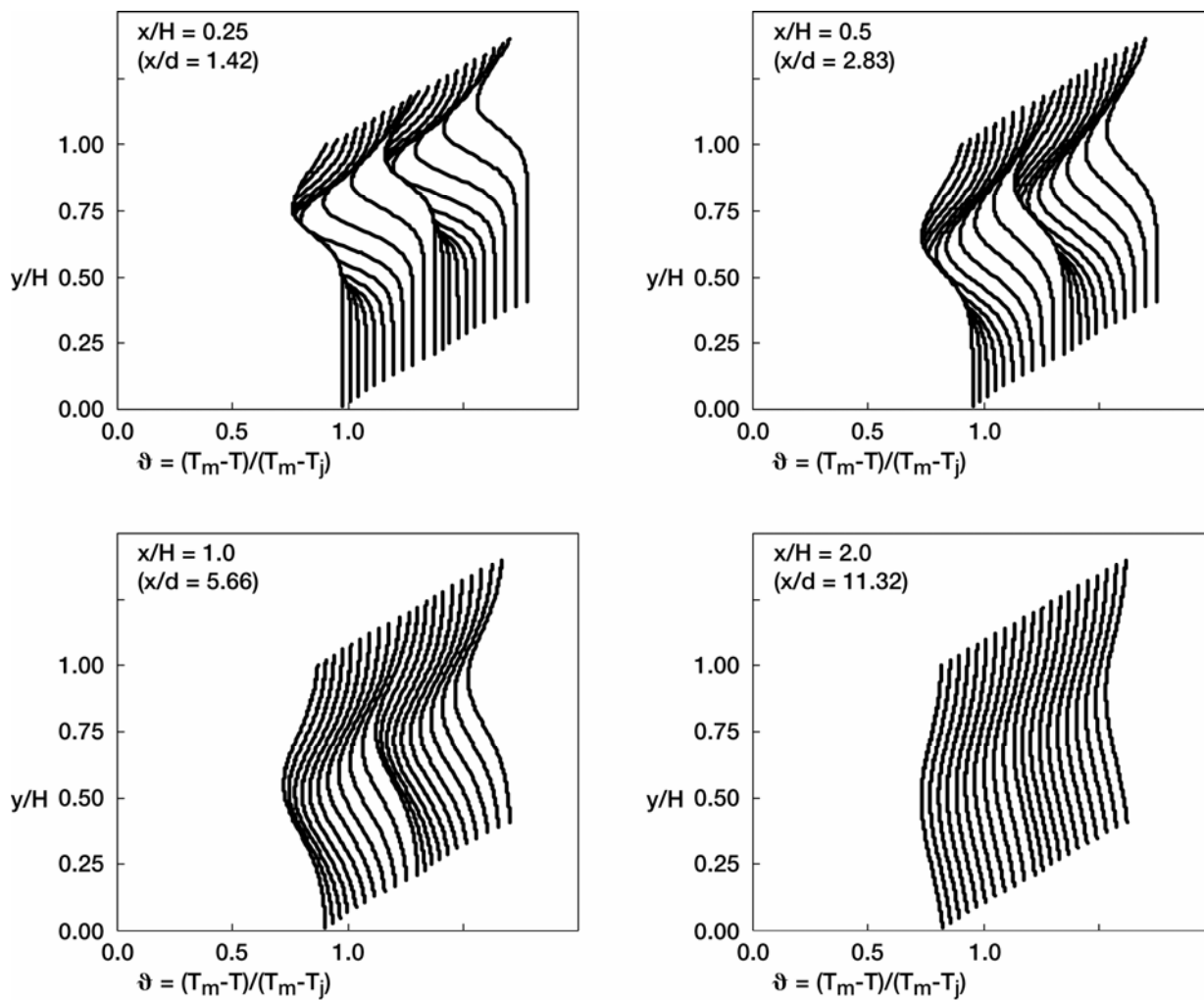


Figure 6.—Variation of "hot" scalar profiles with increasing downstream distance: orifice configuration F in figure 3 (centerplane at edge [-0-0- in spreadsheet]) for  $S/H = 0.5$ ,  $H/d = 5.66$ ,  $(S/d = 2.83)$ ,  $DR = 2.2$ ,  $J = 26.4$ ,  $(M = 7.62, R = 3.46, C = 2.57)$ , and  $Cd = 0.64$ .

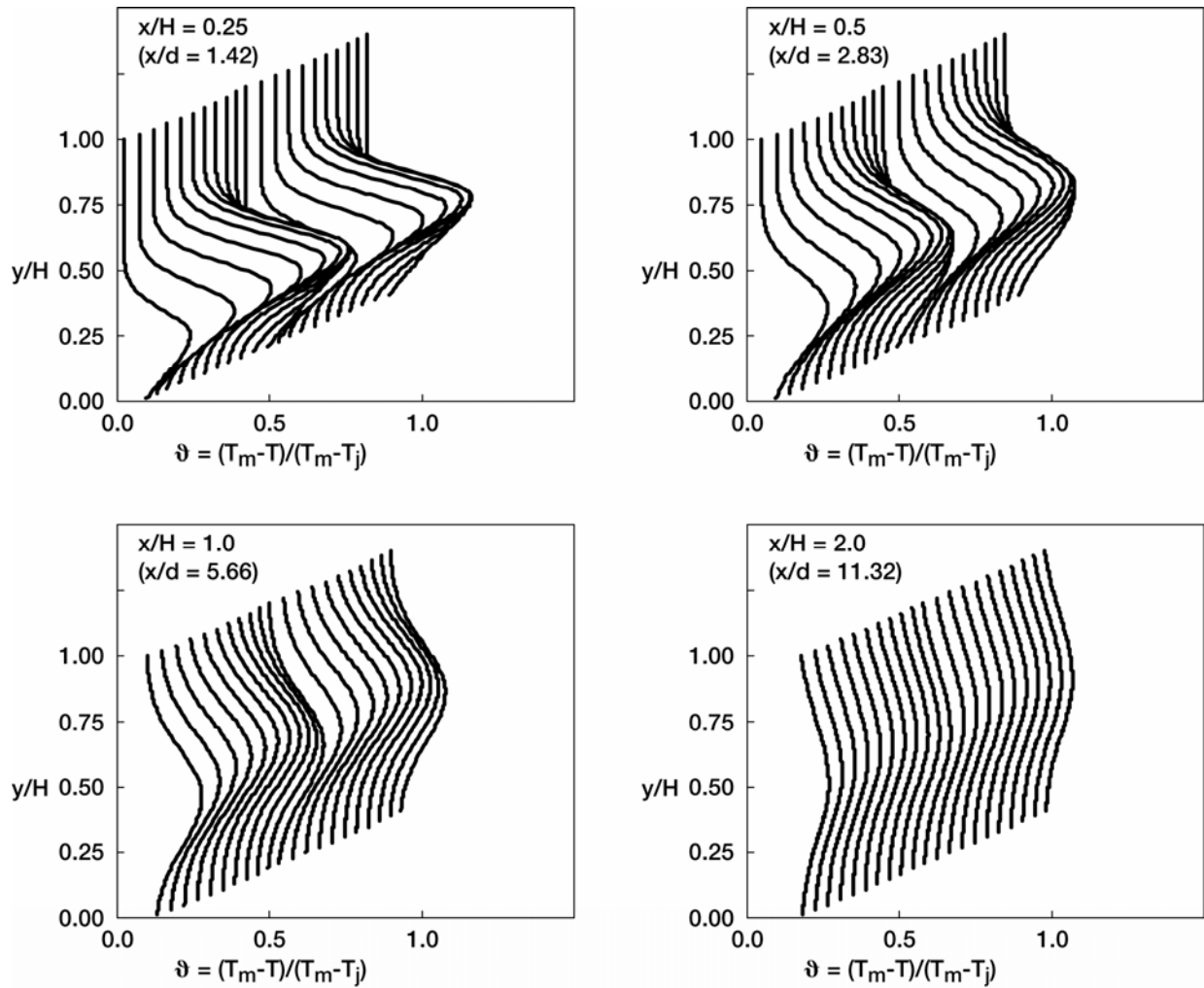


Figure 7.—Variation of bottom injection scalar profiles with increasing downstream distance: orifice configuration F in figure 3 (centerplane at edge [-0-0- in spreadsheet]) for  $S/H = 0.5$ ,  $H/d = 5.66$ , ( $S/d = 2.83$ ),  $DR = 2.2$ ,  $J = 26.4$ , ( $M = 7.62$ ,  $R = 3.46$ ,  $C = 2.57$ ), and  $C_d = 0.64$ .

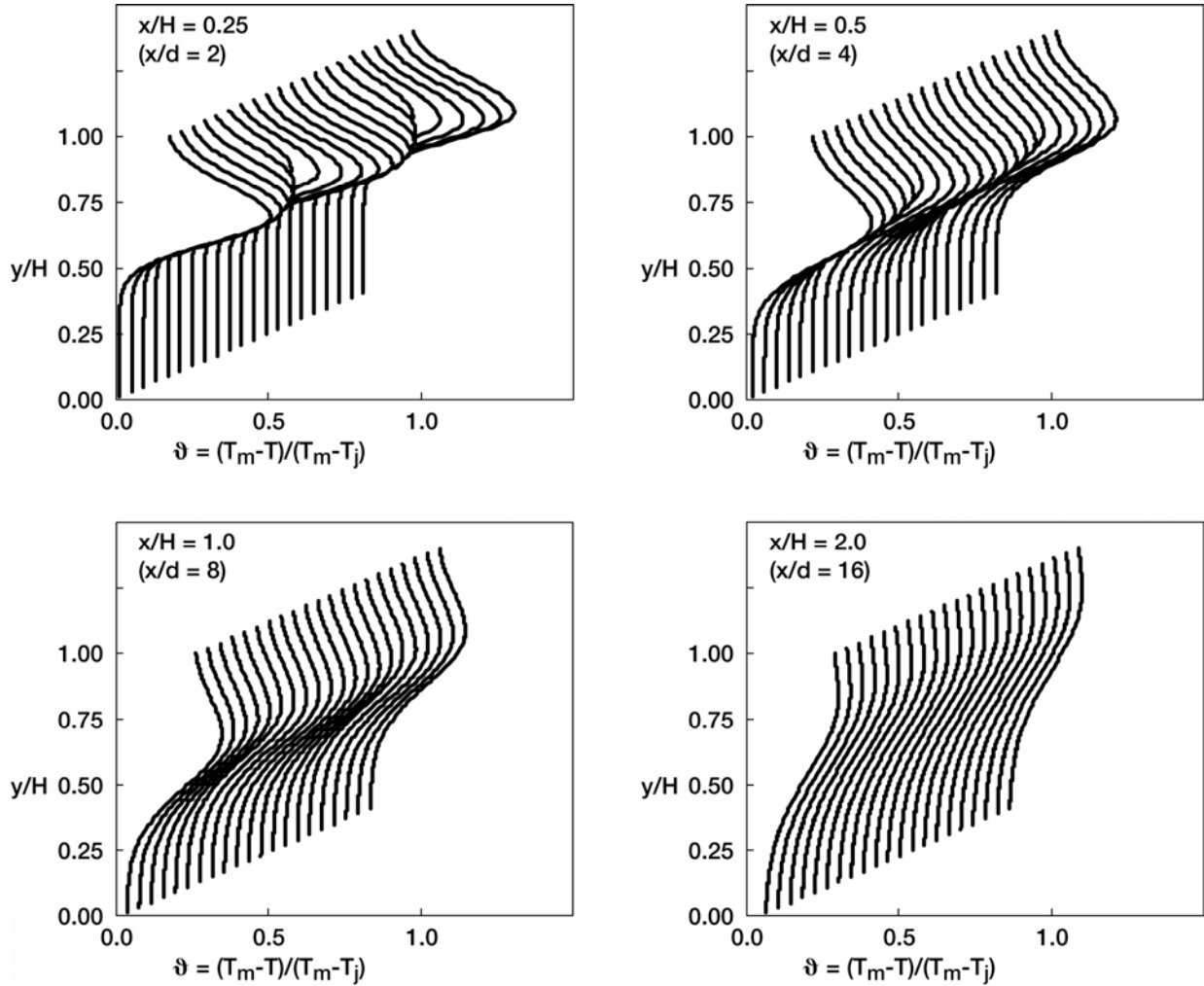


Figure 8a.—Variation in scalar distributions with increasing downstream distance: orifice configuration C in figure 3 (centerplane at edge [ ]–0–( in spreadsheet) for  $S/H = 0.25$ ,  $H/d = 8$ , ( $S/d = 2$ ),  $DR = 2.2$ ,  $J = 26.4$ , ( $M = 7.62$ ,  $R = 3.46$ ,  $C = 1.28$ ), and  $C_d = 0.64$ .

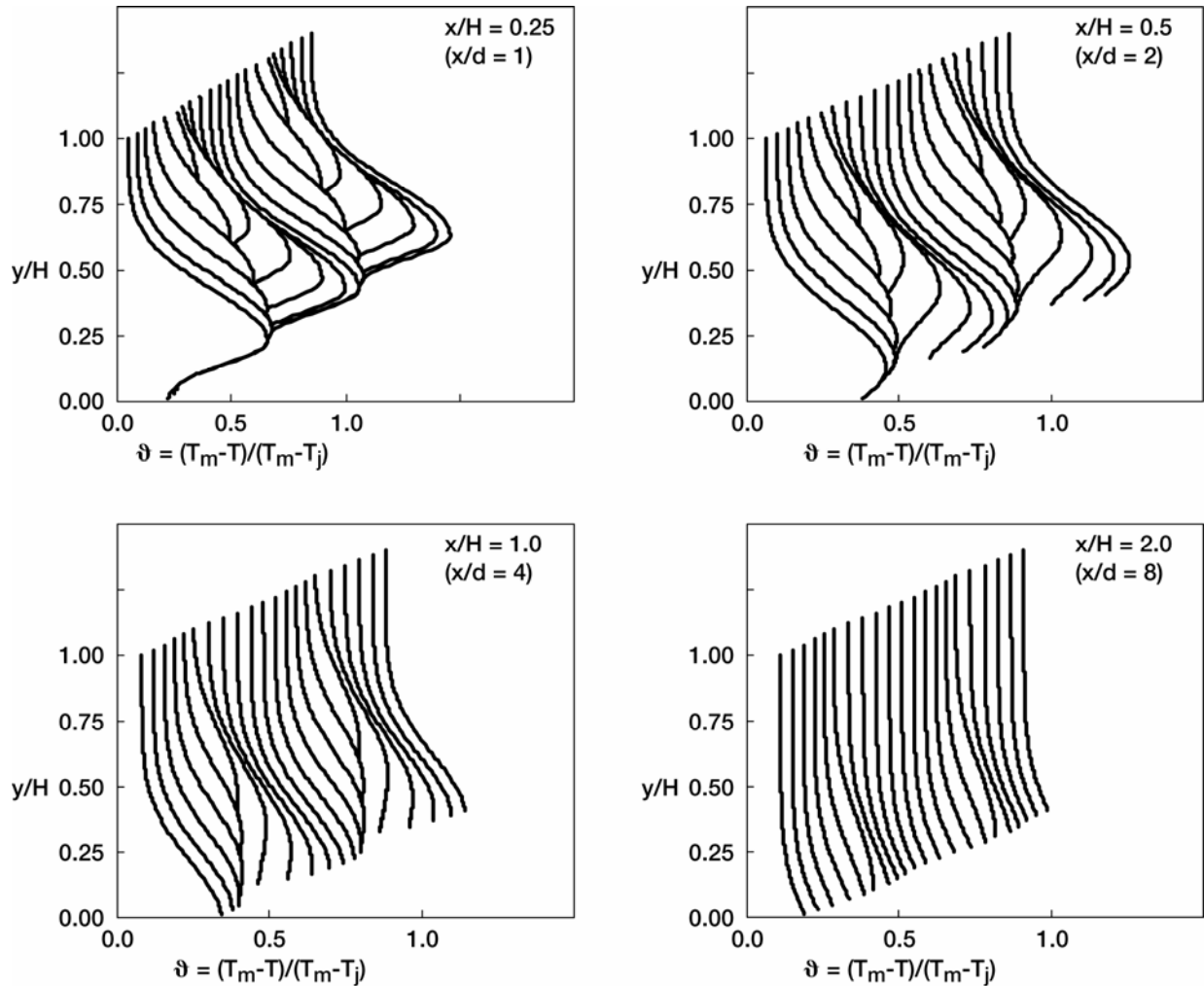


Figure 8b.—Variation in scalar distributions with increasing downstream distance: orifice configuration I in figure 3 (centerplane at edge [ ]–0–( in spreadsheet)) for  $S/H = 1$ ,  $H/d = 4$ ,  $(S/d = 4)$ ,  $DR = 2.2$ ,  $J = 26.4$ ,  $(M = 7.62, R = 3.46, C = 5.14)$ , and  $Cd = 0.64$ .

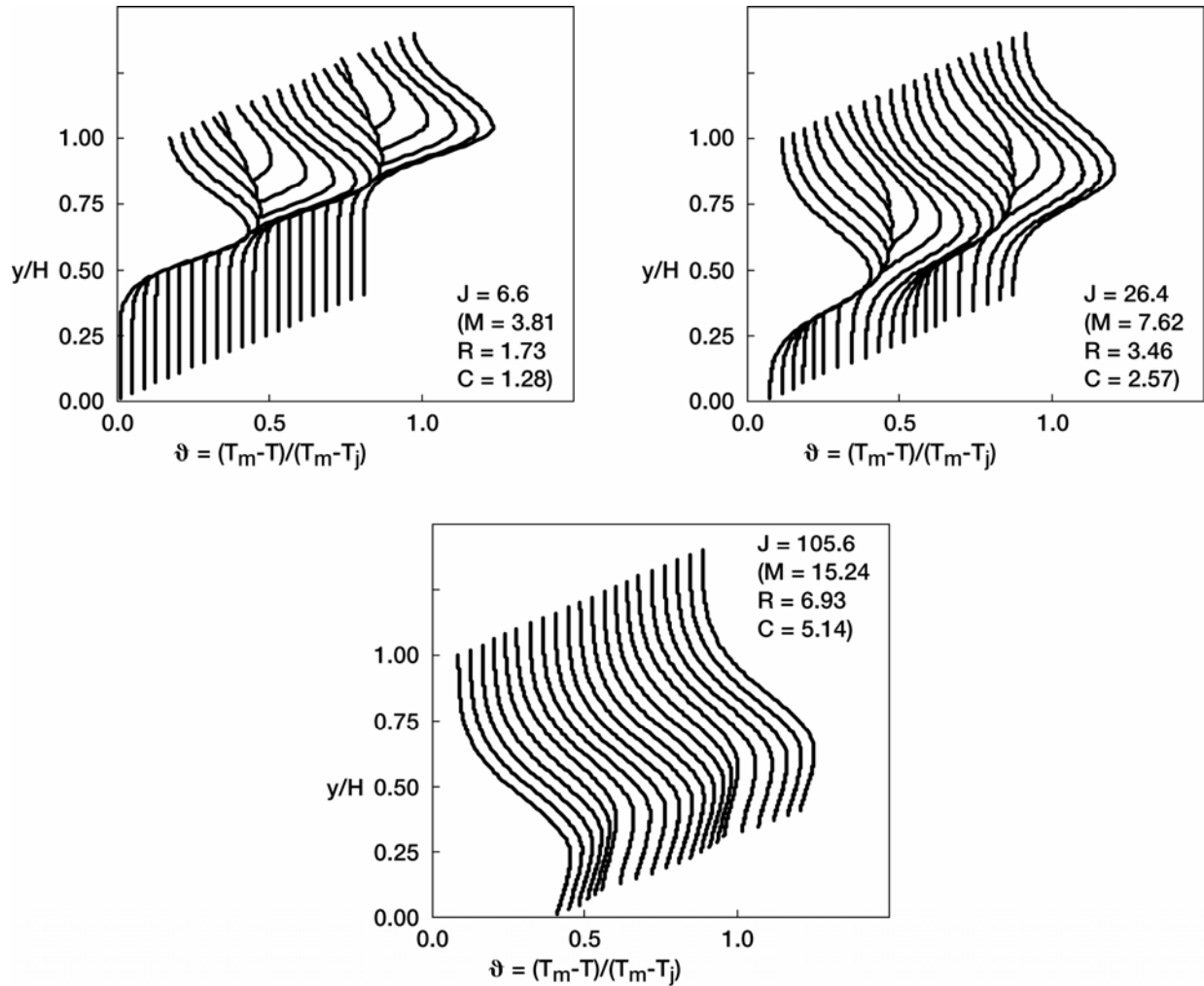


Figure 9.—Variation in scalar distributions with increasing momentum-flux ratio ( $J$ ): orifice configuration F in figure 3 (centerplane at edge [ ]–0–( in spreadsheet)) for  $S/H = 0.5$ ,  $H/d = 5.66$ , ( $S/d = 2.83$ ),  $DR = 2.2$ , and  $C_d = 0.64$  at  $x/H = 0.5$  ( $x/d = 2.83$ ).

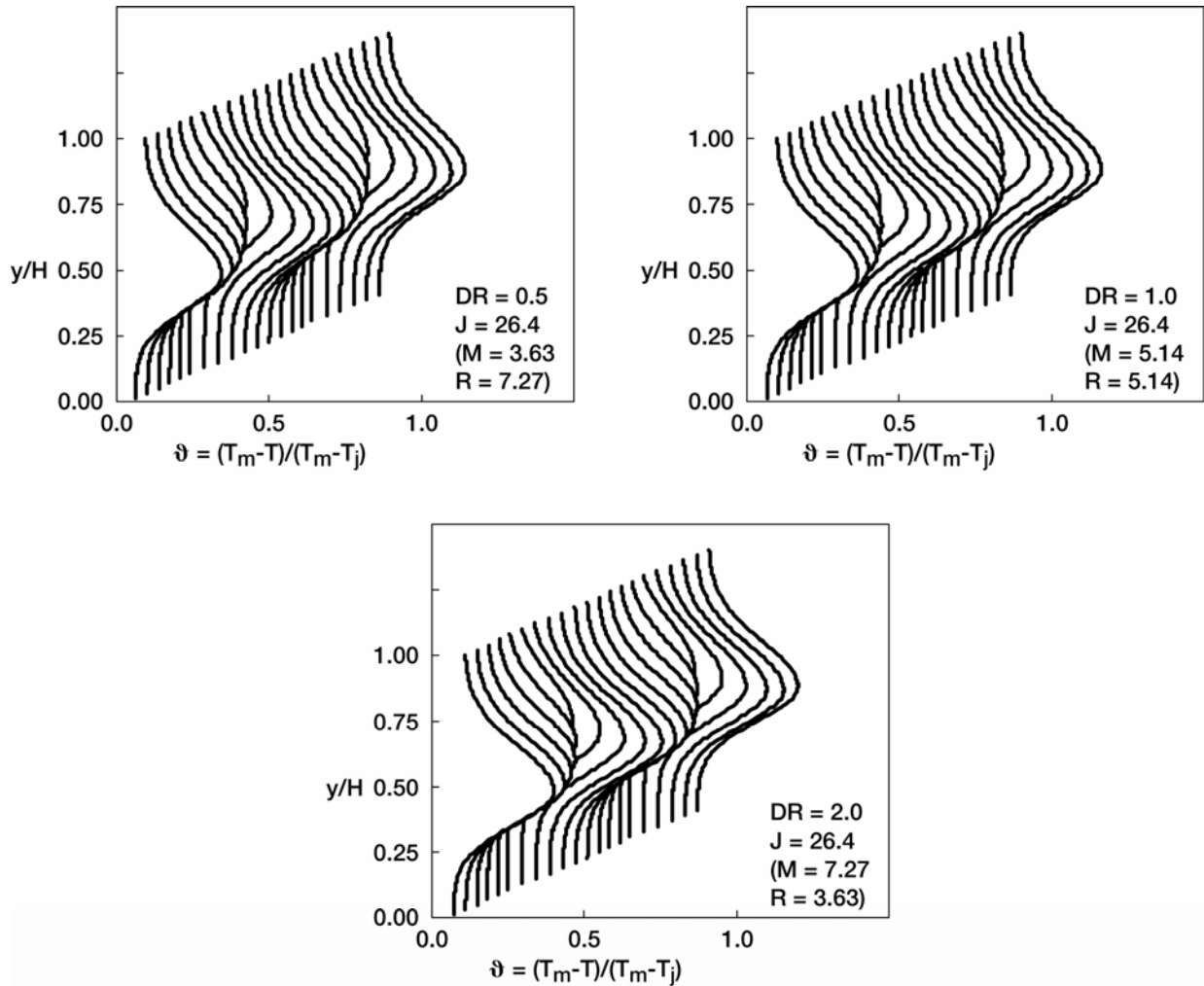


Figure 10.—Variation in scalar distributions with increasing density ratio (DR): orifice configuration F in figure 3 (centerplane at edge [ ]–0–( in spreadsheet)) for  $S/H = 0.5$ ,  $H/d = 5.66$ ,  $(S/d = 2.83, C = 2.57)$  and  $C_d = 0.64$  at  $x/H = 0.5$  ( $x/d = 2.83$ ).

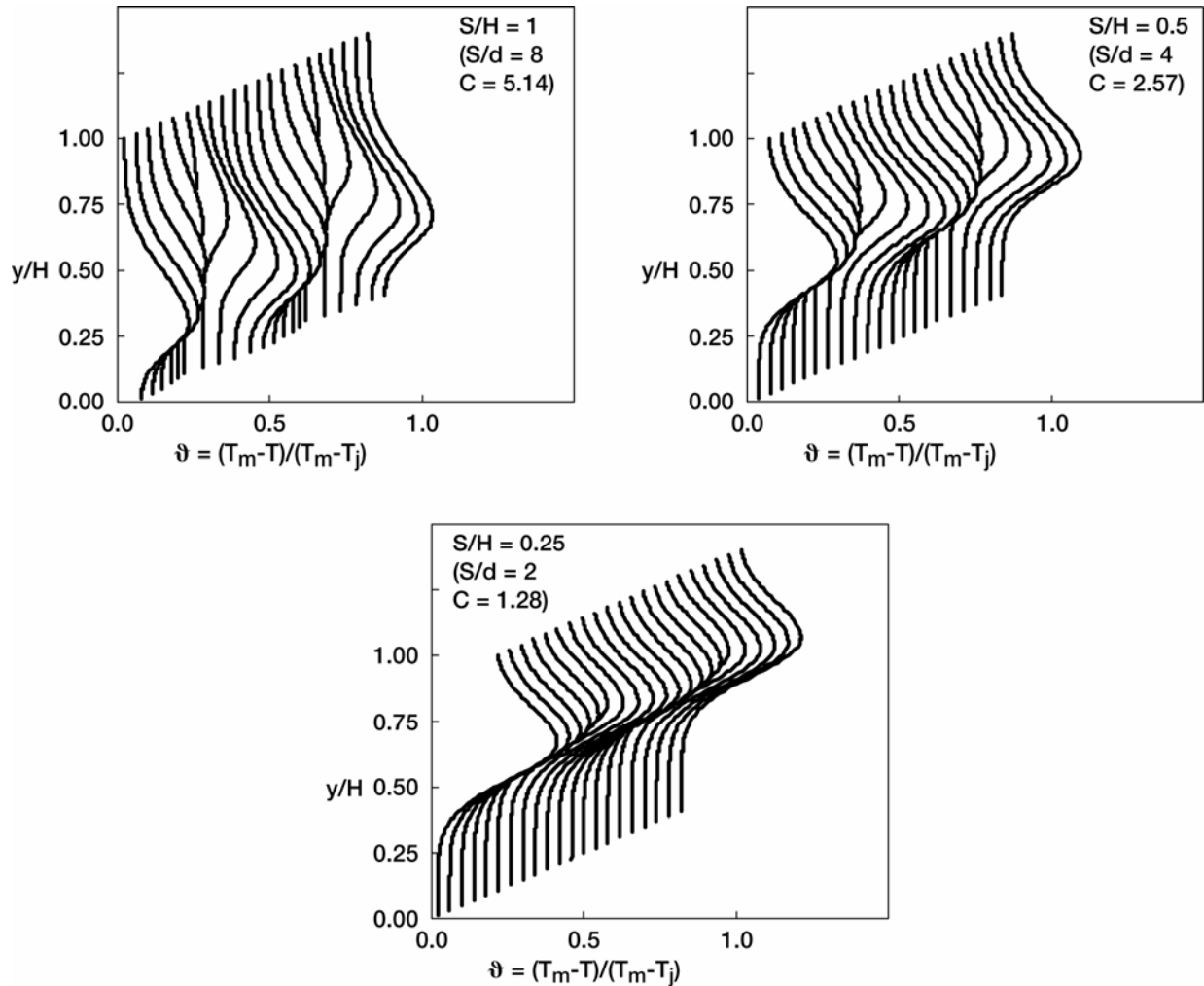


Figure 11.—Variation in scalar distributions with decreasing orifice spacing ( $S/H$ ) at constant orifice diameter: (centerplane at edge [ ]–0–( in spreadsheet)) for ( $H/d = 8$ ,  $DR = 2.2$ ,  $J = 26.4$ , ( $M = 7.62$ ,  $R = 3.46$ , and  $Cd = 0.64$ ) at  $x/H = 0.5$  ( $x/d = 4$ ).

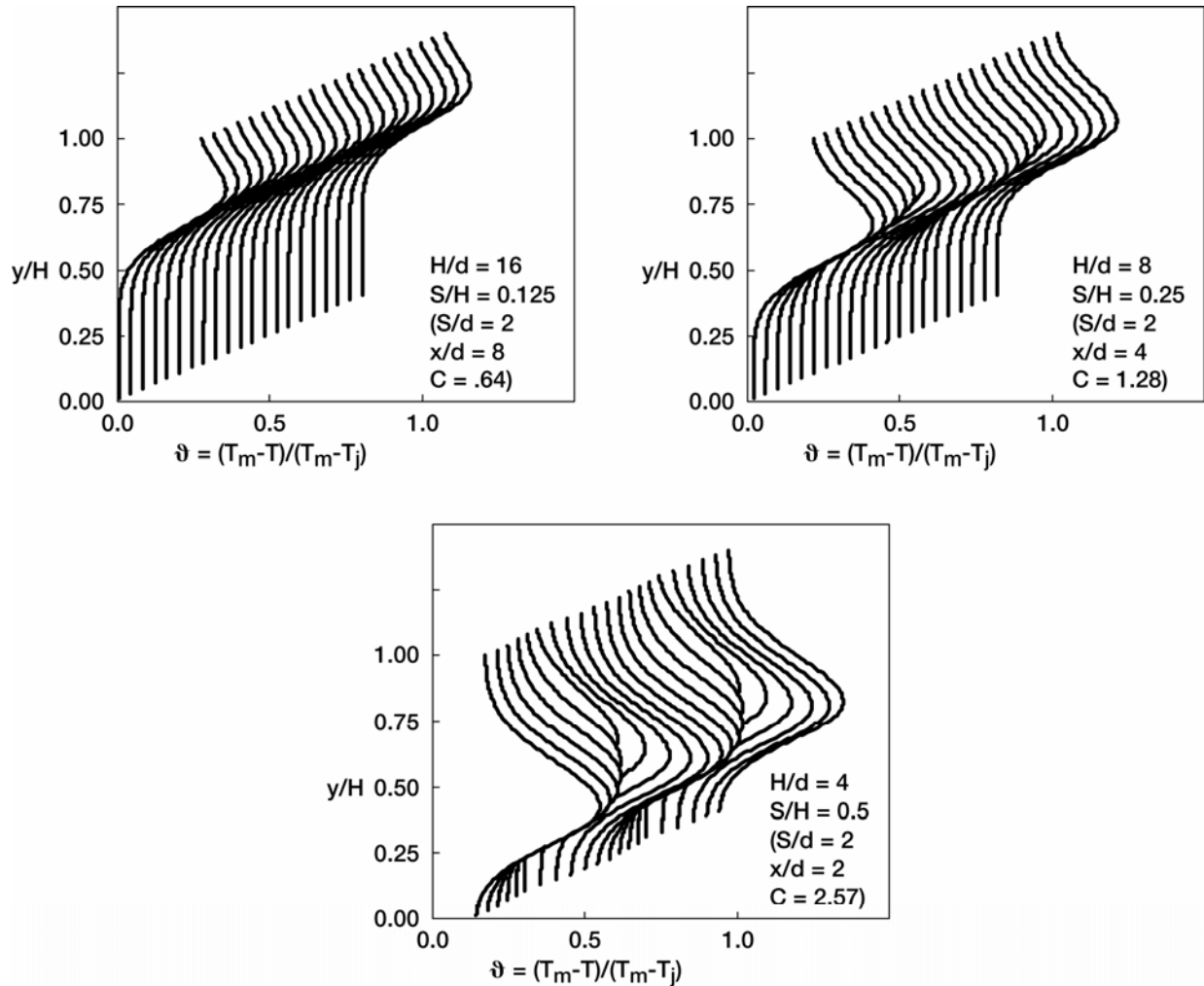


Figure 12.—Variation in scalar distributions with increasing orifice diameter (decreasing  $H/d$ ) at constant  $S/d$ : (centerplane at edge [ ]–0–( in spreadsheet] for  $DR = 2.2$ ,  $J = 26.4$ ,  $(M = 7.62, R = 3.46)$  and  $Cd = 0.64$  at  $x/H = 0.5$ .

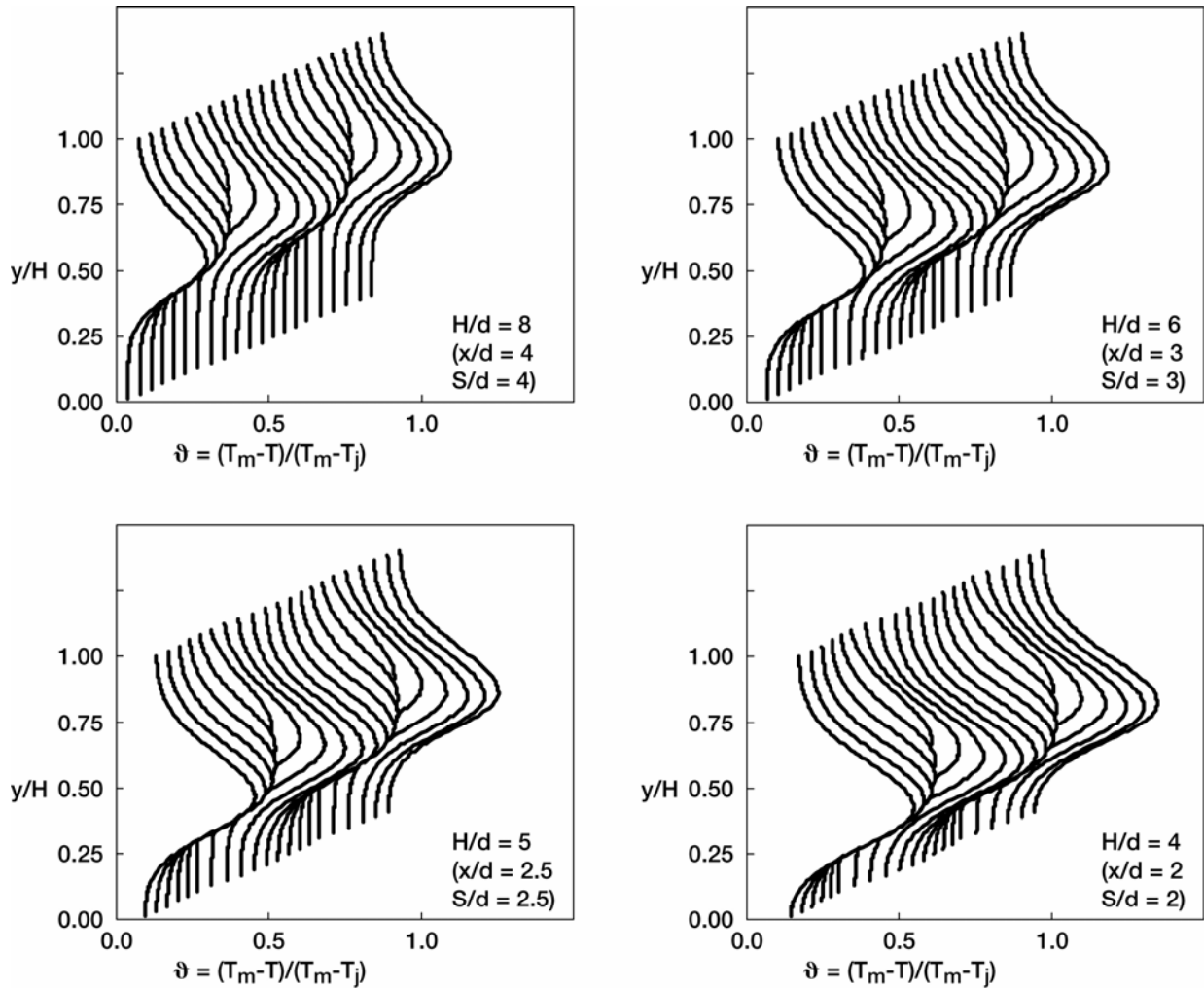


Figure 13a.—Variation in scalar distributions with increasing orifice diameter (decreasing  $H/d$ ) at constant spacing: (centerplane at edge [ ]–0–( in spreadsheet) for  $S/H = 0.5$ ,  $DR = 2.2$ ,  $J = 26.4$ ,  $(M = 7.62, R = 3.46, C = 2.57)$ , and  $Cd = 0.64$  at  $x/H = 0.5$ .

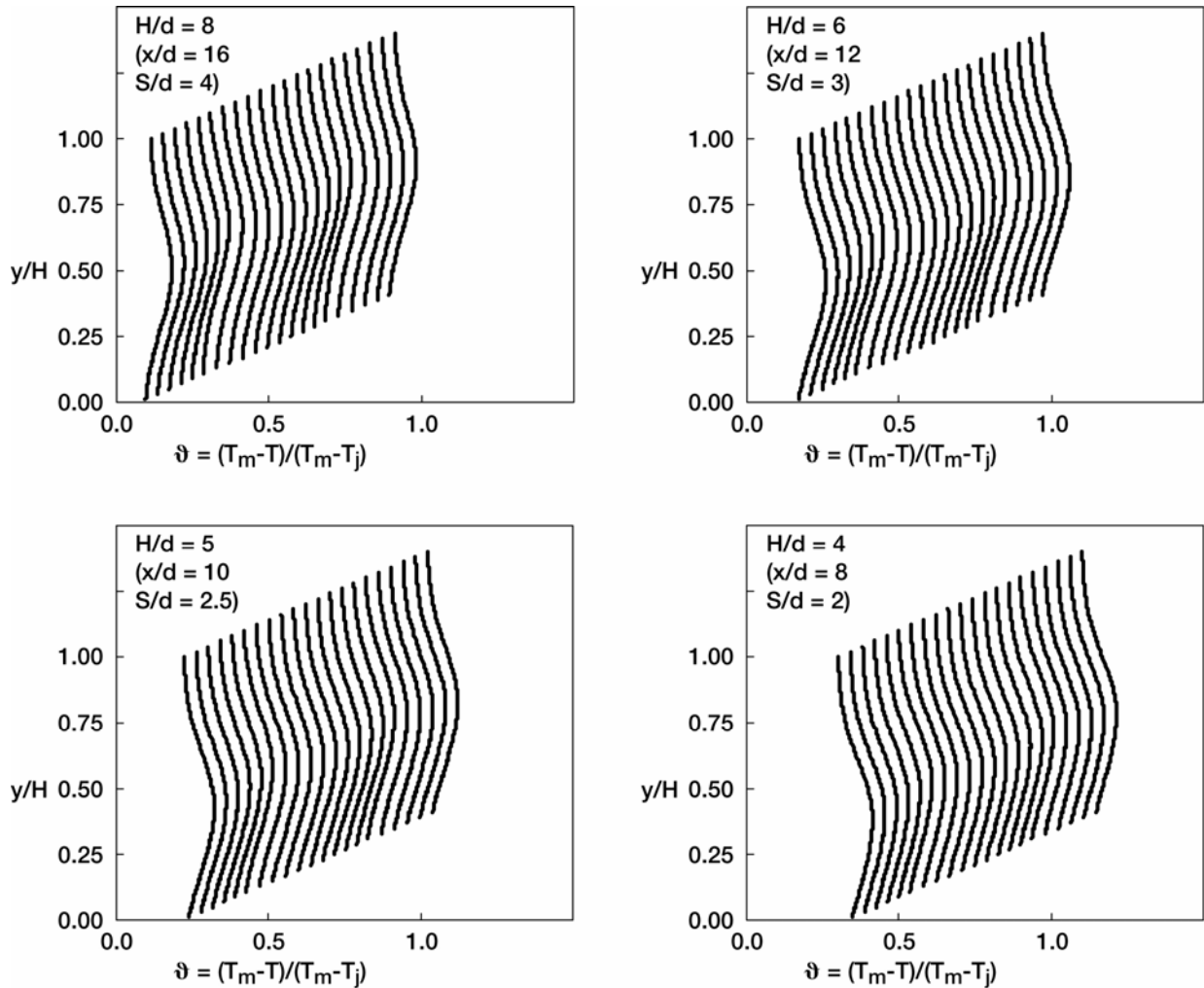


Figure 13b.—Variation in scalar distributions with increasing orifice diameter (decreasing  $H/d$ ) at constant spacing: (centerplane at edge [ ]—0—( in spreadsheet) for  $S/H = 0.5$ ,  $DR = 2.2$ ,  $J = 26.4$ , ( $M = 7.62$ ,  $R = 3.46$ ,  $C = 2.57$ ), and  $Cd = 0.64$  at  $x/H = 2$ .

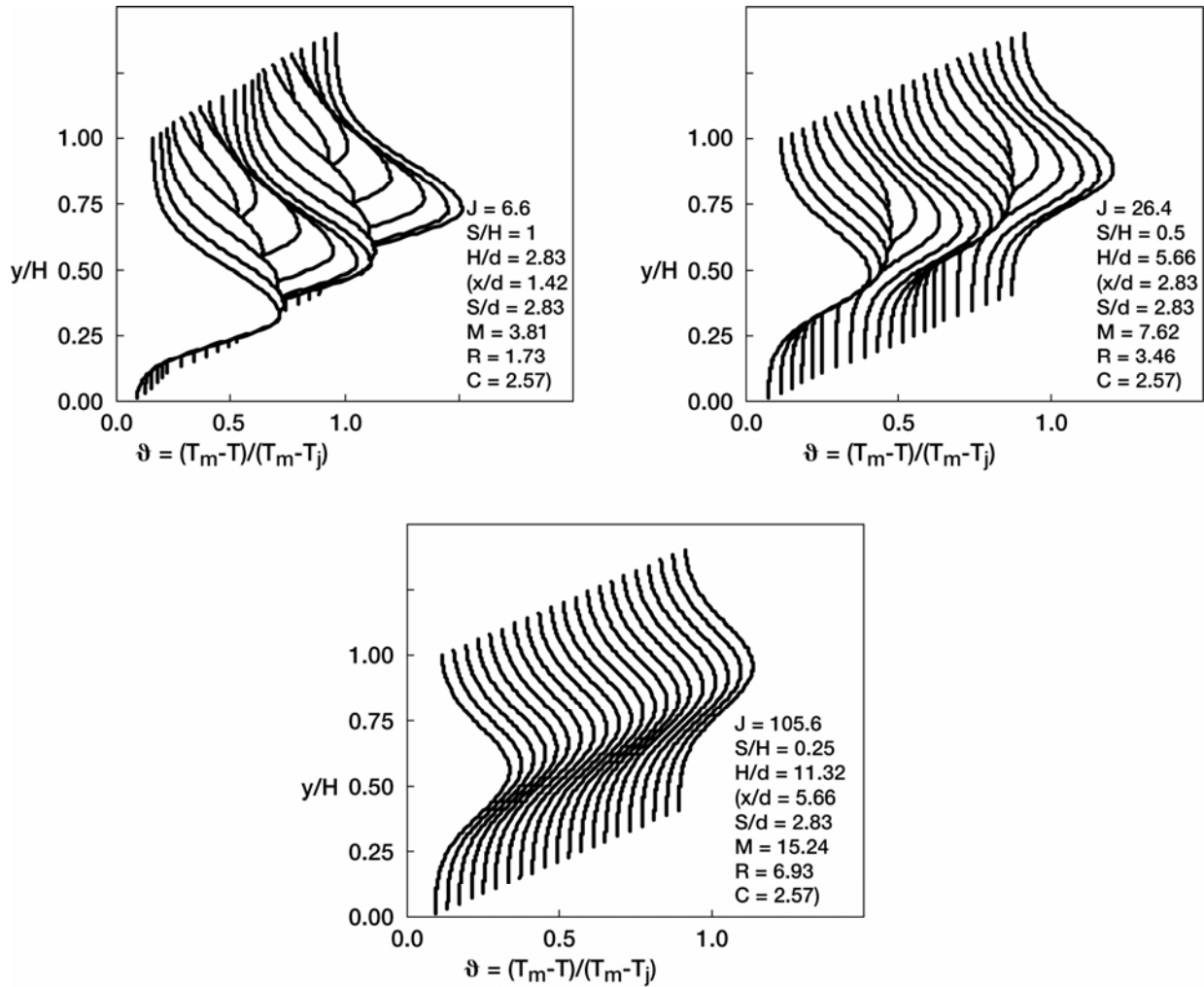


Figure 14a.—Variation in scalar distributions with coupled spacing (S/H) and momentum-flux ratio (J): (centerplane at edge [ ]–0–( in spreadsheet) for DR = 2.2, and Cd = 0.6 at x/H = 0.5.

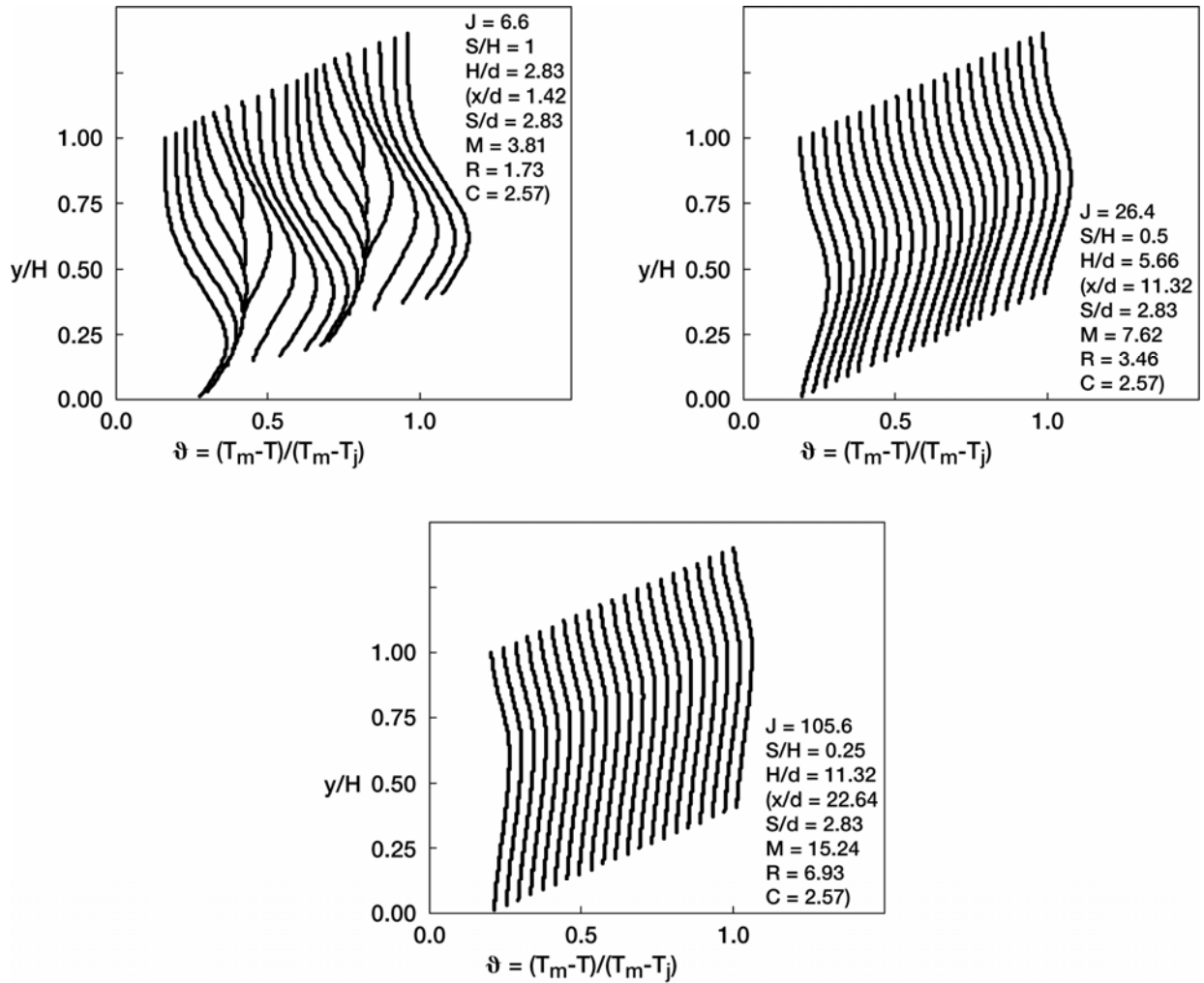


Figure 14b.—Variation in scalar distributions with coupled spacing (S/H) and momentum-flux ratio (J): (centerplane at edge [ ]–0–( in spreadsheet)) for DR = 2.2, and Cd = 0.64 at x/H = 2.

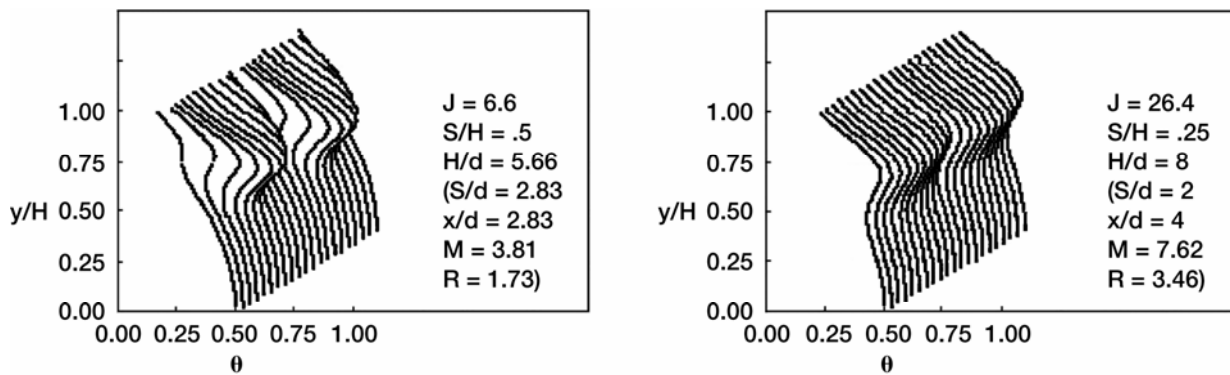


Figure 15a.—Theta profiles for a non-uniform mainstream scalar at x/H = .5 for C = 1.28. (midplane at edge [–0–0– in spreadsheet]) DR = 2.2, Cd = 0.64.

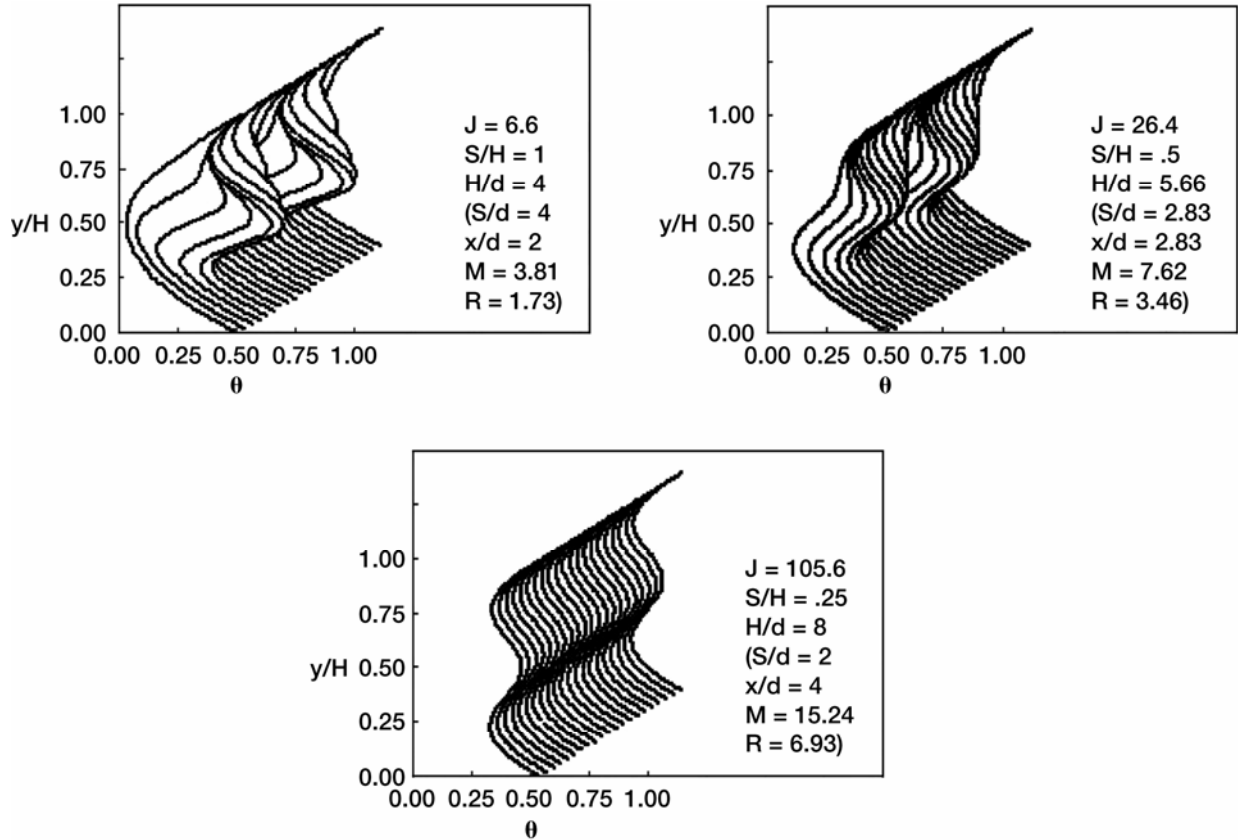


Figure 15b.—Theta profiles for a non-uniform mainstream scalar at  $x/H = .5$  for  $C = 2.57$ . (midplane at edge [-0-0- in spreadsheet])  $DR = 2.2$ ,  $Cd = 0.64$ .

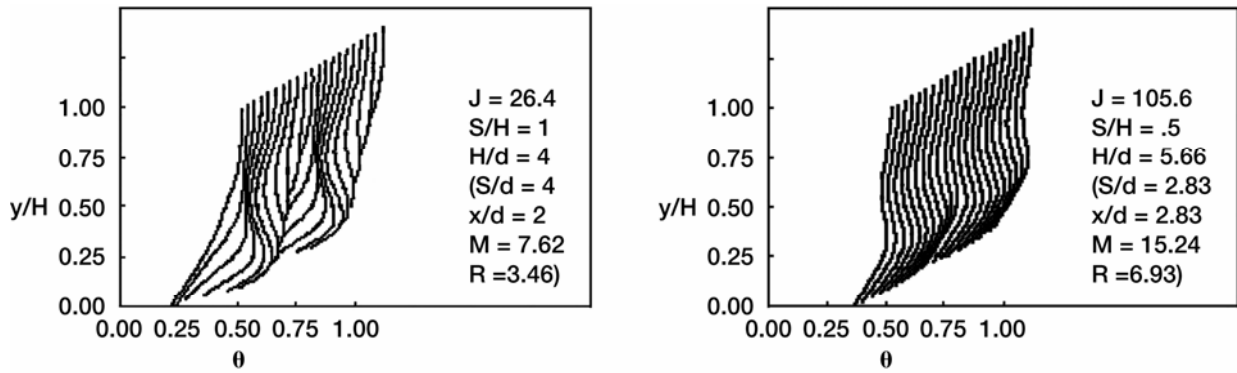


Figure 15c.—Theta profiles for a non-uniform mainstream scalar at  $x/H = .5$  for  $C = 5.14$ . (midplane at edge [-0-0- in spreadsheet])  $DR = 2.2$ ,  $Cd = 0.64$ .

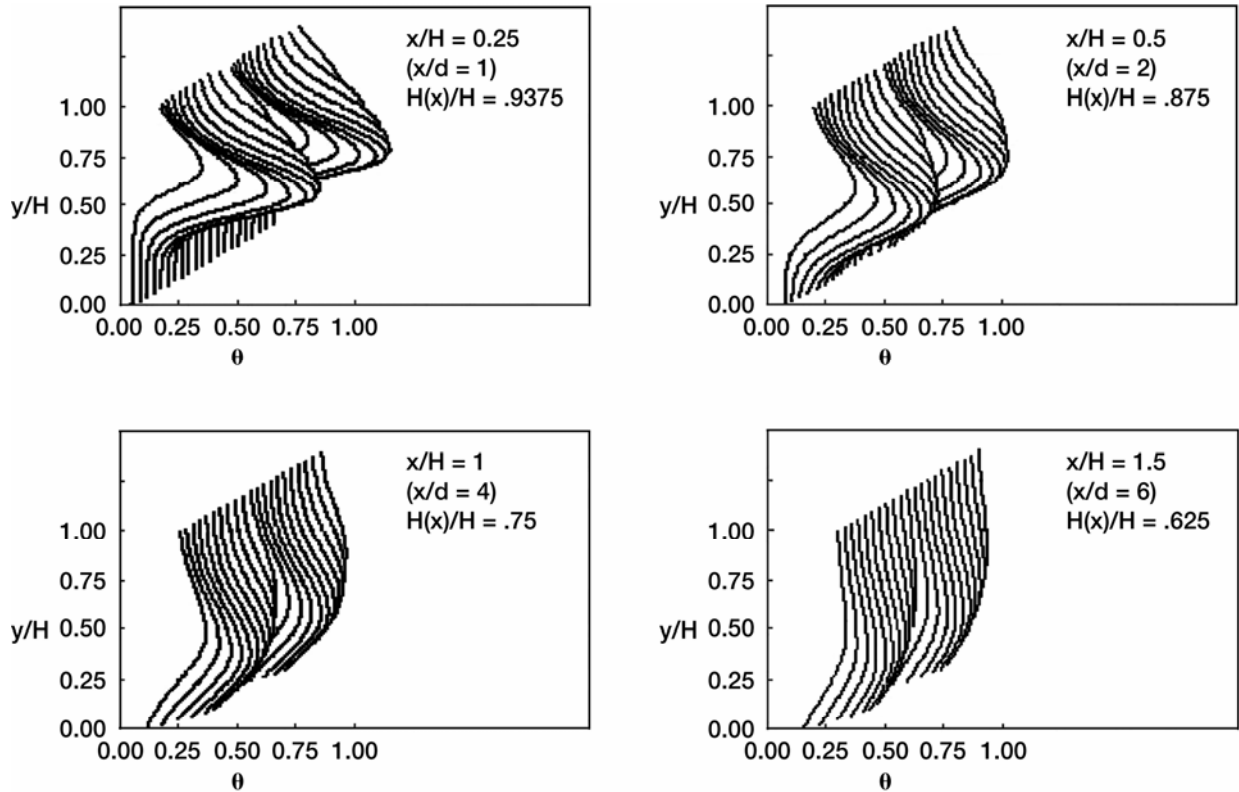


Figure 16a.—Scalar profiles with flow area convergence = .25 cm/cm: orifice configuration H in figure 3 (midplane at edge [-0-0- in spreadsheet]) for  $S/H = .5$ ,  $H/d = 4$ , ( $S/d = 2$ ),  $DR = 2.2$ ,  $J = 26.4$ , ( $M = 7.62$ ,  $R = 3.46$ ,  $C = 2.57$ ), and  $C_d = 0.64$ .

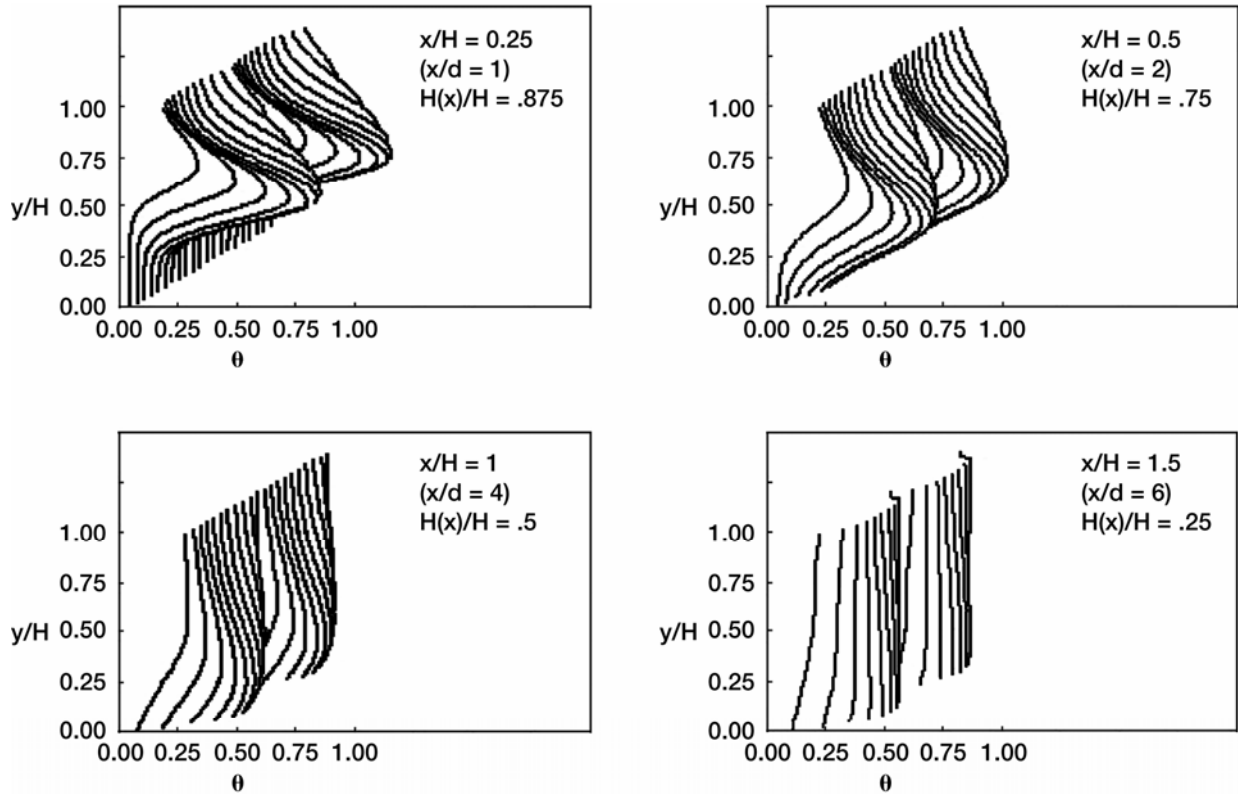


Figure 16b.—Scalar profiles with flow area convergence  $dH/dx = 5 \text{ cm/cm}$ : orifice configuration H in figure 3 (midplane at edge [-0-0- in spreadsheet]) for  $S/H = .5$ ,  $H/d = 4$ , ( $S/d = 2$ ),  $DR = 2.2$ ,  $J = 26.4$ , ( $M = 7.62$ ,  $R = 3.46$ ,  $C = 2.57$ ), and  $Cd = 0.64$ .

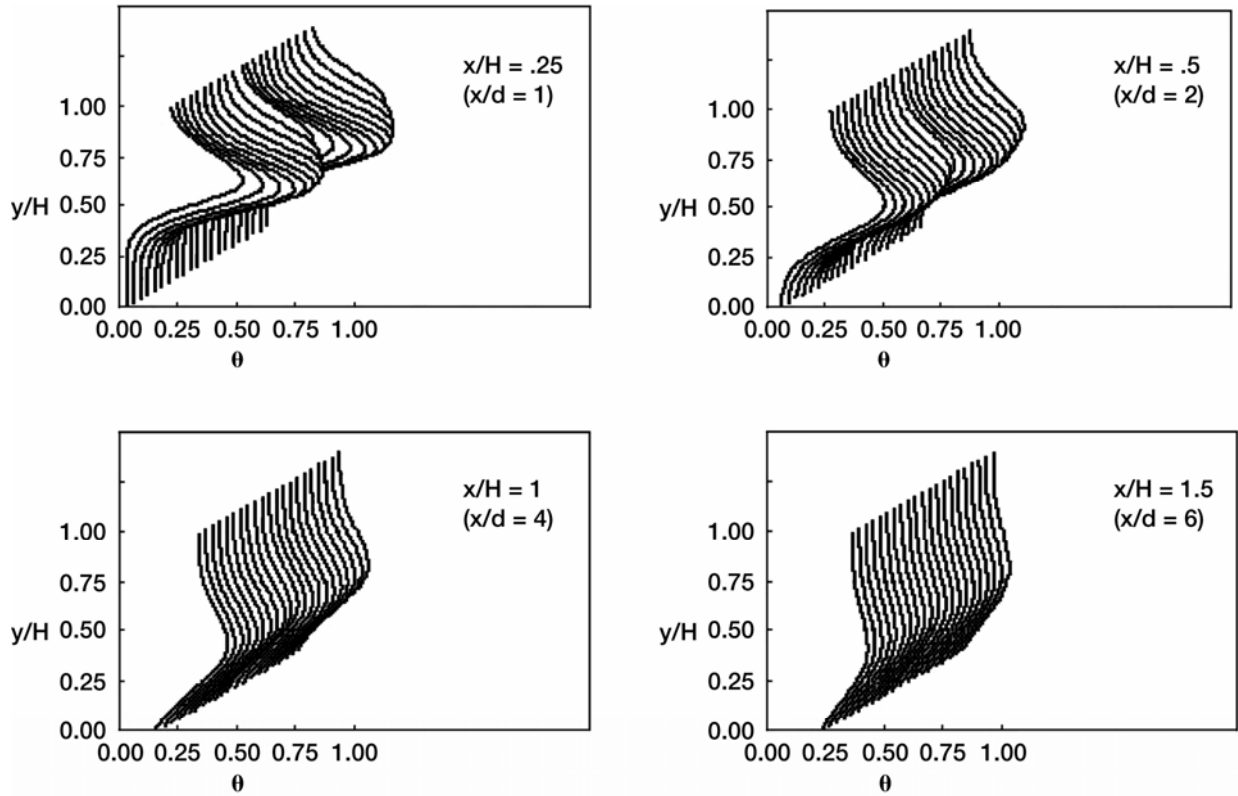


Figure 17a.—Scalar profiles for bluff slots with  $L/W = 2.8$ : orifice configuration K in figure 3 (midplane at edge [-0-0- in spreadsheet]) for  $S/H = .5$ ,  $H/d = 4$ , ( $S/d = 2$ ),  $DR = 2.2$ ,  $J = 26.4$ , ( $M = 7.62$ ,  $R = 3.46$ ,  $C = 2.57$ ), and  $Cd = 0.64$ .

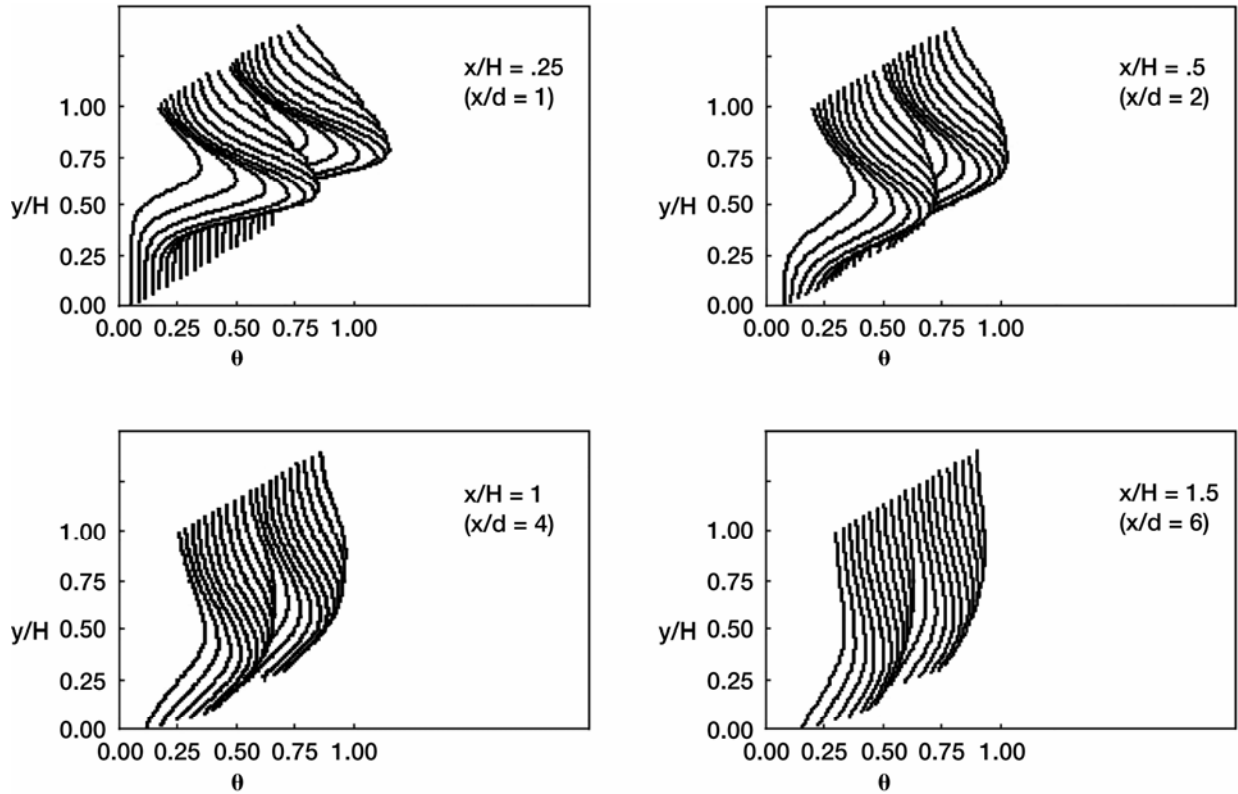


Figure 17b.—Scalar profiles for streamlined slots with  $L/W = 2.8$ : orifice configuration L in figure 3 (midplane at edge [-0-0- in spreadsheet]) for  $S/H = .5$ ,  $H/d = 4$ , ( $S/d = 2$ ),  $DR = 2.2$ ,  $J = 26.4$ , ( $M = 7.62$ ,  $R = 3.46$ ,  $C = 2.57$ ), and  $C_d = 0.64$ .

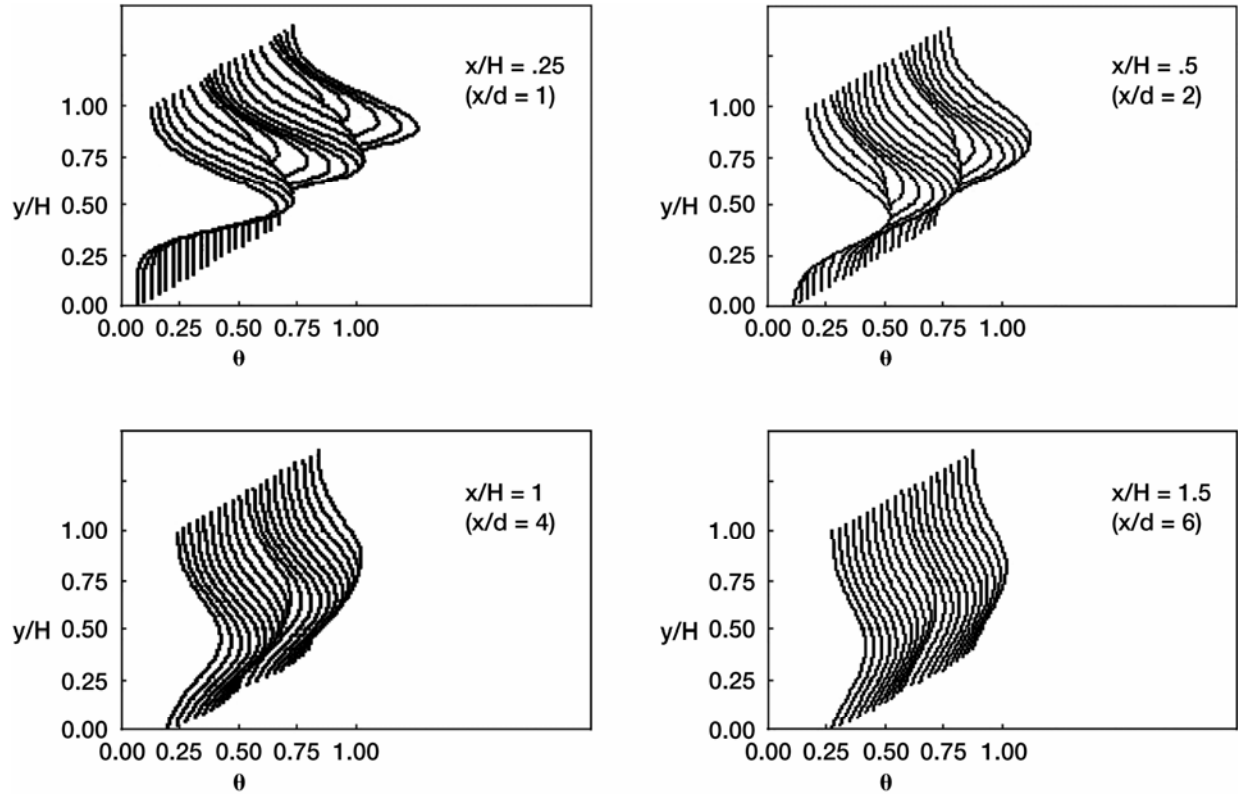


Figure 18.—Scalar profiles for slanted slots with  $L/W = 2.8$ : orifice configuration M in figure 3 (midplane at edge [-0-0- in spreadsheet]) for  $S/H = .5$ ,  $H/d = 4$ , ( $S/d = 2$ ),  $DR = 2.2$ ,  $J = 26.4$ , ( $M = 7.62$ ,  $R = 3.46$ ,  $C = 2.57$ ), and  $Cd = 0.64$ .

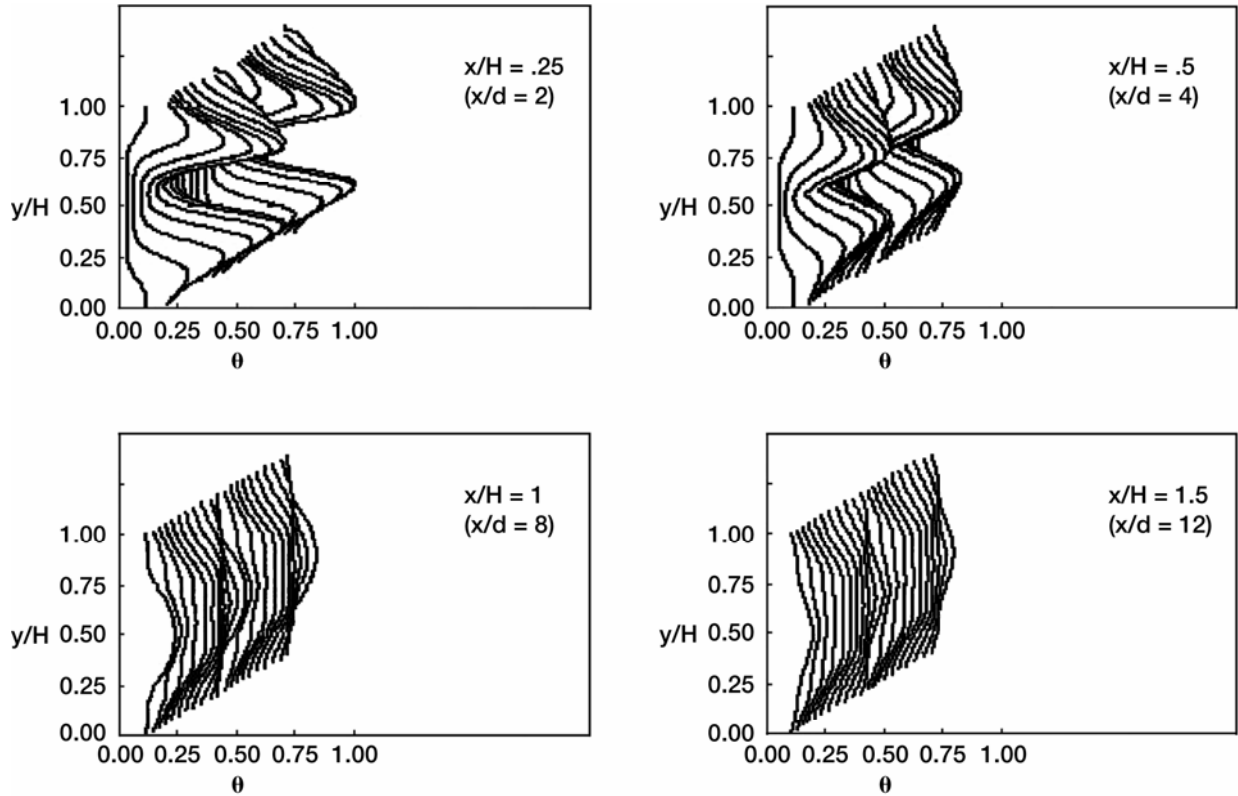


Figure 19a.—Scalar profiles for opposed rows of jets with centerlines in-line: orifice configuration D in figure 3 (midplane at edge [-0-0- in spreadsheet]) for  $S/H = .5$ ,  $H/d = 8$ , ( $S/d = 4$ ),  $DR = 2.2$ ,  $J = 6.6$ , ( $M = 3.81$ ,  $R = 1.73$ ,  $C = 1.28$ ), and  $C_d = 0.64$ .

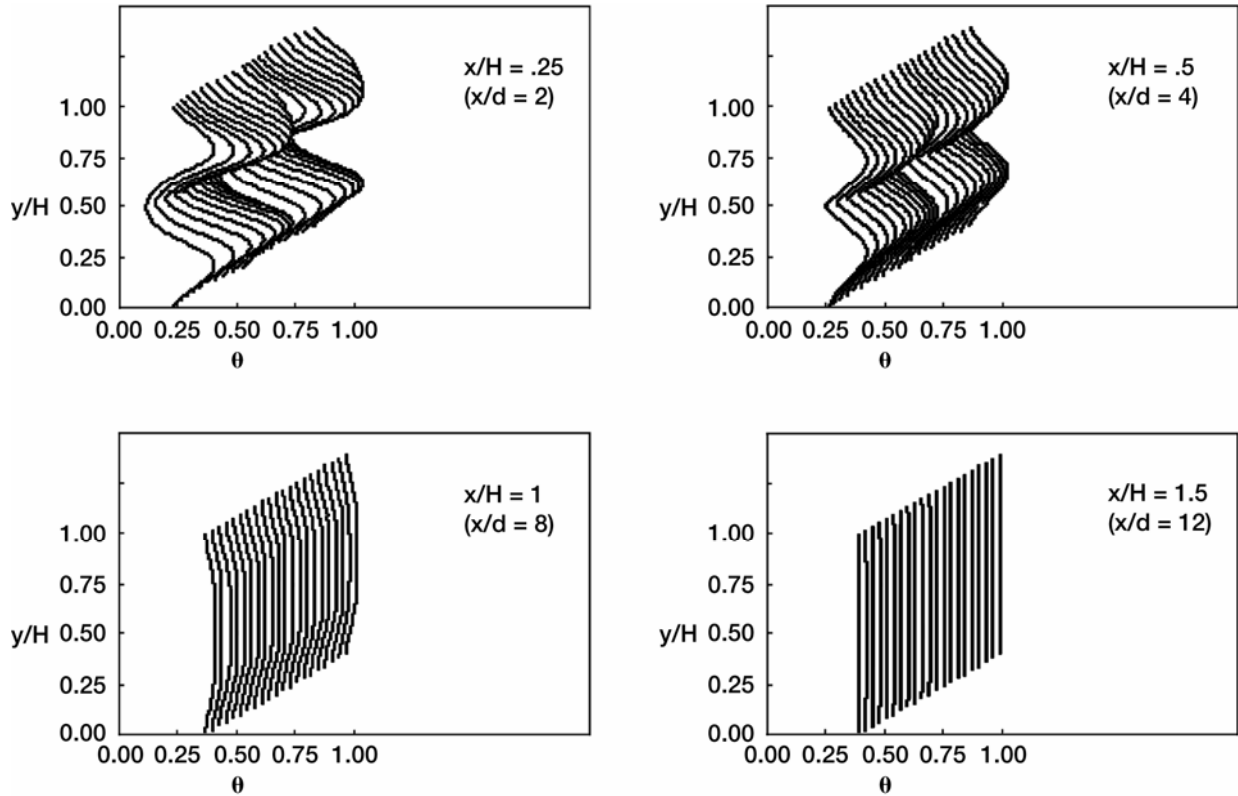


Figure 19b.—Scalar profiles for opposed rows of jets with centerlines in-line: orifice configuration C in figure 3 (midplane at edge [-0-0- in spreadsheet]) for  $S/H = .25$ ,  $H/d = 8$ , ( $S/d = 2$ ),  $DR = 2.2$ ,  $J = 26.4$ , ( $M = 7.62$ ,  $R = 3.46$ ,  $C = 1.28$ ), and  $C_d = 0.64$ .

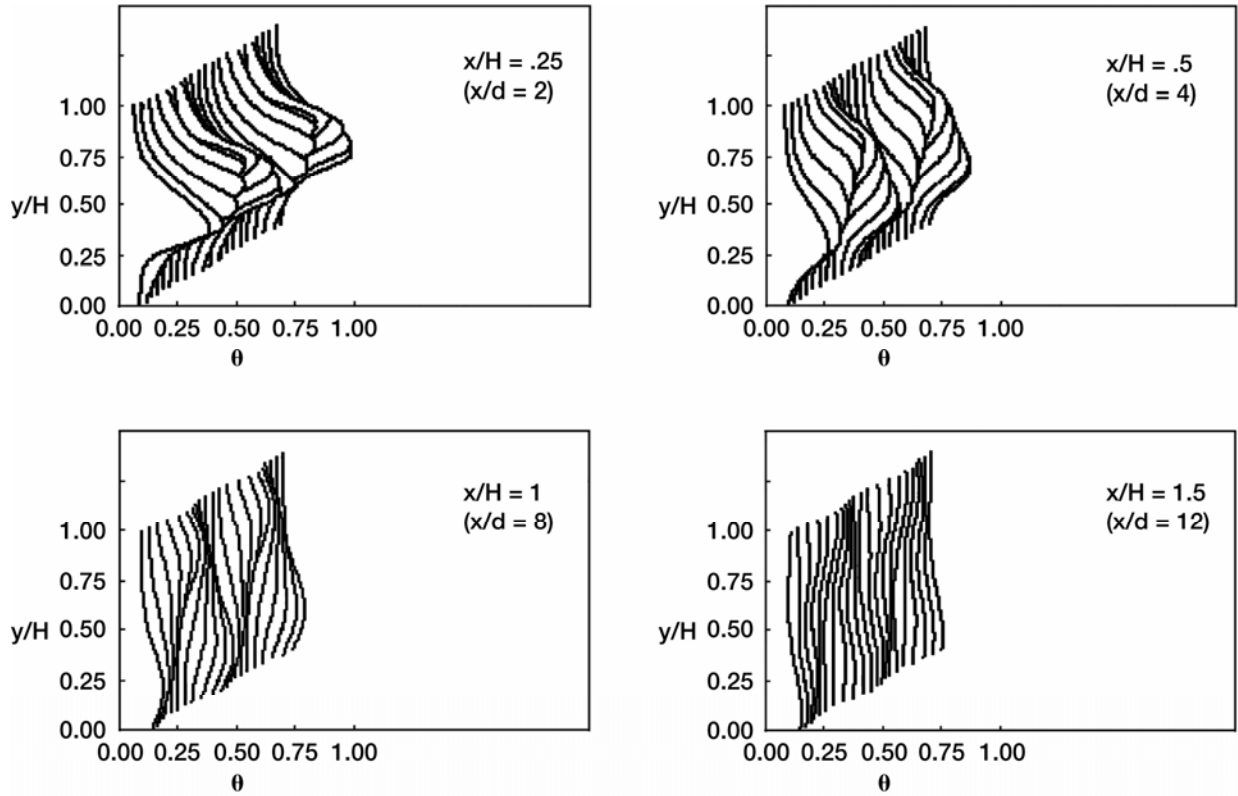


Figure 20a.—Scalar profiles for opposed rows of jets with centerlines staggered: orifice configuration E in figure 3 for  $S/H = 1$ ,  $H/d = 8$ ,  $(S/d = 8)$ ,  $DR = 2.2$ ,  $J = 26.4$ ,  $(M = 7.62, R = 3.46, C = 5.14)$ , and  $Cd = 0.64$ .

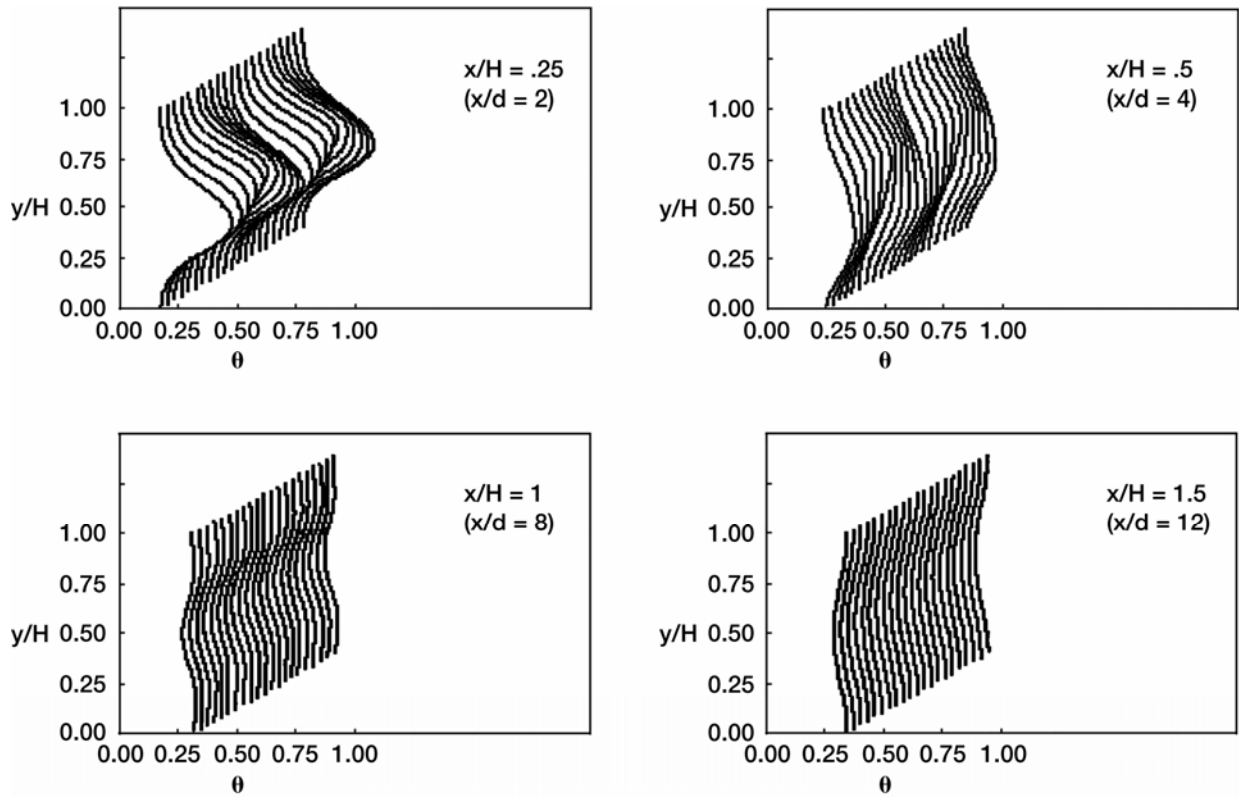


Figure 20b.—Scalar profiles for opposed rows of jets with centerlines staggered: orifice configuration D in figure 3 for  $S/H = .5$ ,  $H/d = 8$ , ( $S/d = 4$ ),  $DR = 2.2$ ,  $J = 105.6$ , ( $M = 15.24$ ,  $R = 6.93$ ,  $C = 5.14$ ), and  $Cd = 0.64$ .

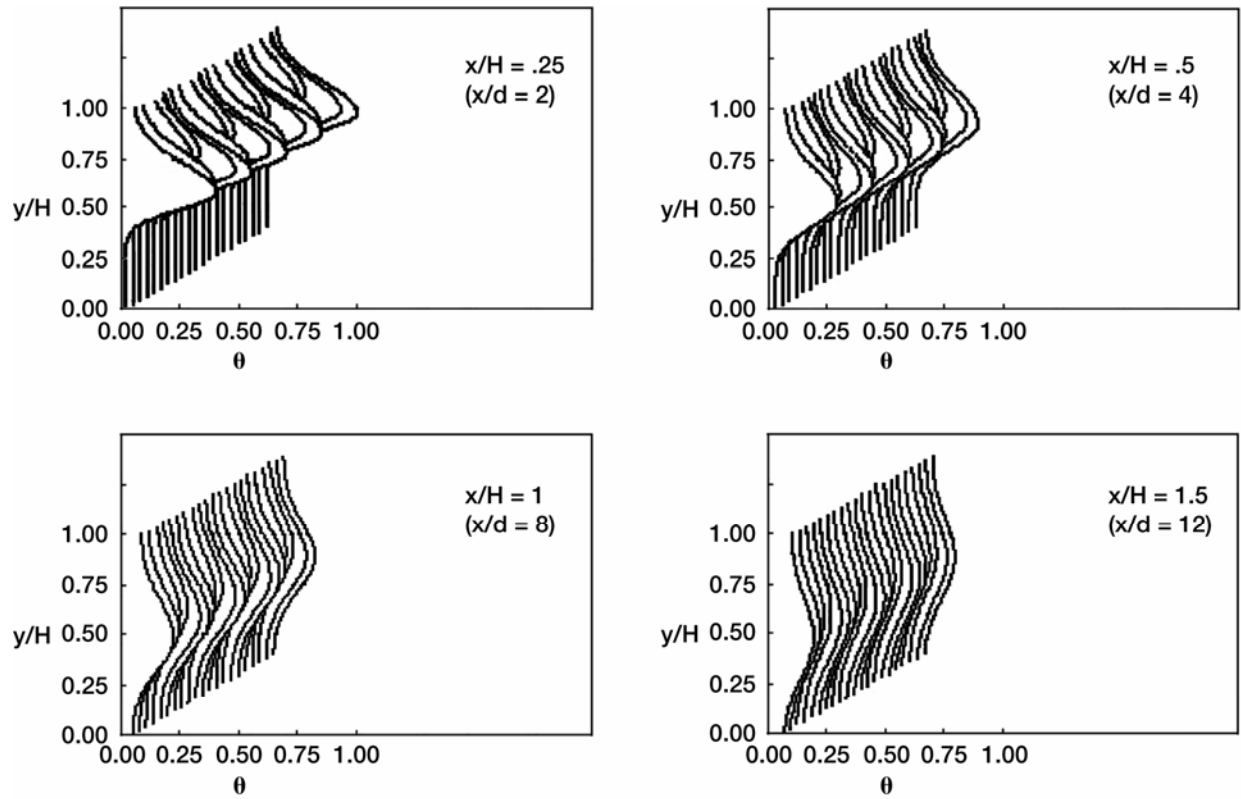


Figure 20c.—Scalar profiles for single-side injection with 4 jets shown: orifice configuration E in figure 3 for  $S/H = .5$ ,  $H/d = 8$ , ( $S/d = 4$ ),  $DR = 2.2$ ,  $J = 26.4$ , ( $M = 7.62$ ,  $R = 3.46$ ,  $C = 2.57$ ), and  $C_d = 0.64$ .

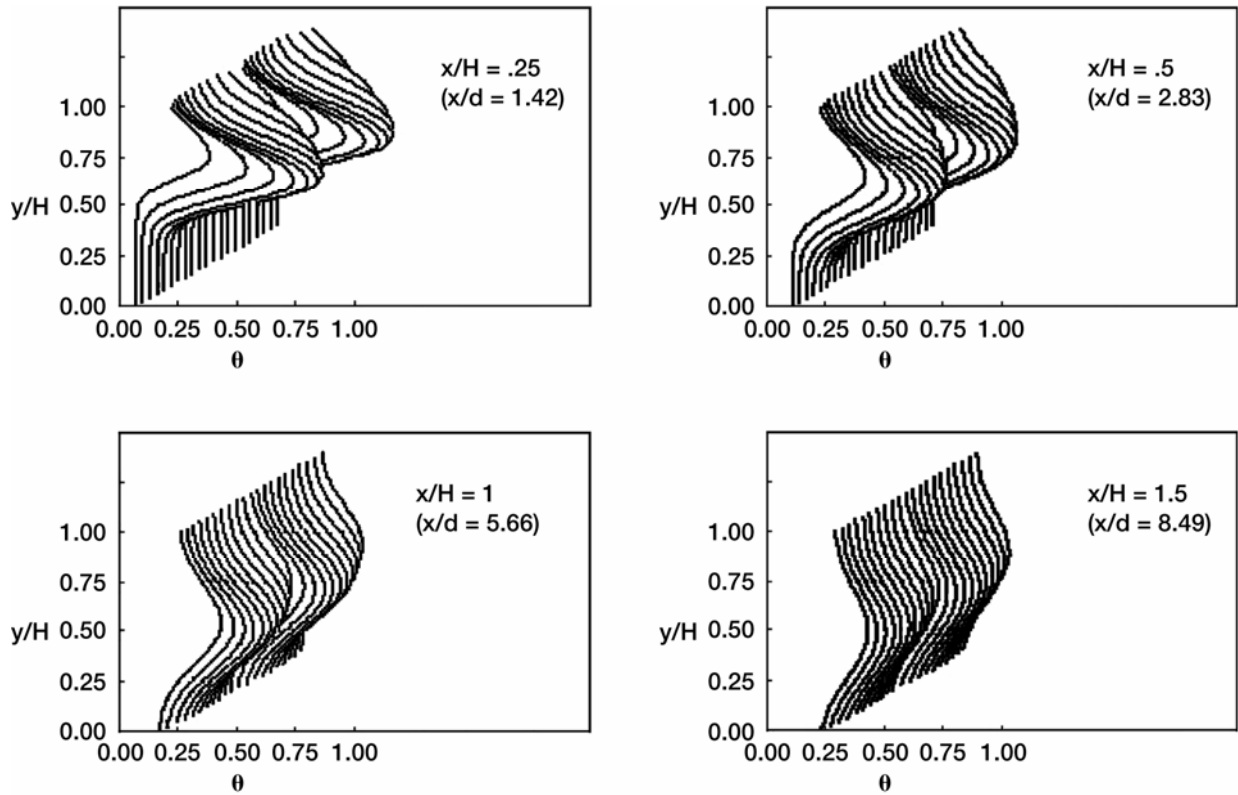


Figure 21a.—Scalar profiles for double rows with centerlines in-line for  $S_x/H = 0$ : orifice configuration F in figure 3 (midplane at edge [-0-0- in spreadsheet]) for  $S/H = .5$ ,  $H/d = 5.66$ , ( $S/d = 2.83$ ),  $DR = 2.2$ ,  $J = 26.4$ , ( $M = 7.62$ ,  $R = 3.46$ ,  $C = 2.57$ ), and  $C_d = 0.64$ . ( $x/H = 0$  at center of 1st row of holes; trailing edge of 2nd row is at  $x/H = .088$ .)

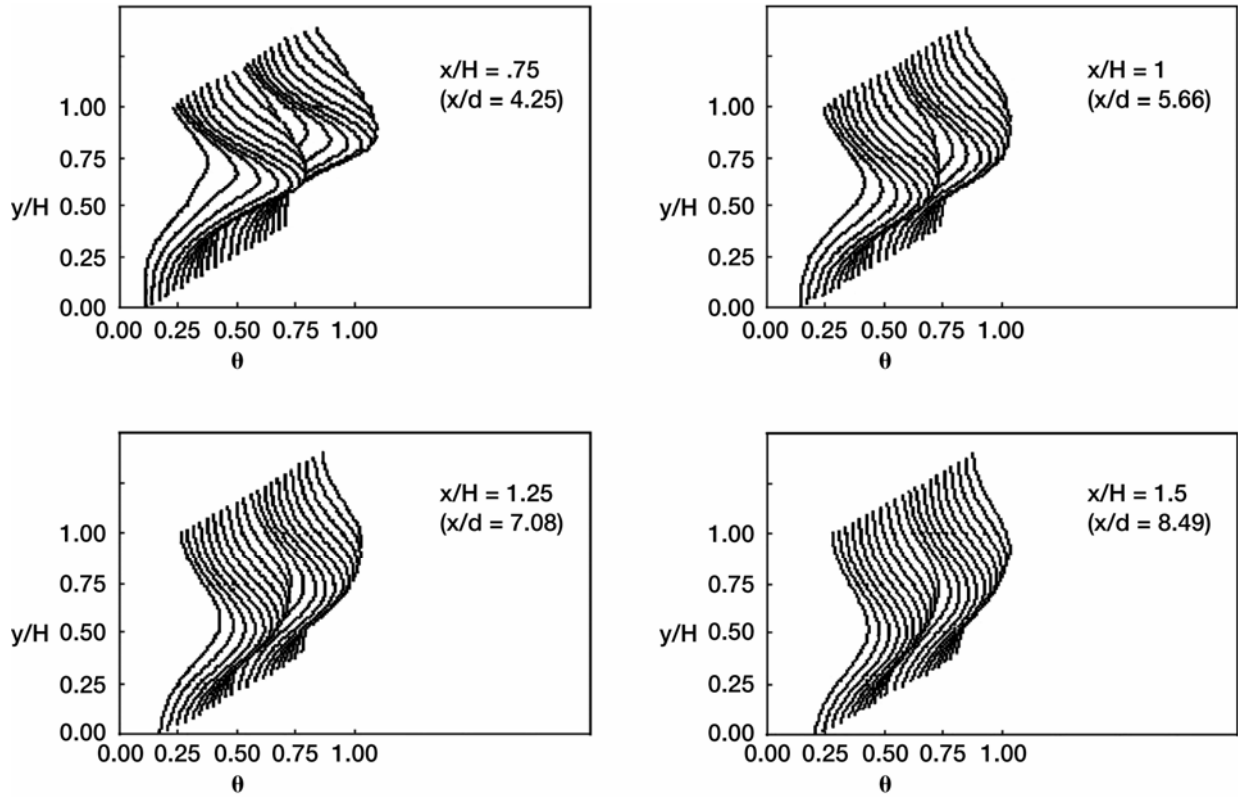


Figure 21b.—Scalar profiles for double rows with centerlines in-line for  $Sx/H = .5$ : orifice configuration F in figure 3 (midplane at edge [-0-0- in spreadsheet]) for  $S/H = .5$ ,  $H/d = 5.66$ , ( $S/d = 2.83$ ),  $DR = 2.2$ ,  $J = 26.4$ , ( $M = 7.62$ ,  $R = 3.46$ ,  $C = 2.57$ ), and  $C_d = 0.64$ . ( $x/H = 0$  at center of 1st row of holes; trailing edge of 2nd row is at  $x/H = .588$ .)

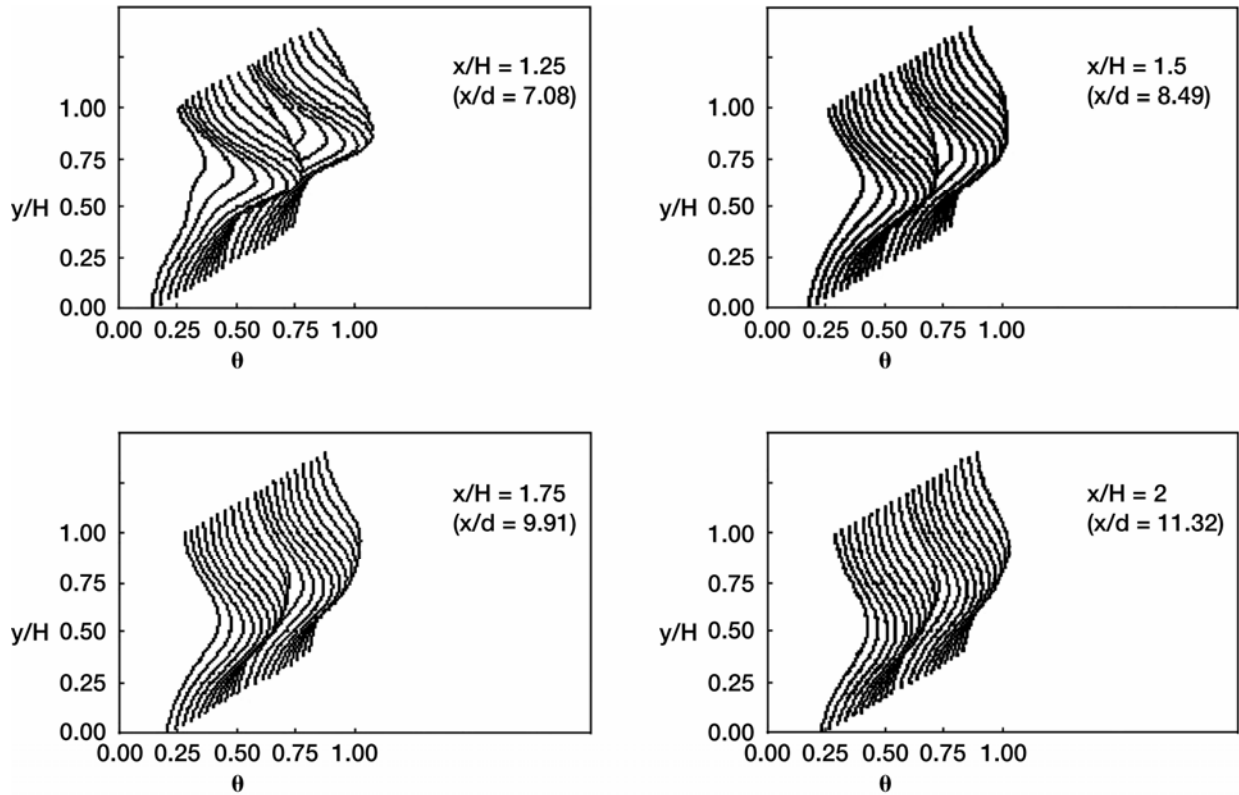


Figure 21c.—Scalar profiles for double rows with centerlines in-line for  $S_x/H = 1$ : orifice configuration F in figure 3 (midplane at edge [-0-0- in spreadsheet]) for  $S/H = .5$ ,  $H/d = 5.66$ ,  $(S/d = 2.83)$ ,  $DR = 2.2$ ,  $J = 26.4$ ,  $(M = 7.62, R = 3.46, C = 2.57)$ , and  $C_d = 0.64$ . ( $x/H = 0$  at center of 1st row of holes; trailing edge of 2nd row is at  $x/H = 1.088$ .)

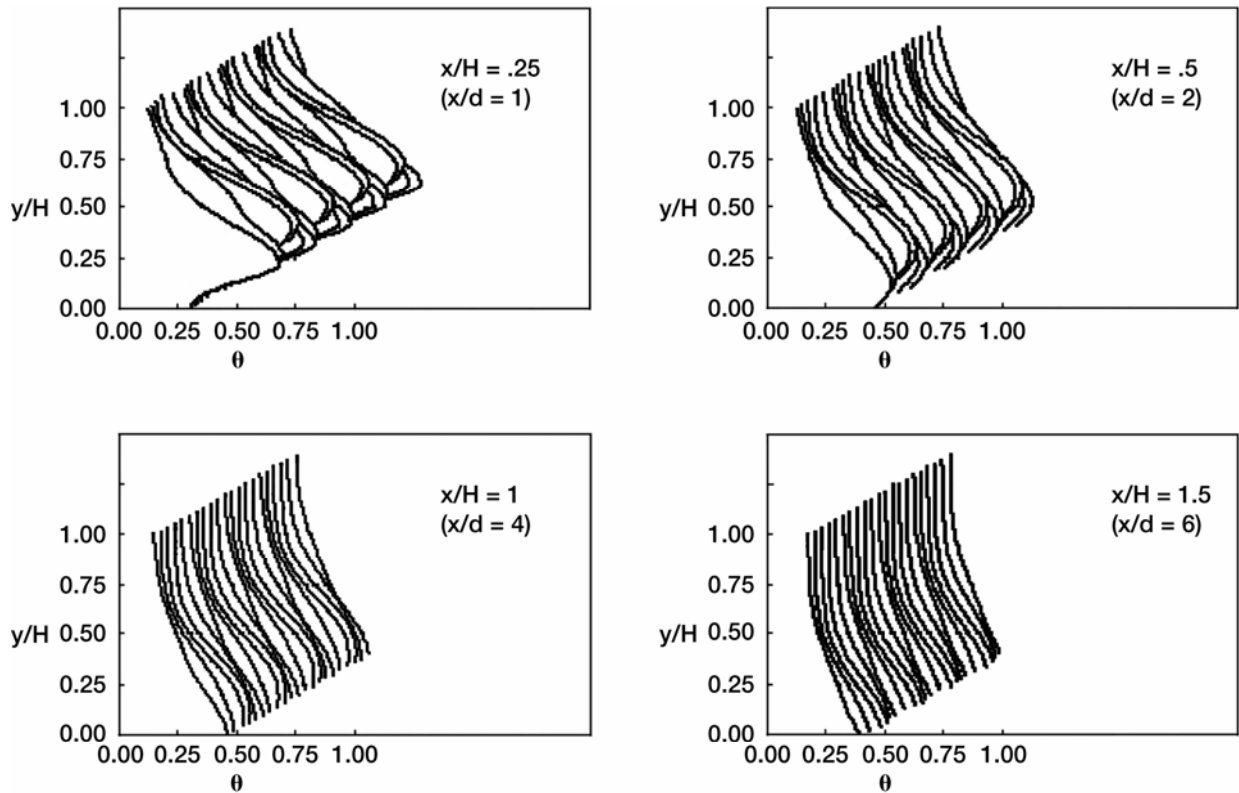


Figure 22a.—Scalar profiles for a single row with 4 holes displayed for  $S/H = .5$ ,  $H/d = 4$ , and  $J = 26.4$  calculated as double rows with centerlines staggered for  $S_x/H = 0$ : orifice configuration I in figure 3 with  $S/H = 1$ ,  $H/d = 4$ , ( $S/d = 4$ ),  $DR = 2.2$ ,  $J = 26.4$ , ( $M = 7.62$ ,  $R = 3.46$ ,  $C = 5.14$ ), and  $C_d = 0.64$ . ( $x/H = 0$  at center of 1st row of holes; trailing edge of 2nd row is at  $x/H = .125$ .)

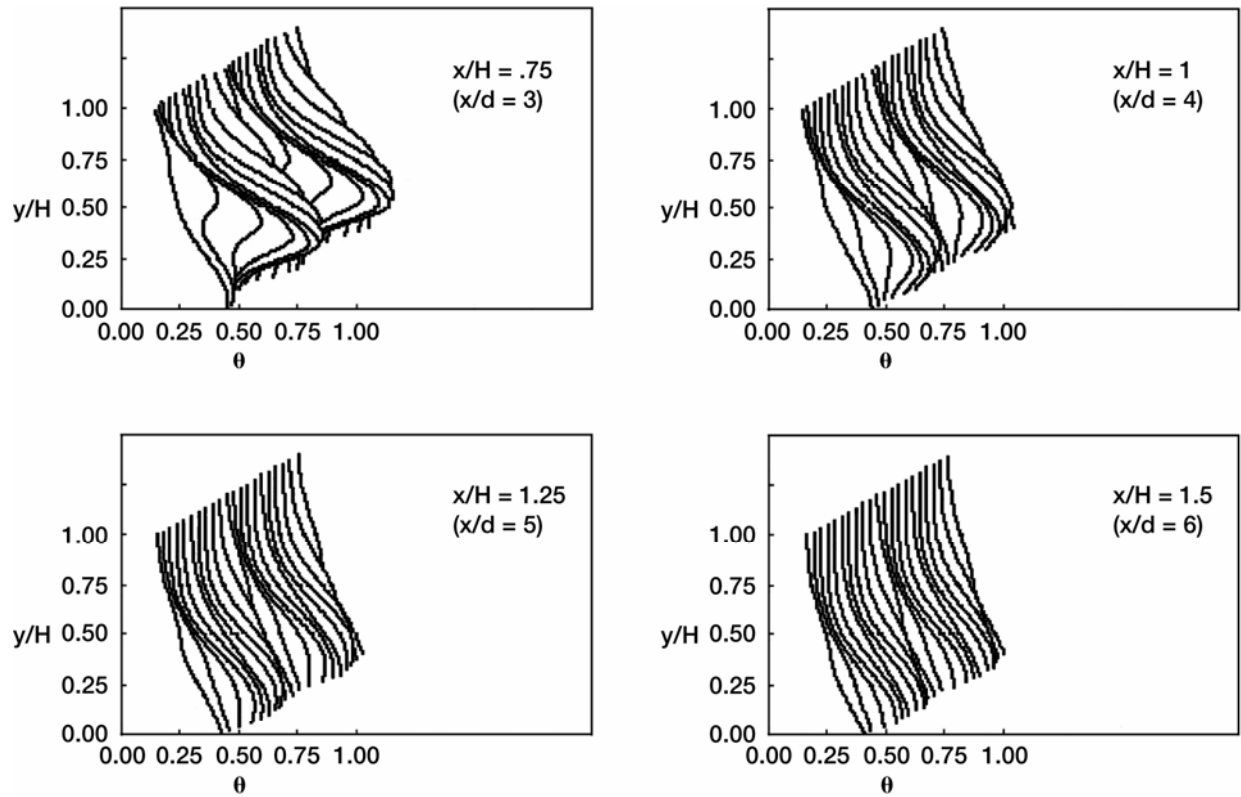


Figure 22b.—Scalar profiles for double rows with centerlines staggered for  $Sx/H = .5$ : orifice configuration I in figure 3 with  $S/H = 1$ ,  $H/d = 4$ , ( $S/d = 4$ ),  $DR = 2.2$ ,  $J = 26.4$ , ( $M = 7.62$ ,  $R = 3.46$ ,  $C = 5.14$ ), and  $C_d = 0.64$ . ( $x/H = 0$  at center of 1st row of holes; trailing edge of 2nd row is at  $x/H = .625$ .)

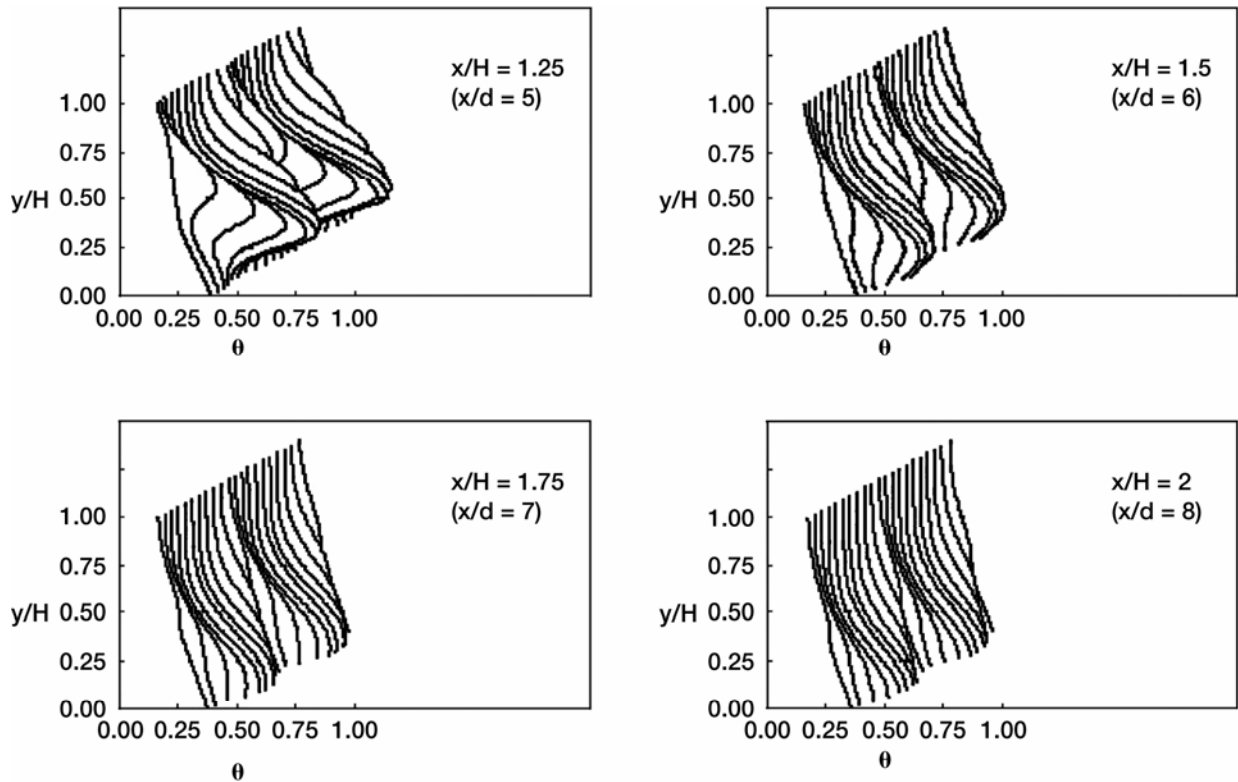


Figure 22c.—Scalar profiles for double rows with centerlines staggered for  $Sx/H = 1$ : orifice configuration I in figure 3 with  $S/H = 1$ ,  $H/d = 4$ ,  $(S/d = 4)$ ,  $DR = 2.2$ ,  $J = 26.4$ ,  $(M = 7.62, R = 3.46, C = 5.14)$ , and  $Cd = 0.64$ . ( $x/H = 0$  at center of 1st row of holes; trailing edge of 2nd row is at  $x/H = 1.125$ .)

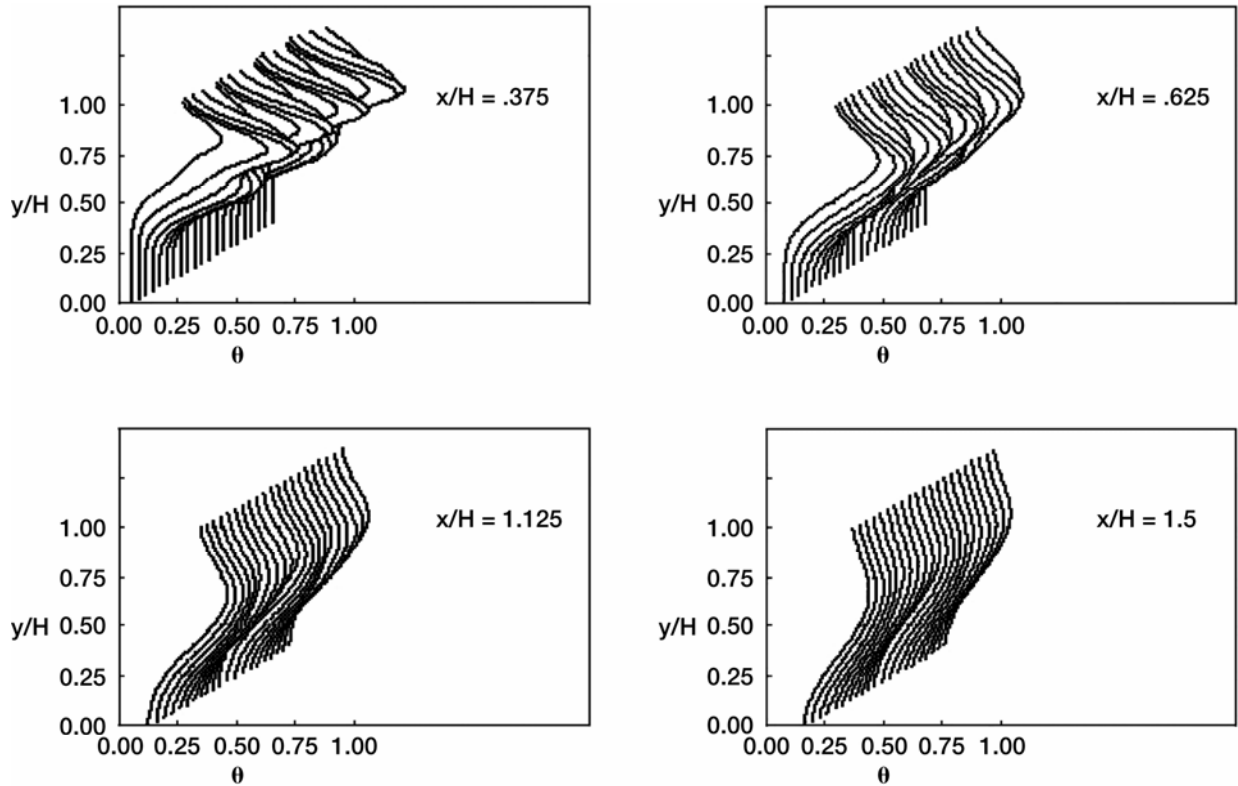


Figure 23a.—Scalar profiles for double rows with different orifice size and spacing for  $Sx/H = .25$ ;  $DR = 2.2$ ,  $J = 26.4$ , ( $M = 7.62$ ,  $R = 3.46$ ), and  $Cd = 0.64$  — Row 1:  $S/H = .5$ ,  $H/d = 5.66$ , ( $S/d = 2.83$ ,  $C = 2.57$ ) — Row 2:  $S/H = .25$ ,  $H/d = 8$ , ( $S/d = 2$ ,  $C = 1.28$ ). ( $x/H$  is from center of 1st row of holes; trailing edge of 2nd row is at  $x/H = .3125$ .)

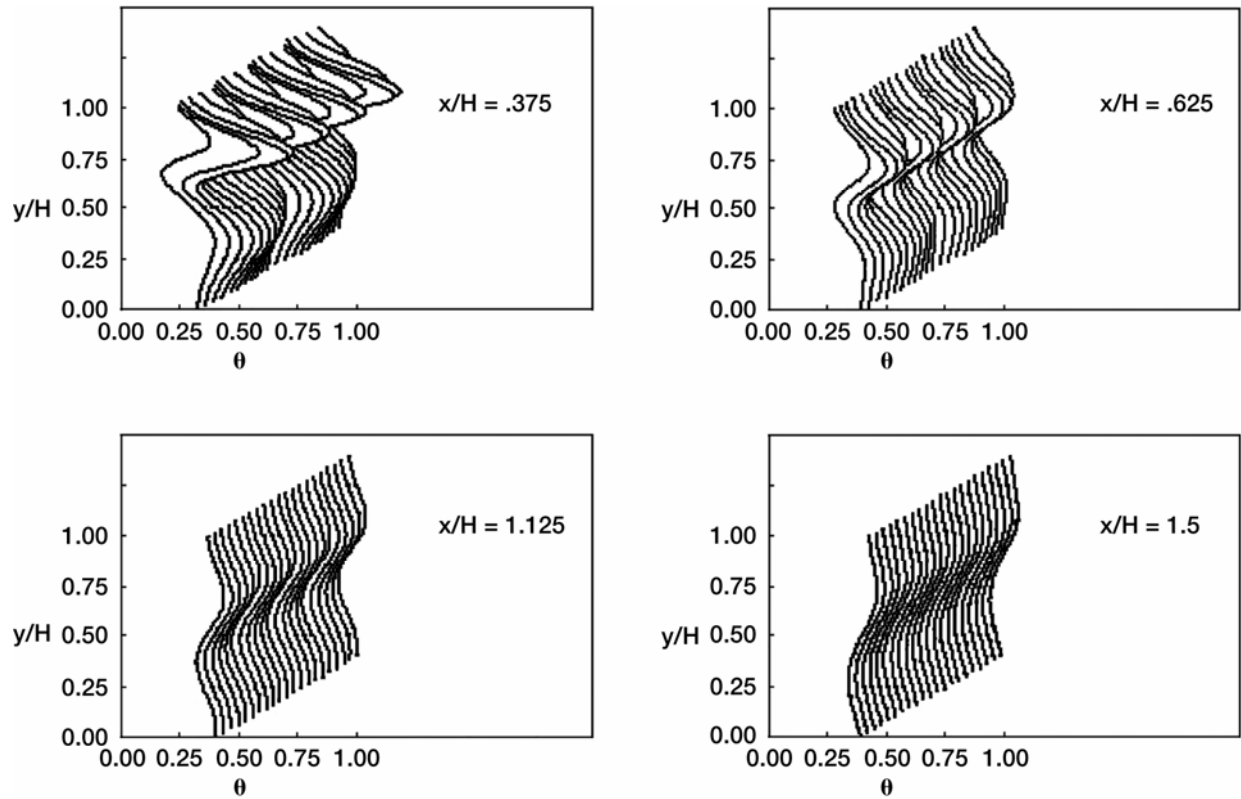


Figure 23b.—Scalar profiles for double rows with different orifice size and spacing for  $S_x/H = .25$ ;  $DR = 2.2$ ,  $C_d = 0.64$  — Row 1:  $S/H = .5$ ,  $H/d = 5.66$ ,  $(S/d = 2.83)$ .  $J = 105.6$ ,  $(M = 15.24, R = 6.93, C = 5.14)$ . — Row 2:  $S/H = .25$ ,  $H/d = 8$ ,  $(S/d = 2)$ ,  $J = 26.4$ ,  $(M = 7.62, R = 3.46, C = 1.28)$ . ( $x/H$  is from center of 1st row of holes; trailing edge of 2nd row is at  $x/H = .3125$ .)

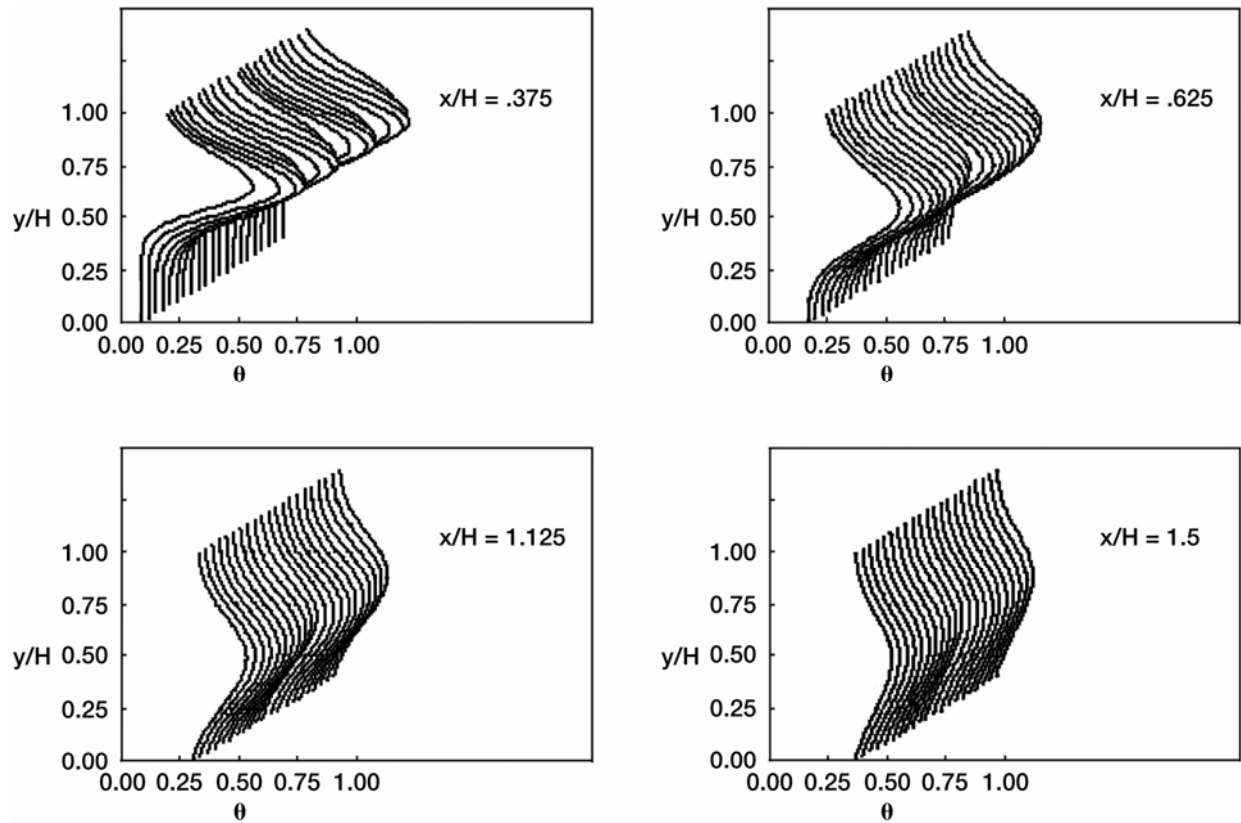


Figure 23c.—Scalar profiles for double rows with different orifice size and spacing for  $S_x/H = .25$ ;  $DR = 2.2$ ,  $C_d = 0.64$  — Row 1:  $S/H = .5$ ,  $H/d = 5.66$ , ( $S/d = 2.83$ ),  $J = 26.4$ , ( $M = 7.62$ ,  $R = 3.46$ ,  $C = 2.57$ ). — Row 2:  $S/H = .25$ ,  $H/d = 8$ , ( $S/d = 2$ ),  $J = 105.6$ , ( $M = 15.24$ ,  $R = 6.93$ ,  $C = 2.57$ ). ( $x/H$  is from center of 1st row of holes; trailing edge of 2nd row is at  $x/H = .3125$ .)

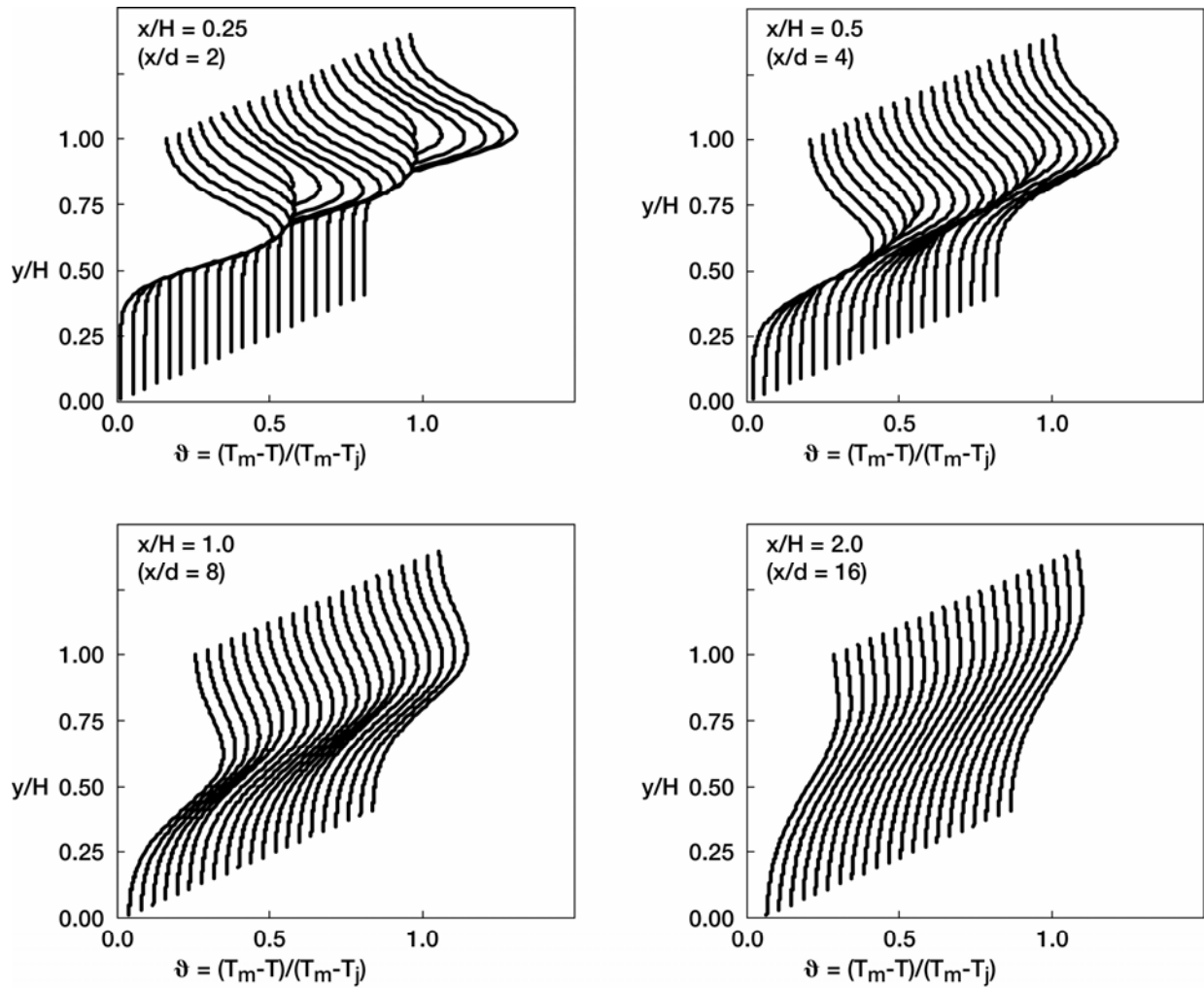


Figure 24a.—Variation in scalar distributions with increasing downstream distance: orifice configuration C in figure 3 (centerplane at edge [ ]–0–( in spreadsheet]) for  $S/H = 0.25$ ,  $H/d = 8$ ,  $(S/d = 2)$ ,  $DR = 2.2$ ,  $J = 26.4$ ,  $(M = 7.62, R = 3.46, C = 1.28)$ , and  $Cd = 0.64$ . (results shown here are based of trajectory equation used in reference 12—compare with figure 8.)

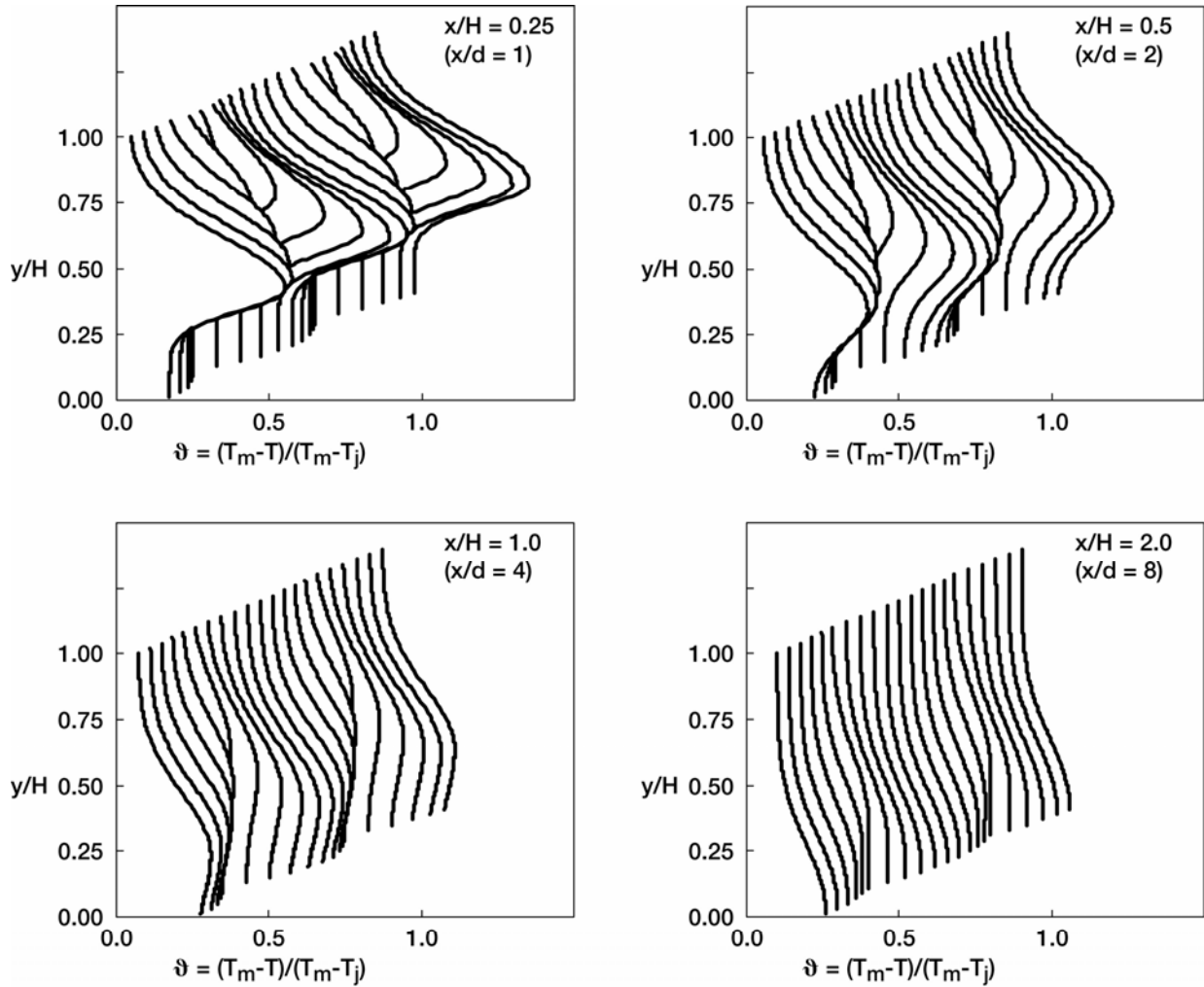


Figure 24b.—Variation in scalar distributions with increasing downstream distance: orifice configuration I in figure 3 (centerplane at edge [ ]-0-( in spreadsheet]) for  $S/H = 1$ ,  $H/d = 4$ , ( $S/d = 4$ ),  $DR = 2.2$ ,  $J = 26.4$ , ( $M = 7.62$ ,  $R = 3.46$ ,  $C = 5.14$ ), and  $C_d = 0.64$ . (results shown here are based of trajectory equation used in reference 12—compare with figure 8.)

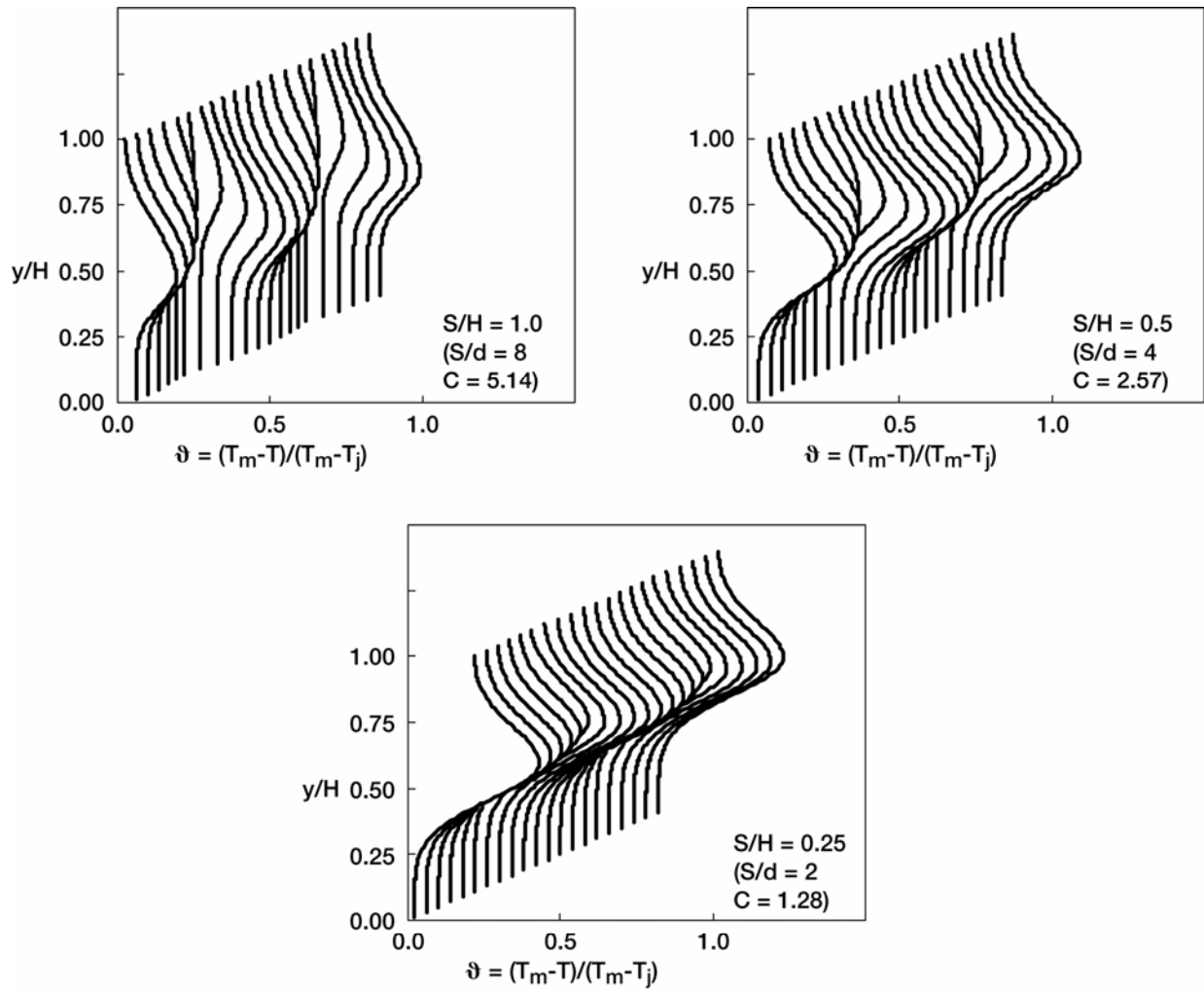


Figure 25.—Variation in scalar distributions with decreasing spacing (S/H) at constant orifice diameter: (centerplane at edge [ ]–0–( in spreadsheet)) for  $H/d = 8.0$ ,  $DR = 2.2$ ,  $J = 26.4$ , ( $M = 7.62$ ,  $R = 3.46$ ), and  $Cd = 0.64$  at  $x/H = 0.5$ . (results shown here are based of trajectory equation used in reference 12—compare with figure 11.)

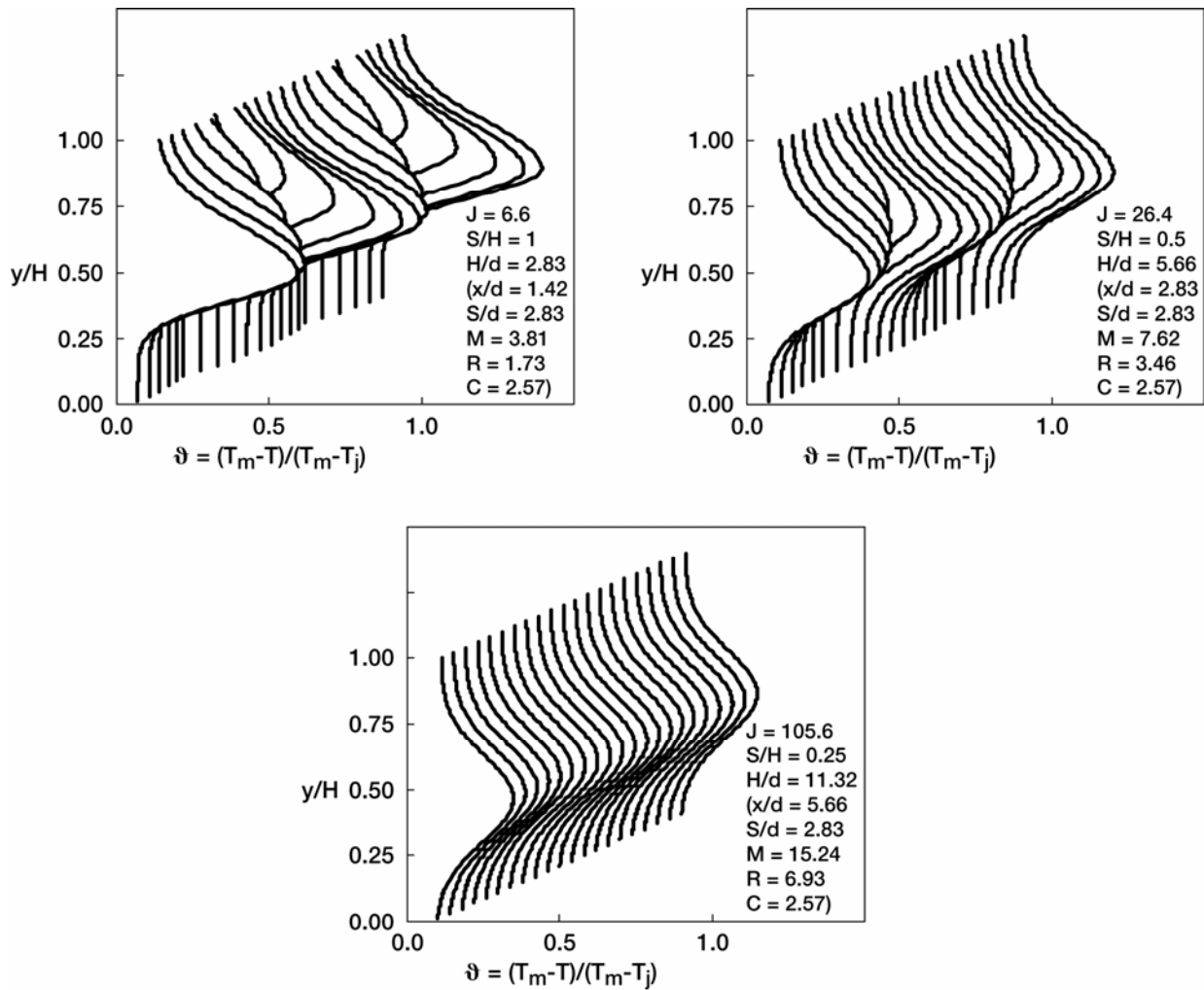


Figure 26a.—Variation in scalar distributions with coupled spacing and momentum-flux ratio, (centerplane at edge [ ]–0–( in spreadsheet)) for  $DR = 2.2$ , and  $Cd = 0.64$  at  $x/H = 0.5$ . (results shown here are based of trajectory equation used in reference 12—compare with figure 14.)

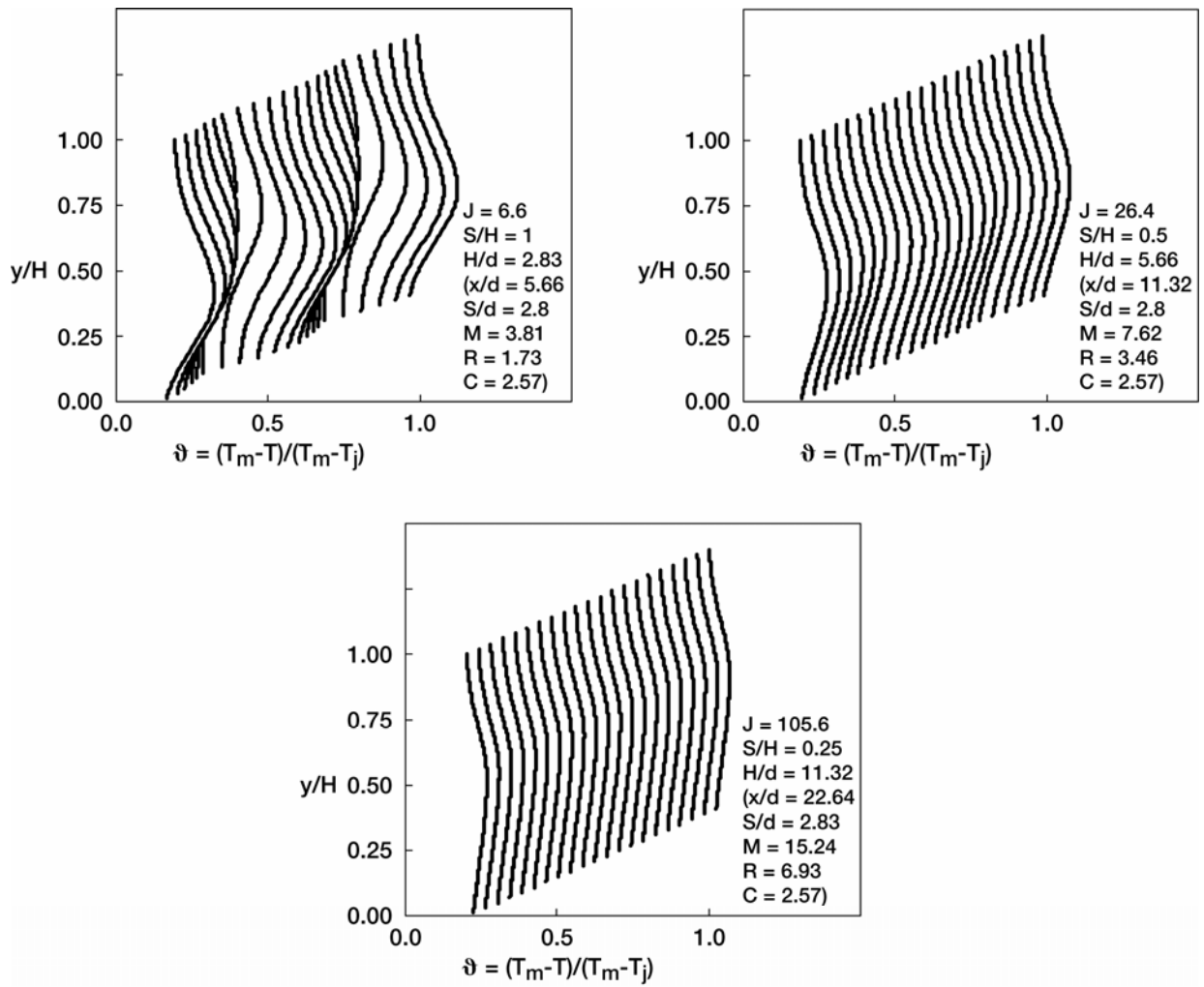


Figure 26b.—Variation in scalar distributions with coupled spacing and momentum-flux ratio, (centerplane at edge [ )-0-( in spreadsheet) for DR = 2.2, and Cd = 0.64 at  $x/H = 2$ . (results shown here are based of trajectory equation used in reference 12—compare with figure 14.)

# REPORT DOCUMENTATION PAGE

*Form Approved*  
*OMB No. 0704-0188*

Public reporting burden for this collection of information is estimated to average 1 hour per response, including the time for reviewing instructions, searching existing data sources, gathering and maintaining the data needed, and completing and reviewing the collection of information. Send comments regarding this burden estimate or any other aspect of this collection of information, including suggestions for reducing this burden, to Washington Headquarters Services, Directorate for Information Operations and Reports, 1215 Jefferson Davis Highway, Suite 1204, Arlington, VA 22202-4302, and to the Office of Management and Budget, Paperwork Reduction Project (0704-0188), Washington, DC 20503.

<b>1. AGENCY USE ONLY</b> ( <i>Leave blank</i> )		<b>2. REPORT DATE</b> February 2005	<b>3. REPORT TYPE AND DATES COVERED</b> Technical Memorandum	
<b>4. TITLE AND SUBTITLE</b>  A Spreadsheet for the Mixing of a Row of Jets With a Confined Crossflow			<b>5. FUNDING NUMBERS</b>  WBS-22-714-20-05	
<b>6. AUTHOR(S)</b>  J.D. Holdeman, T.D. Smith, J.R. Clisset, and W.E. Lear				
<b>7. PERFORMING ORGANIZATION NAME(S) AND ADDRESS(ES)</b>  National Aeronautics and Space Administration John H. Glenn Research Center at Lewis Field Cleveland, Ohio 44135-3191			<b>8. PERFORMING ORGANIZATION REPORT NUMBER</b>  E-14651	
<b>9. SPONSORING/MONITORING AGENCY NAME(S) AND ADDRESS(ES)</b>  National Aeronautics and Space Administration Washington, DC 20546-0001			<b>10. SPONSORING/MONITORING AGENCY REPORT NUMBER</b>  NASA TM-2005-213137	
<b>11. SUPPLEMENTARY NOTES</b>  J.D. Holdeman and T.D. Smith, NASA Glenn Research Center; J.R. Clisset and W.E. Lear, University of Florida, College of Engineering, Department of Mechanical Engineering, Gainesville, Florida 32611. Responsible person, Chi-Ming Lee, organization code RTB, 216-433-3413. There are three sheets in a supplemental Microsoft <sup>®</sup> Excel spreadsheet ( <a href="#">TM-2005-213137/SUPPL1</a> ) included on the CD.				
<b>12a. DISTRIBUTION/AVAILABILITY STATEMENT</b>  Unclassified - Unlimited Subject Category: 07  Available electronically at <a href="http://gltrs.grc.nasa.gov">http://gltrs.grc.nasa.gov</a> This publication is available from the NASA Center for AeroSpace Information, 301-621-0390.			<b>12b. DISTRIBUTION CODE</b>	
<b>13. ABSTRACT</b> ( <i>Maximum 200 words</i> )  An interactive computer code, written with a readily available software program, Microsoft <sup>®</sup> Excel (Microsoft Corporation, Redmond, WA) is presented which displays 3-D oblique plots of a conserved scalar distribution downstream of jets mixing with a confined crossflow, for a single row, double rows, or opposed rows of jets with or without flow area convergence and/or a non-uniform crossflow scalar distribution. This project used a previously developed empirical model of jets mixing in a confined crossflow to create an Microsoft <sup>®</sup> Excel spreadsheet that can output the profiles of a conserved scalar for jets injected into a confined crossflow given several input variables. The program uses multiple spreadsheets in a single Microsoft <sup>®</sup> Excel notebook to carry out the modeling. The first sheet contains the main program, controls for the type of problem to be solved, and convergence criteria. The first sheet also provides for input of the specific geometry and flow conditions. The second sheet presents the results calculated with this routine to show the effects on the mixing of varying flow and geometric parameters. Comparisons are also made between results from the version of the empirical correlations implemented in the spreadsheet and the versions originally written in Applesoft BASIC (Apple Computer, Cupertino, CA) in the 1980's.				
<b>14. SUBJECT TERMS</b> Dilution jets; Jet in crossflow; Gas turbine combustor; Empirical model; Correlations; Multiple jets; RQL; Conserved scalar; Pattern factor; Temperature distribution			<b>15. NUMBER OF PAGES</b> 88	
			<b>16. PRICE CODE</b>	
<b>17. SECURITY CLASSIFICATION OF REPORT</b> Unclassified	<b>18. SECURITY CLASSIFICATION OF THIS PAGE</b> Unclassified	<b>19. SECURITY CLASSIFICATION OF ABSTRACT</b> Unclassified	<b>20. LIMITATION OF ABSTRACT</b>	



